Salmonella-induced SIRT1 and SIRT3 are crucial for maintaining the metabolic switch in bacteria and host for successful pathogenesis

Dipasree Hajra[1], Raju S. Rajmani,[3] Ayushi Devendrasingh Chaudhary[4,5], Shashi Kumar Gupta,[4,5] and Dipshikha Chakravortty[1,2]

[1]Department of Microbiology & Cell Biology, Indian Institute of Science

[2]Adjunct Faculty, School of Biology, Indian Institute of Science Education and Research, Thiruvananthapuram

[3]Centre of Infectious Disease Research, Indian Institute of Science, Bangalore, India

[4]Pharmacology Division, CSIR-Central Drug Research Institute, Lucknow, India

[5]Academy of Scientific and Innovative Research (AcSIR), Ghaziabad, India

Corresponding author: Prof. Dipshikha Chakravortty

Email: dipa@iisc.ac.in

Tel. No. 0091 80 22932842

ABSTRACT

Sirtuins are the major players in host immuno-metabolic regulation. However, the role of sirtuins in the modulation of the immune metabolism pertaining to Salmonellosis is largely unknown. Here, our investigation focussed on the role of two important sirtuins, SIRT1 and SIRT3, shedding light on their impact on intracellular *Salmonella*'s metabolic switch and pathogenesis establishment. Our study indicated the ability of the live *Salmonella* Typhimurium to differentially regulate the levels of SIRT1 and SIRT3 for maintaining the high glycolytic metabolism and low fatty acid metabolism in *Salmonella*. Perturbing SIRT1 or SIRT3 through knockdown or inhibition, resulted in a remarkable shift in the host metabolism

to low fatty acid oxidation and high glycolysis. This switch led to decreased proliferation of *Salmonella* in the macrophages. Further, *Salmonella*-induced higher levels of SIRT1 and SIRT3 led to a skewed polarization state of the macrophages from a pro-inflammatory M1 state toward an immunosuppressive M2 making it more conducive for the intracellular life of *Salmonella*. Alongside, governing immunological functions by modulating p65 NF-κB acetylation, SIRT1, and SIRT3 also skew *Salmonella*-induced host metabolic switch by regulating the acetylation status of HIF-1α and PDHA1. Interestingly, though knock-down of SIRT1/3 attenuated *Salmonella* proliferation in macrophages, in *in vivo* mice-model of infection, inhibition or knockdown of SIRT1/3 led to more dissemination and higher organ burden which can be attributed to enhanced ROS and IL-6 production. Our study hence reports for the first time that *Salmonella* modulates SIRT1/3 levels to maintain its own metabolism for successful pathogenesis.

Keywords: SIRT1 and SIRT3, immune regulation, metabolic shift, macrophage polarization, *Salmonella* metabolism, bacterial dissemination, deacetylation

INTRODUCTION

Sirtuins are NAD+-dependent deacetylases that are present in all forms of life. Sirtuins comprise a conserved core catalytic domain that removes acetyl moiety from the lysine residues of proteins in presence of NAD+ as a cofactor [1] giving rise to 2'O-acetyl-ADP-ribose and free nicotinamide as products[2][3]. Free nicotinamide acts as a non-competitive inhibitor of sirtuins[4]. They possess variable N terminal and C terminal domains that confer different subcellular localization, substrate specificity, and functions[5]. Mammals have seven sirtuins that are responsible for regulating various biological functions such as cell survival, apoptosis, oxidative stress, metabolism, and inflammation[6][7]. SIRT1,6 and 7 have nuclear localization, SIRT2 is cytoplasmic and SIRT 3,4 and 5 comprise the mitochondrial SIRTs. In addition to

their deacetylase activity, they possess ADP ribosylation (SIRT1, SIRT4, and SIRT6), desuccinylation and demalonylation (SIRT5), delipoylation (SIRT4), and demyristoylation and depalmitoylation (SIRT6) enzymatic activities [8]. Previous studies have shown that SIRT1 gets activated in response to acute immune response and it deacetylates RelA/p65 component of NFκB thereby mediating its proteasomal degradation[9]. On the other hand, it activates RelB component of NFκB pathway. RelB causes heterochromatinization of pro-inflammatory genes like TNF-α and IL-β[10]. SIRT1 activates Peroxisome proliferator-activated receptor γ (PPARγ) coactivator-1α (PGC-1α) mediating a metabolic switch from glycolysis toward fatty acid oxidation. SIRT1-mediated RelB activation, in turn, activates SIRT3 causing the promotion of mitochondrial bioenergetics[11]. PGC-1α, a major player in mitochondrial biogenesis, activates SIRT3 [12] which in turn causes activation of PGC-1α, thereby fuelling a positive feedback loop. SIRT3 accounts for the major mitochondrial deacetylase orchestrating several metabolic processes such as fatty acid oxidation, promotion of the TCA cycle, and inhibition of ROS production[13].

Salmonella enterica serovar Typhimurium is a facultative intracellular Gram-negative enteric pathogen, causing a wide array of infections ranging from self-limiting gastroenteritis to diarrhea in humans [14]. *Salmonella enterica* serovar Typhi cause systemic infection in humans with typhoidal symptoms. Recent reports reported incidences of 21 million [15] typhoid cases and 93 million of non-typhoidal [16] cases round the year. The virulence of *Salmonella* is majorly regulated by two pathogenicity islands, namely, SPI-1 and SPI-2. It uses SPI-1 encoded T3SS and the effector proteins to invade host cells [17]. Inside the macrophages, they harbour within the *Salmonella* containing vacuoles (SCV) by virtue of its SPI-2 effectors [18]. Macrophages, dendritic cells and neutrophils are responsible for successful dissemination throughout the body through the reticulo-endothelial system (RES) [17].

Macrophages, serving as an intracellular niche for *Salmonella,* exhibit several continua of polarization states. At the two extreme ends of the spectrum lie the classically polarized M1 macrophages and alternatively activated M2 macrophages. M1 macrophages comprise of the proinflammatory antimicrobial state producing IL-1β, IL-6, TNF-α,IL-12, IFN-γ cytokines and exhibit enhanced expression of CD80, CD86 surface markers. The anti-inflammatory M2 macrophages promote bacterial persistence by producing anti-inflammatory cytokines like IL-10,TGF-β and show increased expression of Arg-1, CD206 surface markers[19][20]. To sustain the continuous production of proinflammatory cytokines M1 macrophages rely on glycolysis for their energy requirements. On the other hand, M2 macrophages are fuelled by enhanced oxidative phosphorylation (OXPHOS) and fatty acid oxidation (FAO)[21].It has been previously reported that sirtuins mediated attuning of metabolism impact polarization of macrophages *in vivo*. SIRT1 has the ability to promote the polarization of M2 macrophages and inhibit inflammation in macrophages of adipose tissue[22][23][24]. SIRT3 suppresses ROS by deacetylating and activating MnSOD[25].

Several bacteria are known to subvert the host immune system toward an immunosuppressive state. *Salmonella* or *Mycobacterium* have evolved mechanisms to counteract the M1 state of the host macrophage. *Salmonella* Typhimurium uses its SPI-2 effectors to inhibit the recruitment of NADPH oxidase to the SCV, thereby preventing oxidative burst mediated microbicidal activity[26]. Similarly, *Mycobacterium bovis* bacillus Calmette-Gue´rin prevents NOS2 recruitment to phagosomes[27]. *Salmonella* Dublin causes inhibition of the production of pro-inflammatory cytokine like IL-18 and IL-12p70[28]. Moreover, *Mycobacteria* inhibits NFκB signalling and IFN-γ mediated downstream pathways[29]. Furthermore, *Yersinia enterocolitica* elicits an M2 response by inducing Arginase-1 expression and TGFβ1 and IL-4production[30]. *Yersinia* TTSS effector LcrV induces an M2 phenotype supposedly by IL-10 production[31].

Since SIRT1 and SIRT3 are the major modulators of the immuno-metabolic paradigm, we intend to decipher the role of SIRT1 and SIRT3 in influencing host and *Salmonella* metabolism. This study highlights the role of SIRT1 and SIRT3 in intracellular pathogen survival by promoting *Salmonella* glycolysis and concomitantly driving host metabolism towards fatty acid oxidation. Additionally, *Salmonella* trigger an immunosuppressive M2 environment conducive to its intravacuolar proliferation by modulating SIRT1 and SIRT3 levels. Here, we have shown that SIRT1 and SIRT3 knockdown cause decreased M2 surface marker expression such as CD206 along with increased production of pro-inflammatory cytokines and ROS generation, together amounting to attenuated bacterial intracellular proliferation within the infected macrophages. Moreover, SIRT1 mediated p65 NF-κB deacetylation played a vital role in immune function regulation within the *Salmonella* infected macrophages with increased interaction of SIRT1 with p65 NF-κB. SIRT1 knockdown or inhibition resulted in hyperacetylation of p65 NF-κB thereby leading to enhanced pro-inflammatory response in *S.* Typhimurium infected macrophages. Further, SIRT1 and SIRT3 knockdown or inhibition skewed the *Salmonella*-induced host metabolic shift by regulating acetylation status of HIF-1α and PDHA. This caused increased host glycolysis and reduced fatty acid oxidation. However, the *Salmonella* shows the opposing metabolic profile with increased fatty acid oxidation and reduced glycolysis upon SIRT1 or SIRT3 inhibition. In the contrary to the macrophages, in *in vivo* mice-model of infection, SIRT1 and SIRT3 inhibition resulted in increased pathogen loads in organs and triggered enhanced bacterial dissemination, together leading to increased susceptibility of the mice to *S.* Typhimurium infection owing to increased ROS and IL-6 production. To the best of our knowledge, this is the first report implying the ability of host Sirtuins in impacting intracellular bacterial metabolism crucial for successful pathogenesis.

RESULTS

Salmonella modulates SIRT1 and SIRT3 expression along its course of infection in macrophages

Upon infection of RAW 264.7 murine macrophages with wildtype *Salmonella* Typhimurium strain 14028S, we observed an increased expression level of *SIRT 1* and *SIRT3* at initial and middle phases of infection, precisely at 2hr and 6hr post infection through qPCR (Fig.1, A and B). The *SIRT1* expression level declined at later phases of infection. On the other hand, the *SIRT3* transcript levels remained elevated at all time points with respect to uninfected control with a marked increment at 16hr time point post-infection which subsided at 20hr post-infection. We even monitored the expression profile of *SIRT1* and *SIRT3* in primary macrophages like peritoneal macrophages of C57BL/6 mice and observed a similar trend of elevated expression at initial (2hr), middle (6hr), and late (16hr) time points post-infection (Fig.1, C and D). In Confocal Laser Scanning Microscopy (CSLM) studies, we observed a similar increase in SIRT1 and SIRT3 expression at 6hr post infection within the infected macrophages RAW264.7 macrophages. (Fig.1, E-H). Immunoblotting revealed increased protein expression of both SIRT1 and SIRT3 at 2hr post-infection in comparison to the uninfected control (Fig. S1). However, SIRT1 expression exhibits a gradual decline at the late phase of infection (Fig. S1A, C). In line with the confocal microscopy data, SIRT3 immunoblotting data shows an increased protein expression profile at 6hr and 16hr post-infection (Fig. S1, B-D). Subsequently, to ascertain whether indeed *Salmonella* could modulate SIRT1 or SIRT3 expression levels, we evaluated the *SIRT1* and *SIRT3* mRNA and SIRT1 and SIRT3 protein expression profile within RAW264.7 macrophages upon infection with wildtype *S*. Typhimurium and SPI-1 (Δ*invC*) (InvC- protein export apparatus) or SPI-2 (Δ*ssaV* and Δ*steE*) (SsaV- Structural component of SPI-2 needle apparatus, SteE- SPI-2 effector protein involved in driving M2 polarization) mutants of *S*. Typhimurium. Our results depict the ability

of wildtype *S*. Typhimurium to induce the expression of both SIRT1 and SIRT3 within the infected RAW264.7 macrophages. However, infection with either SPI-1 or SPI-2 mutant abrogates the induction of *SIRT1* whereas only SPI-2 mutants (Δ*ssaV* and Δ*steE*) and not SPI-1 mutant infection caused reduction in *SIRT3* transcript level expression in the infected macrophages, implicating the role of SPI-1 and SPI-2 genes in triggering SIRT1 and SIRT3 in the infected macrophages (Fig. 1, I-J). However, at the protein level, only SPI-2 mutant infection resulted in a predominant decline in SIRT3 expression and a mild reduction in SIRT1 expression (Fig. S1B). Further, we examined the transcript level profile of *SIRT1* and *SIRT3* in M1 or M2 polarized RAW264.7 macrophages at 16hr post-infection and we observed 20-fold and 5-fold increase in *SIRT1* and *SIRT3* expression in M2 polarized infected macrophages as opposed to 0.5-fold and 0.4 fold downregulation in M1 polarized infected macrophages (Fig. S1C-D). Thus, an increase in expression profile both at transcript and protein levels indicates their role in *Salmonella* pathogenesis.

SIRT1 and SIRT3 play crucial role in intracellular bacterial proliferation in infected murine macrophages

As our previous *SIRT1* and *SIRT3* expression data in the polarized macrophages, hinted at the role of SIRT1 and SIRT3 in driving polarization of macrophages in the infected macrophages. We validated the intracellular replication of *S*. Typhimurium within the infected polarized macrophages. *S.* Typhimurium exhibited increased intracellular fold proliferation within anti-inflammatory M2 polarized macrophages in comparison to the pro-inflammatory M1 polarized RAW264.7 macrophages (Fig. S1 E-F). To evaluate the role of SIRT 1 and SIRT3 in the intracellular proliferation of the bacteria within murine macrophages, we have undertaken knockdown of SIRT1 and SIRT3 in RAW 264.7 (Fig. S2) macrophages through PEI-mediated transfection of shRNA plasmids directed against SIRT1 and SIRT3. Post 48hr of transfection, the transfected cells were infected with MOI=10 of wildtype *S*. Typhimurium and a gentamicin

protection assay was performed. Intracellular proliferation of the bacteria was quantified by plating the cell lysate at 2hr and 16hr post-infection. *Salmonella* exhibits compromised intracellular survival in SIRT1 and SIRT3 knock-down RAW264.7 macrophages in comparison to the un-transfected and scrambled controls (Fig.2, A). Further, we have assessed the intracellular proliferation in peritoneal macrophages isolated from thioglycolate-treated adult C57BL/6 mice post SIRT1 (EX-527) and SIRT3 (3TYP) inhibitor treatment. SIRT1 or SIRT3 inhibitor-treated macrophages exhibited attenuated intracellular replication in comparison to the untreated peritoneal macrophages (Fig,2, B). Together, our results depict the role of SIRT1 and SIRT3 in controlling the intracellular proliferation of *S.* Typhimurium.

SIRT1 and SIRT3 inhibition contribute to skewed inflammatory host responses upon *Salmonella* infection

Several reports indicate the role of SIRT1 and SIRT3 in the modulation of host immune responses pertaining to infection scenarios [35][36][37][38]. Therefore, we intend to check whether SIRT1 or SIRT3 regulates immune functions in *Salmonella*-infected macrophages**.** To delineate the role of SIRT1 and SIRT3 in the modulation of immune responses, we wished to investigate the production of pro-inflammatory and anti-inflammatory cytokines in knockdown (KD) RAW 264.7 macrophages upon *S.* Typhimurium infection. Post 48hr transfection, cells were subjected to wildtype *S.* Typhimurium infection at an MOI of 10. At the indicated time points, cell-free supernatant was harvested and evaluated for pro-inflammatory and anti-inflammatory cytokine production by ELISA. Inhibition of both SIRT1 and SIRT3 increased production of pro-inflammatory cytokine IL-6 significantly at 2hr and 20hr post-infection (Fig.S3, A). Moreover, there was only a significant reduction in anti-inflammatory IL-10 production upon SIRT1 and SIRT3 KD at 2hr and 20hr post-infection (Fig.S3, B). Further, we estimated the production of another pro-inflammatory cytokine, IL-1β at 20hr post-infection under the knockdown condition of SIRT1 and SIRT3 (Fig.S3, C) and we observed heightened

IL-1β production under knockdown of SIRT1 and SIRT3 in comparison to the scrambled infected control. In peritoneal macrophages upon SIRT1(EX-527-1μM) or SIRT3(3-TYP-1μM) chemical inhibitor treatment, an increase in IL-6 and IL-1β cytokine levels was observed at 6hr post-infection (Fig.S3, D-E). This indicates the possible role of SIRT1 and SIRT3 in the regulation of cytokine production upon *Salmonella* infection.

Immune functions are an important determinant of macrophage polarization. Since SIRT1 and SIRT3 played an immune-modulatory role in *Salmonella* infection, we investigated whether *Salmonella* infection is associated with a shift in macrophage polarization status. To assess the ability of the pathogen to alter the polarization state of the macrophage, we have undertaken gene expression profiling of various M1 and M2 markers using nanoString nCounter technology along the course of *Salmonella* Typhimurium infection at the indicated time points in RAW 264.7 macrophages. A gradual shift from pro-inflammatory M1 toward the anti-inflammatory M2 state was observed with the progression of *Salmonella* infection. Along the course of infection, there was a reduction in the expression of M1 markers like *NOS2*, *CD40*,*CD86*, *TNF-α*, *Nfkb2*,*IL-6* and a corresponding increase in the expression of the M2 markers such as *Arg-1*, *CCL-17*, *CD 206*, *IL4ra* with an exception of *Tgf-β* (Fig.3, A).In order to validate the polarization potency of the pathogen, FACS was performed using a pro-inflammatory M1 surface marker, CD86 tagged with PE. The data suggests a distinct decrease in CD86 positive population in the infected sets in comparison to the uninfected and the fixed dead bacteria control along the course of *S.* Typhimurium infection (Fig.3, B, Fig. S4, A). Thus, the live pathogen has a propensity to skew the polarization state of the macrophage toward an anti-inflammatory M2 state to subvert the initial acute inflammatory response mounted by the host immune system.

To assess the role of SIRT1 and SIRT3 in macrophage polarization, we determined anti-inflammatory CD206 surface marker profiling of the infected macrophages through flow

cytometry. Knockdown of SIRT1 or SIRT3 in infected RAW 264.7 macrophages resulted in a reduction in anti-inflammatory CD206 surface marker expression at 16hr post-infection (Fig. 3, C, Fig. S4, B). Moreover, SIRT1 or SIRT3 knockdown led to enhanced intracellular ROS generation within the infected macrophages in comparison to the scrambled or the untransfected control (Fig.S5). Further, the Haematoxylin and Eosin staining of the *S.* Typhimurium infected mice liver tissue sections depicted exacerbated signs of inflammation in the SIRT1 (EX-527) or SIRT3 (3TYP) inhibitor-treated cohorts in comparison to the untreated controls with multiple necrotic foci and increased influx of inflammatory cell inflates. Moreover, these acute inflammatory signs of the liver sections get ameliorated in the SIRT1 (SRT1720) activator-treated infected cohort (Fig.8, T-U) (Data described later). Together, these data suggest the role of SIRT1 and SIRT3 in the modulation of host inflammatory response. Previous literature reports have shown that SIRT1 physically interacts with p65 subunit of NF-κB and inhibits transcription by deacetylating p65 at lysine 310 [39]. Moreover, SIRT1-mediated deacetylation of the p65 subunit of the master regulator of the inflammatory response, NF-κB, results in the reduction of the inflammatory responses mediated by this transcription factor [40]. To evaluate the immune regulatory mechanism of SIRT1 in the *S.* Typhimurium (STM) infection scenario, we undertook SIRT1 immunoprecipitation in the infected RAW264.7 macrophages at 16h post-infection alongside the uninfected macrophages and probed for NF-κB p65 interaction. We observed an increased interaction of SIRT1 with NF-κB p65 in the infected macrophages in comparison to the uninfected control (Fig.4, A). Further, the knockdown of SIRT1 resulted in increased acetylation status of the NF-κB p65 upon infection in comparison to the scrambled, infected control (Fig.4, B, C). To understand whether the enzymatic domain of SIRT1 possess any role in mediating this interaction, we carried out NF-κB p65 immunoprecipitation in infected RAW264.7 macrophages in presence or absence of SIRT1 catalytic chemical inhibitor, EX-527(1μM) treatment at 16h post-

infection. We observed an increased interaction of NF-κB p65 with SIRT1 in the infected untreated macrophages when compared to the untreated uninfected control (Fig.4, D). However, the interaction of NF-κB p65 with SIRT1 gets abrogated under the EX-527 inhibitor treatment in the infected macrophages thereby implying the function of the catalytic domain in mediating the interaction (Fig.4, D). Moreover, an increased acetylation status of NF-κB p65 was observed in the EX-527 treated infected macrophages in comparison to the untreated infected macrophages (Fig. 4 E).

SIRT1 and SIRT3 relieve oxidative stress in infected macrophages and alleviation of the intracellular ROS generation restores intracellular survival of *S.* Typhimurium within the SIRT1 or SIRT3 knockdown macrophages

Previous reports have suggested the role of SIRT1 and SIRT3 in oxidative stress conditions. They are known to act in concert as anti-oxidants by reducing ROS production[41][42][43]. Moreover, enhanced ROS production is also a prototype of the classically activated macrophages[44][45]. Here, we examined the effect of SIRT1 and SIRT3 knockdown in intracellular ROS generation in *S.* Typhimurium infected RAW264.7 macrophages through DCFDA staining in FACS. Results depicted significant enhancement in the production of ROS at 16hr post infection upon knockdown of SIRT1 or SIRT3 in comparison to untransfected or scrambled control (Fig.S5, A,B). Upon detection of extracellular ROS generation through Phenol Red Hydrogen Peroxidase assay, we detected higher ROS generation upon SIRT3 KD at 6hr post infection and greater ROS production at 16hr and 20hr time points in SIRT1 knockdown macrophages (Fig.S5,C). Therefore, SIRT1 and SIRT3 play an important role in mitigating the oxidative burst in *Salmonella* infected macrophages. Our previous findings depicted decreased intracellular burden of *S.* Typhimurium within the SIRT1 or SIRT3 knockdown macrophages along with increase in intracellular ROS generation. Therefore, we speculated that the decreased intracellular proliferation within the SIRT1 or SIRT3 knockdown

macrophages might be on account of increased intracellular ROS production which might lead to increased killing of the intracellular bacteria. This hypothesis led us to evaluate the intracellular bacterial burden within the infected SIRT1 or SIRT3 knockdown RAW264.7 macrophages or SIRT1 or SIRT3 inhibitor treated peritoneal macrophages (isolated from C57BL/6 adult mice post 5th day of thioglycolate injection) in presence of a ROS inhibitor named N-Acetyl Cysteine (NAC). NAC acts as a scavenger of ROS by antagonizing the activity of proteasome inhibitors [46]. The attenuated intracellular proliferation of *Salmonella* Typhimurium within the knockdown or the chemical inhibitor treated macrophages got restored upon 1mM treatment of ROS scavenger, NAC (Fig.S6). Therefore, intracellular ROS production within the knockdown murine macrophages is one of the reasons for the attenuated survival of the bacteria.

SIRT1 and SIRT3 play crucial role in mediating metabolic switch in infected macrophages

Macrophage polarization is not only governed by immunological changes but also contributed by metabolic reprogramming[47][24][48]**.** Since previous data suggested progression of *Salmonella* infection with the shift in polarization state of the macrophage, we decided to investigate alteration of the metabolic state of the macrophages as macrophage polarization is governed by immune-metabolic shift. In pursuit of fulfilling such requirement, we performed gene expression studies of various metabolic genes through nanoString nCounter technology in *S.* Typhimurium infected RAW 264.7 macrophages. Analysis of the gene profile revealed upregulation of genes involved in fatty acid oxidization and tricarboxylic acid cycle and corresponding downregulation of genes involved in glycolysis (Fig.5, A). To validate the findings, we carried out qRTPCR to quantitatively measure the expression of a fatty acid oxidation gene, *PPARδ* in infected RAW 264.7 macrophages. We found that mRNA level was elevated to 2-fold at 2hr and 6hr post-infection. At the late phase of infection, 16hr post

infection around 6-fold upregulation in mRNA transcript was noted (Fig.5, B). Lactate estimation assay of *S.* Typhimurium infected RAW264.7 macrophages at the initial time point of 2hr and at the late time point of 16hr post infection revealed decline in lactate (glycolysis end product) production at 16hr in comparison to 2hr post-infection timepoint (Fig. 5C). Together, these results suggest the capability of the pathogen to drive a shift in the metabolic status of the infected macrophages toward fatty acid oxidation. Next, we evaluated the function of SIRT1 and SIRT3 in influencing the metabolic switch in the infected macrophages through qRT PCR with several host fatty acid oxidizing genes (*Acox*, *Hadha, Pdha, and AcadL)* and glycolytic gene (*PfkL*) in SIRT1 and SIRT3 knockdown macrophages (Fig. S7, A) and via lactate production assay (Fig. 5, D-E). Lactate estimation assay in SIRT1 and SIRT3 knockdown condition revealed enhanced lactate production at 16hr post infection in comparison to the scrambled control which further authenticates the increased host glycolysis upon SIRT1 and SIRT3 knockdown scenario (Fig. 5, D-E). SIRT1 and SIRT3 knockdown RAW 264.7 infected macrophages showed decreased expression of fatty acid oxidizing genes and increased expression of glycolytic *PfkL* gene in comparison to the scrambled infected control (Fig. S7, A). Similar results were obtained in the infected peritoneal macrophages under the SIRT1 or SIRT3 catalytic inhibitor treatment (Fig. S7, B-D). Moreover, qRT PCR-mediated metabolic gene profiling of liver and spleen isolated from wildtype *S.* Typhimurium infected macrophages revealed decreased transcript level expression of murine fatty acid oxidation genes upon treatment with SIRT1 (EX-527) or SIRT3 (3TYP) catalytic inhibitors which got reversed upon SIRT1 activator (SRT1720) treatment (Fig. S7, E-F). Moreover, SIRT1 and SIRT3 knockdown or catalytic inhibition in peritoneal macrophages resulted in increased protein expression of host glycolytic genes such as Phosphoglycerate kinase (Pgk), Phosphofructokinase (Pfk) with concomitant reduction in protein expression of TCA cycle gene like Pyruvate dehydrogenase (Pdha1) and fatty acid oxidation genes such as Hadha and

Acox1 (Fig.5, F, Fig. S7D). Fatty acid oxidation assay in the RAW264.7 macrophages under SIRT1 or SIRT3 knockdown condition or inhibition treatment revealed significant decrease in fatty acid β oxidation activity of the infected macrophages in comparison to the scrambled or the untreated control (Fig.5, G). To investigate whether the host metabolic switch toward increased fatty acid oxidation is being driven by the pathogen, we performed fatty acid β oxidation activity assay under wildtype *S*. Typhimurium (STM WT), SPI-1 (Δ*invC*) or SPI-2 (Δ*ssaV* and Δ*steE*) mutants of *S*. Typhimurium infection condition. We found that the wildtype bacteria with its intact SPI-2 effector secretion apparatus could promote increased host fatty acid β oxidation. In the contrary, the SPI-2 (Δ*ssaV* and Δ*steE*) mutants of *S*. Typhimurium failed to drive host metabolic shift towards increased fatty acid oxidation (Fig. 5, H).

Collectively, these data suggest the role of SIRT1 and SIRT3 in mediating the *Salmonella* induced host metabolic shift in the infected macrophages.

SIRT1 and SIRT3 concomitantly influences *Salmonella* metabolism

Our previous data indicated a shift in host metabolism toward increased fatty acid oxidation along the course of *Salmonella* Typhimurium infection in murine RAW 264.7 macrophages. *Salmonella* Typhimurium drives the metabolism of the infected macrophage toward fatty acid oxidation. This observation led us to investigate the influence of host metabolic shift on the metabolic status of the pathogen harboring inside the infected macrophages[49]. We were intrigued whether increased glucose availability within the fatty-acid oxidizing macrophages is utilized by the bacteria. Thus, we undertook simultaneous gene expression studies of various *Salmonella* genes involved in their pathogenesis and metabolism through nanoString nCounter technology in *S.* Typhimurium infected RAW 264.7 macrophages. The nanoString gene profile revealed enhanced expression of genes involved in *Salmonella* glycolysis and glucose uptake such as *pfkA* and *ptsG*, respectively (Fig.6, A). This finding indicates the ability of the pathogen

to drive the metabolic state of the host toward fatty acid oxidation with corresponding increased glucose utilization by the bacteria favoring their survival inside the host. qRT PCR results with several bacterial fatty acid oxidizing genes (*fadA, fadB,fadL,aceA, aceB*) and glycolytic genes (*ptsG*) in knockdown condition of SIRT1 and SIRT3 in RAW 264.7 macrophages further validated the nanoString gene expression profiles (Fig.6, B). In scrambled control, *Salmonella* infection progresses with increased *Salmonella* glycolysis and reduced bacterial fatty acid oxidation. However, knockdown of SIRT1 and SIRT3 abrogate this bacterial metabolic shift by reducing its glycolysis and by exhibiting enhanced fatty acid oxidation thereby attenuating pathogen intracellular survival. Similar observations were obtained from the qPCR data in the infected mice liver and spleen samples with increased transcript level expression of bacterial fatty acid oxidation genes and decreased expression of bacterial glycolytic genes upon SIRT1 or SIRT3 inhibitor treatment (Fig. 6 C, D). Therefore, SIRT1 and SIRT3 driven host metabolic switch potentially influence the metabolic profile of the intracellular pathogen.

Mechanism behind SIRT1 or SIRT3 mediated metabolic switch

As per our previous findings, SIRT1 or SIRT3 inhibition led to increased host glycolysis and decline in fatty oxidation in the infected macrophages. HIF1α is a master regulator of glycolysis in host during stress conditions [50]. Previous reports have suggested HIF1α to be a target of deacetylation by SIRT1 at Lys 674 which contribute to metabolic reprogramming in cancer cells. During hypoxia, downregulation of SIRT1 leads to increased acetylation and activation of HIF1α [51]. Additionally, in CD4+ T cells, ectopic expression of SIRT1 inhibited IL-9 production and glycolysis by negatively regulating HIF1α [52]. To delve into the mechanism behind SIRT1 mediated modulation of metabolic responses, we assessed the interaction of SIRT1 with HIF-1α in infected RAW264.7 macrophages. The immunoprecipitation studies of SIRT1 showed increased interaction of the SIRT1 with HIF1α in the *S.* Typhimurium infection scenario with respect to the uninfected control (Fig.7, A). Further, we evaluated the acetylation

status of HIF1α in the SIRT1 knockdown status of the infected macrophages. We found that SIRT1 knockdown showed increased acetylation of HIF1α in the infected macrophages in comparison to the scrambled infected control at 16hr post-infection (Fig. 7, B,C). Immunoprecipitation studies under SIRT1 (EX-527) inhibitor treatment in RAW264.7 macrophages revealed increased acetylation of HIF1-α along with reduced interaction of HIF-1α with SIRT1, thereby indicating the probable role of the catalytic domain in influencing the interaction (Fig. 7 D-F). Further, to ascertain the role of HIF-1α in mediating the glycolytic switch in the infected macrophages, we estimated the lactate production under SIRT1 and SIRT3 knockdown conditions in the presence or absence of HIF-1α inhibitor (chetomin)[53]. Our results depicted a decline in lactate production upon chetomine treatment including under SIRT1 and SIRT3 knockdown conditions (Fig.7G). Together, our results implicate the role of SIRT1 in governing glycolytic shift in the infected macrophages by deacetylating HIF1α. Upon SIRT1 knockdown or inhibition, HIF1α gets hyperacetylated which causes activation of the downstream glycolytic genes. Alternatively, several key literatures suggest the role of SIRT3 in modulating metabolic programming by deacetylating several proteins involved in fatty acid oxidation, the tricarboxylic acid cycle and oxidative phosphorylation [54][55]. PDHA1 (Pyruvate Dehydrogenase E1 subunit alpha) is a key enzyme linking glycolysis to TCA cycle and oxidative phosphorylation. SIRT3 regulates PDHA1 acetylation by deacetylating PDHA1 at lysine 385 residue, thereby playing a key role in metabolic reprogramming [55]. PDHA1 acetylation coincides with PDH activity and increased PDHA1 phosphorylation [55]. Therefore, we investigated the role of SIRT3 in the modulation of host fatty acid oxidation upon *S*. Typhimurium infection in RAW264.7 macrophages. To do so, we immunoprecipitated PDHA1 and checked for its interaction with SIRT3 or SIRT1 under the knockdown condition of SIRT3 or upon SIRT3 inhibitor treatment (Fig.7 I-J). We observed an increased interaction of PDHA1 with SIRT3 in the infection scenario in comparison to the uninfected control which

gets eventually abolished under the knockdown condition (Fig.7 I-J) and under the chemical inhibitor treatment of SIRT3 (Fig.7, K-L) suggesting the role of the SIRT3 in mediating the interaction with PDHA1. Alongside the decreased interaction of PDHA1 with SIRT3, increased acetylation of PDHA1 was detected upon SIRT3 inhibitor treatment in infected macrophages (Fig.7, K-L).

SIRT1 or SIRT3 inhibition enhances bacterial burden in mice *in vivo*

6-8 weeks old adult male C57BL/6 mice were treated with SIRT1 inhibitor EX-527, SIRT3 inhibitor 3TYP and SIRT1 activator SRT1720 at a dose of 1mg/kg each via intraperitoneal injection (every alternate Day) (Fig. 8A). Following the inhibitor treatment, the mice were orally gavaged with 10^7 CFU of *S.* Typhimurium 14028S for organ burden evaluation or with 10^8 CFU of wildtype *S.* Typhimurium for survival studies. On day 5th post-infection, mice were sacrificed, and the liver, spleen and Mesenteric Lymph Node (MLN) were harvested for enumeration of the organ burden. The SIRT1 inhibitor, EX-527 and SIRT3 inhibitor, 3TYP-treated mice cohorts exhibited increased organ loads in liver, spleen and MLN in comparison to the vehicle control. On the contrary, the SRT1720 treated mice group showed organ burden comparable to that of the vehicle control (Fig. 8, B). Moreover, the SIRT1 and the SIRT3 inhibitor-treated mice cohorts died earlier than the vehicle-treated control mice group or the SIRT1 activator-treated group (Fig. 8, C). Further, the SIRT1 and the SIRT3 inhibitor-treated mice cohorts showed increased splenic length in comparison to the vehicle-treated mice group and the SIRT1 activator-treated mice cohort (Fig. 8, D). The increased organ burden in the EX-527 or 3TYP treated group might be due to increased bacterial dissemination in blood. To assess bacterial dissemination, blood was collected from infected mice post-inhibitor treatment at specific days post-infection retro-orbitally and plated onto *Salmonella Shigella* (SS) agar plates for bacterial enumeration. Indeed, increased bacterial dissemination was observed in the

blood of mice treated with SIRT1 inhibitor, EX-527 or SIRT3 inhibitor, 3TYP at day 1-, 2-, 3-,4- post-infection in comparison to the vehicle-treated mice (Fig. 8, E). Further, we wanted to examine whether the increased bacterial dissemination was due to increased ROS production or due to the presence of elevated inflammatory cytokine levels like IL-6 and IL-1β. In the wildtype C57BL/6 mice treated with SIRT3 inhibitor 3TYP showed heightened bacterial burden in blood at 5th day post-infection in comparison to the vehicle control. Nevertheless, the *gp91phox*-/- mice group lacking the catalytic subunit of NADPH oxidase did not depict significant variation in the bacterial load among the different mice treatment cohorts (Fig. 8, F). Further, the EX-527 (SIRT1 inhibitor) and the 3TYP (SIRT3 inhibitor) treated mice possessed elevated levels of serum IL-6 (Fig.8G), IL-1β (Fig. S3F) and showed increased intracellular ROS burden in infected liver tissues in comparison to the vehicle-treated control and the SRT1720 (SIRT1 activator) treated mice group (Fig. 8H). The increased mouse serum IL-6 and IL-1β production was in a similar line with the increased IL-6 or IL-1β cytokine generation in EX-527 or 3TYP treated peritoneal macrophages under the infection scenario (Fig. S3, D-E). Moreover, estimation of IL-1β within the infected intestinal ileal sections of the mice revealed increased pro-inflammatory IL-1β generation in the SIRT1 and SIRT3 inhibitor-treated mice groups in comparison to the untreated or the SIRT1-activator treated mice cohorts (Fig. S3G). However, contrary to the *in vitro* studies wherein SIRT1 or SIRT3 knockdown or inhibition resulted in attenuated intracellular proliferation, here in *in vivo* mouse model of infection, we observed increased bacterial organ loads owing to increased bacterial dissemination. To delineate this observation further, we evaluated the bacterial load within splenocytes isolated from control or inhibitor-treated C57BL/6 mice infected with GFP expressing *S.* Typhimurium at 5th day post-infection via flow cytometry. We observed heightened bacterial load in the EX-527 or the 3TYP treated mice cohorts (Fig. 8, I-J). However, when we enumerated the bacterial count within the F4/80+ macrophage population

of the infected splenocytes, we noticed decreased bacterial loads in the EX-527 or 3TYP - treated mice group in comparison to the vehicle-treated control group or the SRT-1720 activator-treated group (Fig. 8, K-L). Further, we evaluated additional splenic populations including CD45+, Ly6C+, and CD11c+ populations. Our results show that the CD45+ splenic population depicts increased bacterial loads like that of the total splenic population within the SIRT1 or SIRT3 inhibitor-treated cohorts. However, CD45+ monocytes and Ly6C positive splenic population exhibit compromised burden within the SIRT1 and SIRT3 inhibitor-treated cohorts. Moreover, CD11c+ population, CD45+ granulocytes, or lymphocytes show comparable organ loads to that of the vehicle control or SIRT1 activator-treated mice group (Fig. 8M-S, Fig. S8). Overall, our data suggest heterogeneous bacterial burden in diverse splenic populations. This opposing phenotype could be attributed to the increased IL-6 and IL-1β cytokine storm and elevated ROS production upon the SIRT1 or SIRT3 inhibitor treatment which in turn resulted in bacterial dissemination *in vivo* and concomitantly restricted the *in vitro* intracellular proliferation within macrophages. To validate this observation, we estimated the ROS levels within the liver and spleen tissues harvested from *S.* Typhimurium infected C57BL/6 mice, treated with specific catalytic inhibitor, activator or vehicle via DCFDA staining using flow cytometry at 5th day post-infection. We detected escalated levels of ROS within both the infected liver and spleen tissues of the EX-527 or 3TYP-treated mice groups in comparison to the vehicle-treated or the SRT1720 treated mice cohorts (Fig. 8, H, S9). Haematoxylin and eosin staining of the liver sections (harvested at 5th day post-infection) revealed increased inflammation with multiple areas of severe acute hepatic necrosis with complete loss of hepatic architecture in the EX-527 and 3-TYP treated liver samples in comparison to the vehicle-treated control and SRT-1720 treated liver samples (Fig. 8, T-U). In line with the inhibitor-treated studies, the increased organ loads, and systemic dissemination driven heightened susceptibility of mice toward *S.* Typhimurium infection were replicated in

in vivo SIRT1 and SIRT3 adeno-associated virus serotype 6 (AAV6) mediated knockdown mice model which showed elevated IL-6 production in comparison to the scrambled control treated mice cohort (Fig. 8, V-X, Fig. S10). Simultaneously, the haematoxylin-eosin-stained sections of the liver tissues harvested from the shSIRT1 or shSIRT3 mice cohorts depicted increased pathological scoring with multiple necrotic areas and severely damaged liver tissue architecture in comparison to the scrambled mice control (Fig. 8, Y). Altogether, our results implicate the role of SIRT1 and SIRT3 in controlling *S*. Typhimurium infection *in vivo*.

DISCUSSION

Several studies have confirmed the propensity of *Salmonella* to skew the polarization state of the infected macrophages toward an immunosuppressive anti-inflammatory state[56][57][58]. We have validated such findings and further elaborated it by depicting the role of SIRT1 and SIRT3 in the modulation of host immune responses as well as host-bacterial metabolism. *Salmonella* Typhimurium infection modulates the expression profile of both SIRT1 and SIRT3 in the infected macrophages at both mRNA and protein level via its SPI-2 effector. Downregulation of SIRT1 and SIRT3 through shRNA mediated knockdown resulted in heightened pro-inflammatory immune responses with increased production of IL-6 cytokine and decreased surface expression of anti-inflammatory CD206. SIRT1 and SIRT3 downregulation also resulted in increased intracellular ROS production in the infected macrophages. SIRT1 and SIRT3 knockdown macrophages not only show altered host immune status but also depicted shift in the metabolic state with increased glycolytic shift. This altered host metabolism upon SIRT1 and SIRT3 knockdown condition influences the outcome of infection by regulating the intracellular bacterial metabolism which shows reduced bacterial glycolysis and increased fatty acid oxidation. All these outcomes account for attenuated intracellular bacterial proliferation in the SIRT1 and SIRT3 knockdown macrophages.

However, in murine model of infection, SIRT1 or SIRT3 inhibitor treatment led to increased organ burden and triggered bacterial dissemination (Fig. S11). Overall, our study highlights the crucial role of SIRT1 and SIRT3 in governing the host immune-metabolic shift during *Salmonella* infection which in turn is vital for maintaining *Salmonella* metabolism.

Previous reports have elucidated the role of SIRT1 and SIRT2 pertaining to *Salmonella* infection. Ganesan et al., have depicted the role of SIRT1 in autophagy in *Salmonella* infection scenario[59]. Gogoi et al., have demonstrated SIRT2 mediated modulation of immune responses in dendritic cells[60]. Till date, there is no report highlighting the role of SIRT3 governing the *Salmonella* pathogenesis. The function of SIRT3 in infection scenario has been explored quite recently. In *Mycobacterium tuberculosis* infection condition, SIRT3 control mitochondrial function and autophagy[38]. SIRT3 downregulation in *Mycobacterium tuberculosis* infected macrophages is associated with dysregulated mitochondrial metabolism and increased cell death[61]. In this study we have explored the role of SIRT1 and SIRT3 in mediating host immune-metabolic switch in *Salmonella* Typhimurium infected macrophages which further govern intracellular bacterial metabolism and pathogenesis.

Our findings suggest the role of SIRT1 and SIRT3 in mediating polarization of the *Salmonella* infected macrophages toward an anti-inflammatory state. Upon knockdown of SIRT1 and SIRT3 in the infected macrophages we detect robust pro-inflammatory response and oxidative burst. This is in line with the findings by S.Elsela et al., wherein SIRT1 knockout RSV(Respiratory Syncytial Virus) - infected BMDCs showed significant increase in *Il1β*, *Il6* and *Il23* expression and ROS generation in comparison to the wild type RSV-infected BMDCs[35]. Also, Kim et al., showed presence of aggravated inflammatory responses in *Mycobacterium tuberculosis* infected SIRT3-/- BMDMs[38]. This heightened pro-inflammatory cytokine and oxidative burst restrict the intracellular survival of the pathogen as

detected by the lower intracellular bacterial burden in the SIRT1 and SIRT3 knockdown murine macrophages. *Salmonella* showed enhanced proliferation in the M2 macrophages owing to the reduced arsenals in terms of pro-inflammatory cytokines and ROS production. Moreover, the M2 macrophages are fuelled by increased fatty acid oxidation and reduced glycolysis[62]. This might facilitate enhanced bacterial proliferation as the host un-utilized intracellular glucose can be readily up taken by the pathogen and used to support its own glycolysis. Similarly, M1 or pro-inflammatory macrophages resort to glycolysis to meet their energy demands[63] thereby limiting the glucose availability for the intracellular pathogen[63][64]. In such condition, bacteria show enhanced fatty acid metabolism to sustain their energy demand[65]. In our study, we found that wild type *S.* Typhimurium infection drive host metabolism toward increased fatty acid oxidation via its SPI-2 effector protein with concomitant increase in the bacterial glycolysis. SIRT1 and SIRT3 inhibition abrogates the metabolic switch and triggers increase in host glycolysis which in turn skew the bacterial metabolism from increased glycolysis to enhanced fatty acid oxidation and reduced glycolysis. Together, these findings implicate the role of SIRT1 and SIRT3 in reprograming the host metabolism which in turn affect the intracellular nutrient niche of the pathogen thereby influencing intracellular *Salmonella* proliferation. However, our *in vivo* findings in the murine model of infection show increased bacterial burden upon SIRT1 or SIRT3 inhibition. This increased burden could be attributed to increased dissemination from the macrophages into the bloodstream owing to the increased level of serum IL-6 levels. This is in concert with previous findings in *Klebsiella pneumoniae* infection in mice wherein increased inflammatory response upon HIF-1α activation induces bacterial dissemination [66]. Further correlation analysis of immune responses to *Salmonella* infection revealed that increased innate immune “cassette” opposes the adaptive immune arm leading to increased bacterial load [67]. Moreover, previous literature studies suggested that a low dose of Sirt1 activator such as resveratrol treatment in rats for 25 days treatment under 5%

DSS (Dextran sulfate sodium)-induced colitis condition led to alterations in gut microbiota profile with increased lactobacilli and bifidobacteria alongside a reduced abundance of enterobacteria [68,69]. This study correlates with our study wherein we have detected enhanced *Salmonella* (belonging to Enterobacteriaceae family) loads under both SIRT1/3 in vivo knockdown or inhibitor-treated condition in C57BL/6 mice alongside reduced burden under SIRT1 activator, SRT1720 treatment.

Future studies might explore the host and bacterial interacting partners of SIRT1 and SIRT3 through mass spectrometry analyses in *Salmonella* infected macrophages which might hint at the underlying mechanism of their action and regulation. Together, this study highlights the complex and multifaceted nature of host-pathogen interactions, and the need for further research to fully understand the role of SIRT1 and SIRT3 in the context of *Salmonella* infection.

MATERIALS AND METHODS

Bacterial Strains, and culture conditions

Salmonella enterica serovar Typhimurium (STM) strain ATCC 14028S or ATCC 14028S constitutively expressing green fluorescent protein (eGFP) or mCherry (RFP) through pFPV plasmid were used. 4% paraformaldehyde fixed STM (PFA) was used as the killed fixed bacteria control. The above-mentioned live bacterial strain was grown overnight in LB broth in 37 ^{0}C at 160 rpm shaking condition in presence or absence of appropriate antibiotic (Ampiciilin-50µg/ml) (Table-1) after revival of the bacterial strains from glycerol stock (stored at -80 ^{0}C).

Table:1: List of strains and plasmids used in this study

Strains/Plasmids	Characteristics	Source

Salmonella enterica serovar Typhimurium ATCC strain 14028S (STM)	Wild Type (WT)	Gifted by Prof. M. Hensel
pFPV:GFP	Amp^R	Laboratory Stock
pFPV:mCherry	Amp^R	Laboratory Stock
pLKO.2 : shRNA	Amp^R	Gifted by Prof. Subba Rao Gangi Setty
STM Δ *invC*	Kan^R	Laboratory Stock
STM Δ *ssaV*	Chl^R	Laboratory Stock
STM Δ *steE*	Kan^R	Laboratory Stock

Cell Culture

RAW 264.7 murine macrophages were cultured in DMEM (Lonza) containing 10% FBS (Gibco) at 37 ^{0}C in a humified incubator with 5% CO_2. Prior to each experiment, cells were seeded into 24 well or 6 well plate as per requirement at a confluency of 60%.

For macrophage polarization experiments, the seeded macrophages were subjected to 100ng/ml LPS + 20ng/ml IFN-γ treatment for M1 polarization and 20ng/ml IL-4 treatment for M2 polarization for 24 hrs. Post- polarization, the cell supernatant were collected for validation of polarization status by ELISA and was further subjected to infection protocol.

Peritoneal macrophages were collected in PBS from the peritoneal cavity of C57BL/6 mice aseptically post thioglycolate treatment using 20G needle and 5ml syringe. Following centrifugation, cell pellet was resuspended in RPMI-1640 (Lonza) containing 10% heat-inactivated FBS (Gibco), 100 U/ml penicillin and 100 μg/ml streptomycin and seeded into 6 well- plate. 6hr prior to infection, antibiotic-containing media was replaced with Penicillin-Streptomycin free RPMI-1640 (Lonza) containing 10% heat-inactivated FBS (Gibco).

Transfection

shRNA mediated knockdown was carried out by PEI mediated transfection protocol. Plasmid harbouring shRNA in pLKO.2 vector backbone specific to SIRT1 and SIRT3 were used for transfection. Plasmid harbouring scrambled sequence of shRNA, served as a control, was also used for transfection. Plasmid DNA was used at a concentration of 500ng and 1µg per well of a 24-well plate and 6-well plate respectively. Plasmid and PEI were added in 1:2 ratio in serum free DMEM media and incubated for 20 mins at room temperature. Post incubation, the DNA: PEI cocktail was added to the seeded RAW 264.7 macrophages. After 6-8hrs of incubation, serum-free media was replaced with complete media containing 10% FBS. Post 48hr of transfection, transfected cells were either harvested for knockdown confirmation studies or subjected to infection with STM.

Table 2: List of shRNA used for knockdown

Sirtuins	**Construct ID**	**TRC ID**	**Sequence (5'---3')**
SIRT1	C4	TRCN0000218734	GTACCGGCATGAAGTGCCTCAGATATTACTCGAGTAATATCTGAGGCACTTCATGTTTTTTG
SIRT1	C12	TRCN0000018979	CCGGGCAAAGCCTTTCTGAATCTATCTCGAGATAGATTCAGAAAGGCTTTGCTTTTT
SIRT3	E8	TRCN0000038889	CCGGCCCAACGTCACTCACTACTTTCTCGAGAAAGTAGTGAGTGACGTTGGGTTTTTG

SIRT3	E12	TRCN0000038893	CCGGCCACCTGCACAGTCTGCCAAACTCGAGTTTGGCAGACTGTGCAGGTGGTTTTTG

Infection Protocol

Macrophages were infected with stationary-phase bacterial culture with MOI of 10. For synchronization of the infection, tissue culture plates were subjected to centrifugation at 600xg for 5 min and incubated at 37 ^{0}C humified incubator with 5% CO_2 for 25 min. Cells were washed with PBS and were treated with DMEM (Sigma) + 10% FBS (Gibco) containing 100 µg/ml gentamicin for 1 hr. Subsequently, the gentamicin concentration was reduced to 25 µg/ml and maintained until the cells were harvested. For the inhibitor treatment studies, along with 25 µg/ml containing complete media 1µM of SIRT1 (EX-527) inhibitor or SIRT3 (3TYP) or 10mM of N-Acetyl Cysteine (NAC, Sigma) or 50nM of chetomin (Sigma) were added to the cells.

Immunofluorescence confocal microscopic studies

At the specified time points post infection with GFP tagged STM, cells were fixed with 3.5% paraformaldehyde for 15 min. Primary antibody staining was performed with specific primary antibody in the presence of a permeabilizing agent, 0.01% saponin (Sigma) dissolved in 2.5% BSA containing PBS at 4°C for overnight or for 6hr at room temperature (RT). Following this, cells were washed with PBS stained with appropriate secondary antibody tagged with fluorochrome for 1 hr at RT. This was followed by DAPI staining and mounting of the coverslip onto a clean glass slide using the mounting media containing the anti-fade agent. The coverslip sides were sealed with a transparent nail paint. All immunofluorescence images were obtained using Zeiss LSM 710 or Zeiss LSM 880 and were analyzed using ZEN black 2012 software.

Quantitative Real Time PCR

Total RNA was isolated at specific time points post infection by using TRIzol (Takara) as per manufacturer's protocol. Quantification of RNA was performed in Nano Drop (Thermo-Fischer scientific). Quality of isolated RNA was detected by performing 2% agarose gel electrophoresis. 2 µg of RNA was subjected to DNaseI (Thermo Fischer Scientific) treatment at 37°C for 1 hr followed by addition of 0.5M EDTA (final concentration 5mM) and heat inactivation at 65°C for 10 mins. The mRNA was reverse transcribed to cDNA using oligo $(dT)_{18}$ primer, buffer, dNTPs and reverse transcriptase (Takara) as per manufacturer's protocol. The expression profile of target gene was evaluated using specific primers (Table-3) by using SYBR green RT-PCR master mix (Takara) in BioRad Real time PCR instrument. β-actin was used as an internal control for mammalian genes and for bacterial genes 16S rRNA was used. All the reaction was setup in 384 well plate with two replicates for each sample.

Table 3: List of primers

Primer Name	**Sequence (5'---3')**
SIRT1 FP	ACAAAGTTGACTGTGAAGCTGTAC
SIRT1 RP	GTTCATCAGCTGGGCACCTA
SIRT3 FP	GCTGCTTCTGCGGCTCTATAC
SIRT3 RP	GAAGGACCTTCGACAGACCGT
PPARδ FP	CACAACGCTATCCGCTTTGG
PPARδ RP	ATGCTCCGGGCCTTCTTTTT
βactin FP	CAGCAAGCAGGAGTACGATG
βactin RP	GCAGCTCAGTAACAGTCCG
Acadl FP	CTTGGGAAGAGCAAGCGTACT
Acadl RP	CTGTTCTTTTGTGCCGTAATTCG

Hadha FP	AGCAACACGAATATCACAGGAAG
Hadha RP	AGGCACACCCACCATTTTGG
Acox1 FP	TCGAAGCCAGCGTTACGAG
Acox1 RP	ATCTCCGTCTGGGCGTAGG
Pdha1 FP	TGTCGGTTCCCAGTCCATCA
Pdha1 RP	CGTTTCCTTTTCACAGCACATGA
Pfkl FP	GAACTACGCACACTTGACCAT
Pfkl RP	CTCCAAAACAAAGGTCCTCTGG
ptsG FP	TATCTGGGCTTCTTTGCGGG
ptsG RP	ACCAGGCAACGCTCGATAAA
fadA FP	TCTGGGATTGATGGAGCAGA
fadA RP	AGACCAATACACATCGTCGC
fadB FP	GTCCCCGAAGAGCAGTTAAG
fadB RP	CCAGTTTAGTTTCCGGCAGA
aceA FP	CGATCTGGTATGGTGCGAAA
aceA RP	TTCTGCCAGTTGAAGGATGG
aceB FP	AGCGTTTCAATCAACAGGGT
aceB RP	CCCGTATTTTTACCTGCCGA
Salmonella 16S rRNA FP	GTGAGGTAACGGCTCACCAA
Salmonella 16S rRNA RP	TAACCGCAACACCTTCCTCC

Intracellular proliferation or gentamicin protection assay

Following infection of the transfected cells with STM at an MOI of 10, cells were treated with DMEM (Sigma) + 10% FBS (Gibco) containing 100 μg/ml gentamicin for 1 hr. Subsequently,

the gentamicin concentration was reduced to 25 µg/ml and maintained until the specified time point. Post 2hr and 16hr post-infection, cells were lysed in 0.1% triton-X-100. Lysed cells were serially diluted and plated on *Salmonella-Shigella* (SS) agar to obtain colony-forming units (cfu). Fold proliferation was calculated as cfu at 16hr divided by cfu at 2hr.

Fold Proliferation= [CFU at 16h]/[CFU at 2h]

Western Blotting

Post appropriate time points of infection, the cells were washed in PBS and subsequently harvested in PBS. The cell pellets were obtained after centrifugation at 300g for 7 minutes at 4ºC. Cells were lysed in 1X RIPA (10X-0.5M NaCl, 0.5M EDTA pH-8.0, 1M Tris, NP-40, 10% sodium deoxycholate, 10% SDS) buffer containing 10% protease inhibitor cocktail (Roche) for 30 min on ice. Total protein was estimated using Bradford (Bio-Rad) method of protein estimation. Protein samples were subjected to 12 % SDS polyacrylamide gel electrophoresis and then were transferred onto 0.45µm PVDF membrane (18V, 2 hrs). The membrane was blocked using 5% skim milk in TBST (Tris Buffered Saline containing 0.1% Tween-20) for 1hr at RT and subsequently probed with appropriate primary antibody (Table-4) for overnight at 4°C. Following wash in TBST, blot was probed with specific HRP conjugated secondary antibody for 1hr at RT. The membrane was developed using ECL (Advansta) and images were captured using ChemiDoc GE healthcare. All densitometric analysis was performed using ImageJ software.

Table 4: List of Antibodies

Antibody Name	**Catalogue Number**
SIRT1 Polyclonal Antibody	Cat #PA5-85921 (ThermoFisher Scientific)

SIRT3 Polyclonal Antibody	**Cat#** PA5-13222(ThermoFisher Scientific)
CD 86	**Cat#**12-086282PE(ThermoFisherScientific)
CD 206	**Catalog#** 17-2069-42 (ThermoFisherScientific)
F4/80 Antibody	BD Horizon, Cat-565411
HIF-1α	**sc-13515 SCBT**
NF-κβ p65	CST(D14E12)XP® RabbitmAb #8242
Acetylated-Lysine Antibody	**Cat #9441(Cell Signaling Technology)**
PDHA1	**Catalog No. A13687 (ABclonal)**
HADHA	**Catalog No. A5346 (ABclonal)**
ACOX1	**Catalog No. A8091 (ABclonal)**
PGK	**Catalog No. A12686 (ABclonal)**
PFK	**Catalog No. A5477 (ABclonal)**
β actin	A3854 (Sigma)

Immunoprecipitation

For co-immunoprecipitation, cells were washed with PBS and were lysed in native lysis buffer containing 1% Nonidet P-40, 20 mM Tris (pH 8), 2 mM EDTA, 150 mM NaCl and protease

inhibitors mixture (Roche Diagnostics) for 30 min at 4°C. Cell debris was removed by centrifugation at 10,000 rpm for 10 min and the supernatant was treated with the specific antibody against the protein to be precipitated. Antibody-lysate complexes were immunoprecipitated using Protein A/G- linked magnetic beads (MagGenome) according to the manufacturer's protocol. Beads were extensively washed with washing buffer and denatured at 95 ^{o}C for 10 min. Denatured precipitates were subjected to SDS-PAGE (12% gel) followed by transfer to 0.45 μ PVDF membrane. The membrane was blocked using 5% skimmed milk in TBST (Tris Buffered Saline containing 0.1% Tween-20) for 1h at room temperature and eventually probed for the target primary antibodies or Anti-acetylated Lysine (Ac-K) primary antibody overnight at 4°C. The blot was probed with a specific HRP-conjugated secondary antibody for 1hr at RT after rigorous washing in TTBS. ECL (BioRad) was used for detection and images were captured using ChemiDoc GE healthcare.

ELISA

Estimation of cytokines in cell-free supernatant or in mice serum was performed according to the manufacturer's instructions. Briefly, 96-well ELISA plates (BD Bioscience) were coated overnight with capture antibody at 4°C. Following day, plates were washed with 0.1% Tween-20 containing PBS and blocked with 10% FBS for 1 h. Following blocking, wells were washed and incubated with 100 μL of test samples for 2 h at room temperature. Subsequently, plates were washed and incubated with detection antibody and enzyme reagent for 1 h at room temperature (BD Bioscience). TMB (Sigma) was used as a substrate and reactions were stopped with 2 N H_2SO_4. For the estimation of IL-1β, pre-coated ELISA (SARD Biosciences) plates were used, and ELISA was performed as per manufacturer's protocol. Absorbance was measured at 450 nm wavelength in Tecan Plate reader and the concentration of cytokines were interpolated from a standard curve.

Flow cytometry

After specific time points post infection, cells were washed and harvested in PBS. Following centrifugation, cell pellet was resuspended in FACS buffer comprised of 1% BSA in PBS. Blocking was performed with Fc blocker (purified Anti-mouse CD16/CD32, eBioscience) dissolved in FACS blocking buffer for 30 min on ice. Following a washing step with PBS, antibody staining was performed with PE-conjugated CD86 antibody or APC-conjugated CD206 (Thermo Scientific) for 45 min on ice. After washing in PBS, the cell pellet was resuspended in 1% PFA in PBS. Subsequently, PFA was removed, and cells were resuspended in FACS buffer and reading was taken in BD FACSVerse instrument. For flow cytometry studies in mice tissues , the harvested liver or spleen was homogenized into single-cell suspension post RBC lysis (RBC lysis Buffer, Sigma). The homogenized cell suspension was washed and resuspended in FACS buffer containing the PE-conjugated Rat anti-mouse F4/80 antibody (BD Horizon, Cat-565411) or eFluor450-conjugated anti-mouse CD11c antibody (eBioscience), or FITC-conjugated anti-mouse Ly6C antibody (BD Pharmingen) or Alexa647-conjugated anti-mouse CD45 antibody (BioLegend). Following staining protocol, the cells were washed in PBS and the cells were resuspended in FACS buffer and the FACS protocol was performed either in BD FACSVerse or CytoFLEX flow cytometer (Beckman).

For DCFDA staining, one hour before the indicated time point of infection, cells were incubated with 10µM DCFDA containing DMEM media at 37°C humidified incubator with 5% $CO_2$for 45 min. Post incubation, cells were washed and harvested in PBS. Readings were measured in BD FACSVerse instrument.

All analysis was done using BD FACSuite software.

Phenol Red-Hydrogen Peroxidase Assay

Post 48hr of transfection, cells were infected with STM culture at an MOI of 10. Cells were incubated with Phenol Red solution containing hydrogen peroxidase enzyme (8.5U/ml). At, the designated time points post-infection, the supernatant was collected, and the absorbance was taken at 610 nm in Tecan Plate reader. The exogenously produced H2O2 was quantified using a standard curve of known concentration of H_2O_2.

Gene expression studies by nanoString nCounter technology

Total RNA was isolated at specific time points post infection by using TRIzol (Takara) as per manufacturer's protocol. Quantification of RNA was performed in Nano Drop (Thermo-Fischer scientific) and Qubit Bioanalyzer (Agilent 2100 Bioanalyzer). Quality of isolated RNA was detected by performing 2% agarose gel electrophoresis. Post quality check, samples were subjected to nanoString nCounter technology (theraCUES). This technology allows multi-plex, spatially resolved RNA expression quantification with appropriate probes designed against the target gene.

Lactate Estimation Assay

Cell-supernatant was harvested at the specific time-points post-infection and the lactate content of the sample was estimated using the Lactate Assay Kit (Sigma, Catalog Number-MAK064) as per manufacturer's protocol. Briefly, 50µl of the sample was added to each 96 well-plate and each of the well 50µl of the master reaction mix containing 46µl of lactate assay buffer, 2µl of lactate enzyme mix, and 2µl of lactate probe was added. After the addition of the master reaction mix to the sample, they were mixed by horizontal shaker or via pipetting. The plate was incubated for 30 minutes in dark at room temperature. Post incubation, absorbance was measured at 570nm. The lactate content of the sample was estimated from the lactate standard curve ranging from 0-10 nmole/µl.

Fatty Acid Oxidation Assay

At 16h post-infection, cell pellets were harvested and stored at-80ºC. The fatty acid oxidation assay protocol was followed as per manufacturer's instructions (AssayGenie Fatty Acid Oxidation (FAO) Assay Kit, Catalogue Code-BR00001). Briefly, cell pellets were lysed using 1X Cell lysis buffer (provided in the kit) and the cell supernatant were obtained post centrifugation of the cell lysate in a cold microfuge at 14,000rpm for 5min. The protein content of the cell supernatants was estimated using Bradford (Bio-Rad) method. 20µl of the protein sample was added to each 96-well plate in duplicate on ice. Each sample was treated with 50µl of control solution and 50µl of reaction solution by swiftly adding one 50µl of control solution to one set of wells and 50µl of reaction solution to the other set of wells. The contents were gently mixed for 10s. The plate is covered and incubated in a 37ºC incubator for 30-60 min (without CO_2). After incubation cherry red colour appears in the wells. The O.D. is measured at 492nm using a plate reader at 30 min,60 min or 120 min. The control well reading was subtracted from the reaction well reading for each sample for each time point. The subtracted reading is used for enzyme activity calculation by considering the incubation time.

Animal Experiment

For all experiments, 6–8 weeks old C57BL/6 or *gp91phox*-/- mice were used. For organ burden analysis, 6 weeks old C57BL/6 or *gp91phox*-/- mice were infected with 10^7 CFU bacteria via oral gavaging. For bacterial enumeration via flow cytometry, mice were infected with 10^7 GFP-expressing bacteria orally. Infected mice were intraperitoneally injected on every other day with either 1 mg/kg body weight of SIRT1 inhibitor EX-527 (Sigma-Aldrich) [32], or SIRT3 inhibitor 3TYP (Selleck Chemical) [33] or SIRT1 activator SRT1720 (Calbiochem, Sigma-Aldrich) [34] or treated with vehicle alone. 5 days post infection, mice were sacrificed, and bacterial organ load was estimated by plating the tissue homogenates on SS agar plates. For calculating percentage survival, 6 weeks old C57BL/6 mice were infected with 10^8 bacteria orally and monitored till fatality. For flow cytometry studies, the harvested liver or spleen were

homogenized into single cell suspension and were subjected to flow cytometry. The animal experiments were carried out in accordance with the approved guidelines of the institutional animal ethics committee at the Indian Institute of Science, Bangalore, India (Registration No: 48/1999/CPCSEA). All procedures involving the use of animals were performed according to the Institutional Animal Ethics Committee (IAEC)-approved protocol.

In vivo knockdown

For in vivo knockdown adeno-associated virus serotype 6 (AAV6) was used. AAV6 viruses were produced in HEK293T cells. Briefly, HEK293T cells were transfected with AAV plasmid encoding shRNAs targeting SIRT1, SIRT3 and scramble control under U6 promoter together with helper plasmid using PEI Max 40000 (Polysciences USA). Next day transfection medium was removed, and fresh culture medium was added. Forty-eight hours later, medium was collected, and fresh culture medium was added and incubated for next forty-eight hours. Again, culture medium was collected and cells were harvested by trypsinization. Collected medium containing secreted AAV viral particles was incubated with 40% PEG 8000 overnight. Precipitated viral particles were then collected by centrifugation and re-suspended in PBS. Cells containing AAV viral particles were then lysed with citrate buffer and incubated with 40% PEG 8000 and processed similarly to medium for viral particle precipitation. Precipitated viral particles were then cleaned with chloroform and loaded on iodixanol gradient for further cleaning using ultracentrifugation. Cleaned viral particles were collected from the forty percent gradient and loaded on Amicon 100K cut-off columns. Purified AAV particles were then titrated by real-time PCR. For infection of AAV6, the mice were intravenously injected with a volume of 200 µl containing approximately 10^{12} viral particles harbouring the respective scrambled or shRNA constructs. The mice were infected at 7th day after injection of the virus with 10^6 cfu units of *S*. Typhimurium orally. Fifth day post-infection, mice were euthanized,

and dissected out for organ harvesting and blood collection. The knockdown was validated by performing western blotting and qPCR of the harvested liver tissue (Fig. S10).

Haematoxylin and Eosin Staining

6-8 weeks old C57BL/6 mice were infected with 10^7 bacteria orally. Infected mice were intraperitoneally injected every alternate with either 1 mg/kg body weight of SIRT1 inhibitor EX-527, or SIRT3 inhibitor 3TYP or SIRT1 activator SRT1720 or treated with vehicle alone. 5 days post infection, mice were euthanized, and livers were collected and fixed using 3.5% paraformaldehyde. The fixed liver was then dehydrated using a gradually increasing concentration of ethanol and embedded in paraffin. 5μm sections were collected on coated plates. Sections were further rehydrated and then stained with hematoxylin and eosin. Images were collected in a Leica microscope. **Scoring system:-** according to pathological changes the tissue sections are scored as 0 for normal pathology, 1 for mild/ minor pathology, 2 for moderate pathology, and 3 for severe pathological changes.

Statistical analysis

Data were analyzed and graphed using the GraphPad Prism 8 software (San Diego, CA). Statistical significance was determined by Student's t-test or Two-way ANOVA and Bonferroni post-t-test to obtain p values. Adjusted p-values below 0.05 are considered statistically significant. The results are expressed as mean ± SD or SEM of three independent experiments.

ACKNOWLEDGEMENT

We duly thank Prof. Subba Rao Gangi Setty and Prof. Michael Hensel for providing us with the shRNA knockdown constructs and the *S*. Typhimurium 14028S strain, respectively.

FUNDING

This work was supported by the DAE SRC fellowship (DAE00195) and DBT-IISc partnership umbrella program for advanced research in biological sciences and Bioengineering to DC. Infrastructure support from ICMR (Centre for Advanced Study in Molecular Medicine), DST (FIST), and UGC (special assistance) is highly acknowledged. DH sincerely acknowledges the CSIR- SPM fellowship for her financial support. SKG is supported by Ramalingaswami Re-entry Fellowship BT/RLF/re-entry/14/2019 from DBT, Government of India. The funders had no role in study design, data collection and analysis, decision to publish, or preparation of the manuscript.

AUTHOR CONTRIBUTION

DH and DC have conceptualized the study. DH has contributed to the experiment designing, visualization, methodology, investigation, formal analysis, literature survey, validation, writing (original draft), reviewing, and editing of the manuscript. RSR has performed the histopathological scoring of the liver sections and the retro-orbital injection of the adenoviral constructs in mice. ADC and SKG have prepared and provided AAV6, for *in vivo* mice knockdown experiments. DC has contributed to the funding acquisition, project administration, and overall supervision of the work. All authors approved the final version of the manuscript.

DECLARATION OF INTEREST

The authors are unaware of any conflicting interests and thereby declare no conflict of interest.

REFERNCES

1. Landry J, Sutton A, Tafrov ST, Heller RC, Stebbins J, Pillus L, et al. The silencing protein SIR2 and its homologs are NAD-dependent protein deacetylases. Proc Natl Acad Sci U S A. 2000;97(11):5807–11.

2. Jackson MD, Denu JM. Structural identification of 2'- and 3'-O-acetyl-ADP-ribose as novel metabolites derived from the Sir2 family of beta -NAD+-dependent histone/protein deacetylases. J Biol Chem. 2002;277(21):18535-18544. doi:10.1074/jbc.M200671200

3. Sauve AA, Celic I, Avalos J, Deng H, Boeke JD, Schramm VL. Chemistry of gene silencing: The mechanism of NAD+-dependent deacetylation reactions. Biochemistry. 2001;40(51):15456–63.

828 4. Bitterman KJ, Anderson RM, Cohen HY, Latorre-Esteves M, Sinclair DA. Inhibition of silencing and
829 accelerated aging by nicotinamide, a putative negative regulator of yeast Sir2 and human SIRT1. J
830 Biol Chem. 2002;277(47):45099–107.

831 5. Sanders BD, Jackson B, Marmorstein R. Structural basis for sirtuin function: What we know and
832 what we don't. Biochim Biophys Acta - Proteins Proteomics 2010;1804(8):1604–16. Available from:
833 http://dx.doi.org/10.1016/j.bbapap.2009.09.009 10. Lin Z, Fang D. The Roles of SIRT1 in Cancer.
834 Genes and Cancer. 2013;4(3–4):97– 104.

835 6. Lin Z, Fang D. The Roles of SIRT1 in Cancer. Genes and Cancer. 2013;4(3–4):97–104.

836 7. Guarente L. Sirtuins in aging and disease. Cold Spring Harb Symp Quant Biol. 2007;72:483–8.

837 8. Martínez-Redondo P, Vaquero A. The Diversity of Histone Versus Nonhistone Sirtuin Substrates.
838 Genes and Cancer. 2013;4(3–4):148–63.

839 9. Liu TF, Yoza BK, El Gazzar M, Vachharajani VT, McCall CE. NAD+-dependent SIRT1 deacetylase
840 participates in epigenetic reprogramming during endotoxin tolerance. J Biol Chem.
841 2011;286(11):9856–64.

842 10. El Gazzar M, Yoza BK, Hu JYQ, Cousart SL, McCall CE. Epigenetic silencing of tumor necrosis factor
843 α during endotoxin tolerance. J Biol Chem. 2007;282(37):26857–64.

844 11. Liu TF, Vachharajani V, Millet P, Bharadwaj MS, Molina AJ, McCall CE. Sequential actions of
845 SIRT1-RELB-SIRT3 coordinate nuclear-mitochondrial communication during immunometabolic
846 adaptation to acute inflammation and sepsis. J Biol Chem. 2015;290(1):396–408.

847 12. Kong X, Wang R, Xue Y, et al. Sirtuin 3, a new target of PGC-1alpha, plays an important role in the
848 suppression of ROS and mitochondrial biogenesis. PLoS One. 2010;5(7):e11707.

849 13. van de Ven RAH, Santos D, Haigis MC. Mitochondrial Sirtuins and Molecular Mechanisms of
850 Aging. Trends Mol Med. 2017;23(4):320–31.

851 14. Garai, P., D.P. Gnanadhas, and D. Chakravortty, Salmonella enterica serovars Typhimurium and
852 Typhi as model organisms: revealing paradigm of host-pathogen interactions. Virulence, 2012. **3**(4): p.
853 377-88

854 15.Bhutta ZA, Threlfall J. Addressing the global disease burden of typhoid
855 fever. *JAMA*.2009;302(8):898-899. doi:10.1001/jama.2009.1259

856 16. Majowicz SE, Musto J, Scallan E, et al. The global burden of nontyphoidal Salmonella
857 gastroenteritis. Clin Infect Dis. 2010;50(6):882-889. doi:10.1086/650733

858 17. Haraga, A., M.B. Ohlson, and S.I. Miller, Salmonellae interplay with host cells. Nat Rev Microbiol,
859 2008. **6**(1): p. 53-66.

860 18. Hajra, D., A.V. Nair, and D. Chakravortty, An elegant nano-injection machinery for sabotaging the
861 host: Role of Type III secretion system in virulence of different human and animal pathogenic
862 bacteria. Phys Life Rev, 2021. **38**: p. 25-54.

863 19. Lawrence T, Natoli G. Transcriptional regulation of macrophage polarization: Enabling diversity
864 with identity. Nat Rev Immunol. 2011;11(11):750–61.

865 20. Martinez FO, Helming L, Gordon S. Alternative Activation of Macrophages: An Immunologic
866 Functional Perspective. Annu Rev Immunol. 2009;27(1):451–83.

867 21. Namgaladze D, Brüne B. Fatty acid oxidation is dispensable for human macrophage IL-4-induced
868 polarization. Biochim Biophys Acta - Mol Cell Biol Lipids 2014;1841(9):1329–35.

869 22. Hui X, Zhang M, Gu P, Li K, Gao Y, Wu D. Adipocyte SIRT 1 controls systemic insulin sensitivity by
870 modulating macrophages in adipose tissue. 2017;18(4):645–57.

871 23. Jia Y, Han S, Li J, et al. IRF8 is the target of SIRT1 for the inflammation response in macrophages.
872 Innate Immun. 2017;23(2):188-195. doi:10.1177/1753425916683751

873 24. Kratz M, Coats BR, Hisert KB, Hagman D, Mutskov V, Peris E, et al. Metabolic dysfunction drives a
874 mechanistically distinct proinflammatory phenotype in adipose tissue macrophages. Cell Metab
875 2014;20(4):614–25. Available from: http://dx.doi.org/10.1016/j.cmet.2014.08.010

876 25. Cimen H, Han MJ, Yang Y, Tong Q, Koc H, Koc EC. Regulation of succinate dehydrogenase activity
877 by SIRT3 in mammalian mitochondria. Biochemistry. 2010;49(2):304–11.

878 26. Vazquez-Torres A, Xu Y, Jones-Carson J, Holden DW, Lucia SM, Dinauer MC, et al. Salmonella
879 pathogenicity island 2-dependent evasion of the phagocyte NADPH oxidase. Science (80-).
880 2000;287(5458):1655–8.

881 27. Miller BH, Fratti RA, Poschet JF, Timmins GS, Master SS, Burgos M, et al. Mycobacteria Inhibit
882 Nitric Oxide Synthase Recruitment to Phagosomes during Macrophage Infection. Infect Immun.
883 2004;72(5):2872–8.

884 28. Bost KL, Clements JD. Intracellular Salmonella dublin induces substantial secretion of the 40-
885 kilodalton subunit of interleukin-12 (IL-12) but minimal secretion of IL-12 as a 70-kilodalton protein
886 in murine macrophages. Infect Immun. 1997;65(8):3186–92.

887 29. Pathak SK, Basu S, Basu KK, Banerjee A, Pathak S, Bhattacharyya A, et al. Direct extracellular
888 interaction between the early secreted antigen ESAT-6 of Mycobacterium tuberculosis and TLR2
889 inhibits TLR signaling in macrophages. Nat Immunol. 2007;8(6):610–8.

890 30. Tumitan ARP, Monnazzi LGS, Ghiraldi FR, Cilli EM, De Medeiros BMM. Pattern of macrophage
891 activation in yersinia-resistant and yersinia-susceptible strains of mice. Microbiol Immunol.
892 2007;51(10):1021–8.

893 31. Brubaker RR. Interleukin-10 and inhibition of innate immunity to Yersiniae: Roles of Yops and
894 LcrV (V antigen). Infect Immun. 2003;71(7):3673–81.

895 32. Morató L, Astori S, Zalachoras I, et al. eNAMPT actions through nucleus accumbens NAD^+/SIRT1
896 link increased adiposity with sociability deficits programmed by peripuberty stress. Sci Adv.
897 2022;8(9):eabj9109. doi:10.1126/sciadv.abj9109.

898 33. Hu B, Wang P, Zhang S, et al. HSP70 attenuates compression-induced apoptosis of nucleus
899 pulposus cells by suppressing mitochondrial fission via upregulating the expression of SIRT3. Exp Mol
900 Med. 2022;54(3):309-323. doi:10.1038/s12276-022-00745-9.

901 34. Tan P, Wang M, Zhong A, et al. SRT1720 inhibits the growth of bladder cancer in organoids and
902 murine models through the SIRT1-HIF axis. *Oncogene*. 2021;40(42):6081-6092. doi:10.1038/s41388-
903 021-01999-9.

904 35. Elesela S, Morris SB, Narayanan S, Kumar S, Lombard DB, Lukacs NW. Sirtuin 1 regulates
905 mitochondrial function and immune homeostasis in respiratory syncytial virus infected dendritic
906 cells. PLoS Pathog. 2020;16(2):e1008319.

907 36. Liu G, Bi Y, Xue L, et al. Dendritic cell SIRT1-HIF1α axis programs the differentiation of CD4+ T
908 cells through IL-12 and TGF-β1. Proc Natl Acad Sci U S A. 2015;112(9):E957-E965.
909 doi:10.1073/pnas.1420419112.

910 37. Yang H, Hu J, Chen Y (Jason), Ge B. Role of Sirt1 in innate immune mechanisms against
911 Mycobacterium tuberculosis via the inhibition of TAK1 activation. Arch Biochem Biophys
912 2019;667(October 2018):49–58. Available from: https://doi.org/10.1016/j.abb.2019.04.006

913 38. Kim TS, Jin YB, Kim YS, Kim S, Kim JK, Lee HM, et al. SIRT3 promotes antimycobacterial defenses
914 by coordinating mitochondrial and autophagic functions Vol. 15, Autophagy. Taylor & Francis; 2019.
915 1356–1375 p. Available from: https://doi.org/10.1080/15548627.2019.1582743.

916 39. Yeung F, Hoberg JE, Ramsey CS, et al. Modulation of NF-kappaB-dependent transcription and cell
917 survival by the SIRT1 deacetylase. EMBO J. 2004;23(12):2369-2380. doi:10.1038/sj.emboj.7600244.

918 40. Yang H, Zhang W, Pan H, et al. SIRT1 activators suppress inflammatory responses through
919 promotion of p65 deacetylation and inhibition of NF-κB activity. PLoS One. 2012;7(9):e46364.
920 doi:10.1371/journal.pone.0046364.

921 41. Singh CK, Chhabra G, Ndiaye MA, Garcia-peterson LM, Mack NJ, Ahmad N. The Role of Sirtuins in
922 Antioxidant and Redox Signaling. 2018;28(8):643–61.

923 42. Kitada M, Ogura Y, Monno I, Koya D. Sirtuins and Type 2 Diabetes: Role in Inflammation,
924 Oxidative Stress, and Mitochondrial Function. Front Endocrinol (Lausanne). 2019;10:187.

925 43. Merksamer PI, Liu Y, He W, Hirschey MD, Chen D, Verdin E. The sirtuins, oxidative stress and
926 aging: an emerging link. Aging (Albany NY). 2013;5(3):144-150. doi:10.18632/aging.100544.

927 44. Rendra E, Riabov V, Mossel DM, Sevastyanova T, Harmsen MC, Kzhyshkowska J. Immunobiology
928 Reactive oxygen species (ROS) in macrophage activation and function in diabetes. Immunobiology
929 2019;224(2):242–53. Available from: https://doi.org/10.1016/j.imbio.2018.11.010

930 45. Zhou Y, Que KT, Zhang Z, et al. Iron overloaded polarizes macrophage to proinflammation
931 phenotype through ROS/acetyl-p53 pathway. Cancer Med. 2018;7(8):4012-4022.
932 doi:10.1002/cam4.1670.

933 46. Halasi M, Wang M, Chavan TS, Gaponenko V, Hay N, Gartel AL. ROS inhibitor Nacetyl-L-cysteine
934 antagonizes the activity of proteasome inhibitors. Biochem J. 2013;454(2):201–8.

935 47.De Santa F, Vitiello L, Torcinaro A, Ferraro E. The Role of Metabolic Remodeling in Macrophage
936 Polarization and Its Effect on Skeletal Muscle Regeneration. Antioxid Redox Signal.
937 2019;30(12):1553-1598. doi:10.1089/ars.2017.7420.

938 48. Galván-Peña S, O'Neill LAJ. Metabolic reprogramming in macrophage polarization. Front
939 Immunol. 2014;5(AUG):1–6.

940 49. Taylor SJ, Winter SE. Salmonella finds a way: Metabolic versatility of Salmonella enterica serovar
941 Typhimurium in diverse host environments. PLoS Pathog 2020;16(6):10–5. Available from:
942 http://dx.doi.org/10.1371/journal.ppat.1008540

943 50. Kierans SJ, Taylor CT. Regulation of glycolysis by the hypoxia-inducible factor (HIF): implications
944 for cellular physiology. J Physiol. 2021;599(1):23-37. doi:10.1113/JP280572.

945 51. Lim JH, Lee YM, Chun YS, Chen J, Kim JE, Park JW. Sirtuin 1 modulates cellular responses to
946 hypoxia by deacetylating hypoxia-inducible factor 1alpha. Mol Cell. 2010;38(6):864-878.
947 doi:10.1016/j.molcel.2010.05.023.

948 52. Wang Y, Bi Y, Chen X, et al. Histone Deacetylase SIRT1 Negatively Regulates the Differentiation of
949 Interleukin-9-Producing CD4(+) T Cells. Immunity. 2016;44(6):1337-1349.
950 doi:10.1016/j.immuni.2016.05.009

951 53. Viziteu E, Grandmougin C, Goldschmidt H, et al. Chetomin, targeting HIF-1α/p300 complex,
952 exhibits antitumour activity in multiple myeloma. Br J Cancer. 2016;114(5):519-523.
953 doi:10.1038/bjc.2016.20

954 54. Hirschey MD, Shimazu T, Goetzman E, et al. SIRT3 regulates mitochondrial fatty-acid oxidation by
955 reversible enzyme deacetylation. Nature. 2010;464(7285):121-125. doi:10.1038/nature08778

956 55. Zhang Y, Wen P, Luo J, et al. Sirtuin 3 regulates mitochondrial protein acetylation and
957 metabolism in tubular epithelial cells during renal fibrosis. Cell Death Dis. 2021;12(9):847.

958 56. Panagi I, Jennings E, Zeng J, Günster RA, Stones CD, Mak H, et al. Salmonella Effector SteE
959 Converts the Mammalian Serine/Threonine Kinase GSK3 into a Tyrosine Kinase to Direct
960 Macrophage Polarization. Cell Host Microbe. 2020;27(1):41-53.e6.

961 57. Stapels DAC, Hill PWS, Westermann AJ, Fisher RA, Thurston TL, Saliba AE, et al. Salmonella
962 persisters undermine host immune defenses during antibiotic treatment. Science.
963 2018;362(6419):1156–60.

964 58. Pham THM, Brewer SM, Thurston T, Massis LM, Honeycutt J, Lugo K, et al. Salmonella-Driven
965 Polarization of Granuloma Macrophages Antagonizes TNFMediated Pathogen Restriction during
966 Persistent Infection. Cell Host Microbe. 2020;27(1):54-67.e5. Available from:
967 https://doi.org/10.1016/j.chom.2019.11.011

968 59. Ganesan R, Hos NJ, Gutierrez S, Fischer J, Stepek JM, Daglidu E, et al. Salmonella Typhimurium
969 disrupts Sirt1/AMPK checkpoint control of mTOR to impair autophagy. PLoS Pathog. 2017;13(2):1–
970 22.

971 60. Gogoi M, Chandra K, Sarikhani M, Ramani R, Sundaresan NR, Chakravortty D. Salmonella escapes
972 adaptive immune response via SIRT2 mediated modulation of innate immune response in dendritic
973 cells. PLoS Pathog. 2018;14(11):1–22.

974 61. Smulan LJ, Martinez N, Kiritsy MC, Kativhu C, Cavallo K, Sassetti CM, et al. Sirtuin 3
975 downregulation in mycobacterium tuberculosis-infected macrophages reprograms mitochondrial
976 metabolism and promotes cell death. MBio. 2021;12(1):1–15.

977 62. Eisele NA, Ruby T, Jacobson A, Manzanillo PS, Cox JS, Lam L, et al. Salmonella require the fatty
978 acid regulator PPARδ for the establishment of a metabolic environment essential for long-term
979 persistence. Cell Host Microbe 2013;14(2):171– 82. Available from:
980 http://dx.doi.org/10.1016/j.chom.2013.07.010

981 63. Cramer T, Yamanishi Y, Clausen BE, et al. HIF-1alpha is essential for myeloid cell mediated
982 inflammation. Cell. 2003;112(5):645-657. doi:10.1016/s0092-8674(03)00154-5.

64. Merrill GF, Kurth EJ, Hardie DG, Winder WW. AICA riboside increases AMP activated protein kinase, fatty acid oxidation, and glucose uptake in rat muscle. Am J Physiol. 1997;273(6):E1107-E1112. doi:10.1152/ajpendo.1997.273.6.E1107.

65. Reens AL, Nagy TA, Detweiler CS. Salmonella enterica Requires Lipid Metabolism Genes To Replicate in Proinflammatory Macrophages and Mice. Infect Immun. 2019;88(1):e00776-19

66. Holden VI, Breen P, Houle S, Dozois CM, Bachman MA. Klebsiella pneumoniae Siderophores Induce Inflammation, Bacterial Dissemination, and HIF-1α Stabilization during Pneumonia. mBio. 2016;7(5):e01397-16. Published 2016 Sep 13. doi:10.1128/mBio.01397-16

67. Hotson AN, Gopinath S, Nicolau M, et al. Coordinate actions of innate immune responses oppose those of the adaptive immune system during Salmonella infection of mice. Sci Signal. 2016;9(410):ra4. Published 2016 Jan 12. doi:10.1126/scisignal.aaa9303

68. Lakhan SE, Kirchgessner A. Gut microbiota and sirtuins in obesity-related inflammation and bowel dysfunction. J Transl Med. 2011;9:202. Published 2011 Nov 24. doi:10.1186/1479-5876-9-202

69. Larrosa M, Yañéz-Gascón MJ, Selma MV, et al. Effect of a low dose of dietary resveratrol on colon microbiota, inflammation and tissue damage in a DSS-induced colitis rat model. J Agric Food Chem. 2009;57(6):2211-2220. doi:10.1021/jf803638d

MAIN FIGURE LEGENDS

Fig.1- *Salmonella* modulates the expression of SIRT1 and SIRT3 along its course of infection

A-B. Expression studies of *SIRT1* and *SIRT3* through qPCR in RAW 264.7 macrophages. Data is representative of N=4, n=2. Unpaired two tailed Student's t test was performed to obtain the p values. (****p<0.0001,***p < 0.001, ** p<0.01, *p<0.05)

C-D-Expression studies of *SIRT1* and *SIRT3* through qPCR in peritoneal macrophages derived from C57BL/6. Data is representative of N=3, n=2. . Unpaired two tailed Student's t test was performed to obtain the p values. (****p<0.0001,***p < 0.001, ** p<0.01, *p<0.05)

E. Representative confocal images of RAW264.7 macrophages exhibiting SIRT1 expression upon *S.* Typhimurium infection at indicated time points post infection. Data is representative of N=3, n=80 (microscopic field).

F. Quantitative representation of the expression profile as depicted in the confocal images (E) in terms of Mean Fluorescence Intensity (MFI). Unpaired two tailed Student's t test was performed to obtain the p values. (****p<0.0001,***p < 0.001, ** p<0.01)

G. Representative confocal images of RAW264.7 macrophages exhibiting SIRT3 expression upon *S.* Typhimurium infection at indicated time points post infection. Data is representative of N=3, n=80 (microscopic field).

H. Quantitative representation of the expression profile as depicted in the confocal images (G) in terms of Mean Fluorescence Intensity (MFI). Unpaired two tailed Student's t test was performed to obtain the p values. (****p<0.0001, *** p < 0.001, ** p<0.01)

I. qPCR mediated expression of *SIRT1* in RAW264.7 macrophages upon infection with wildtype *S*. Typhimurium or SPI-1 (Δ*invC*)or SPI-2 (Δ*ssaV* and Δ*steE*) *m*utants of *S*. Typhimurium. Data is representative of N=3,n=3. Unpaired two tailed Student's t test was performed to obtain the p values. (****p<0.0001,***p < 0.001, ** p<0.01)

J. qPCR mediated expression of *SIRT3* in RAW264.7 macrophages upon infection with wildtype *S*. Typhimurium or SPI-1 (Δ*invC*) or SPI-2 (Δ*ssaV* and Δ*steE*) *m*utants of *S*. Typhimurium. Data is representative of N=3, n=3. Unpaired two tailed Student's t test was performed to obtain the p values. (****p<0.0001,***p < 0.001, ** p<0.01)

Fig.2- Effect of SIRT1 and SIRT3 knockdown in intracellular bacterial proliferation within RAW 264.7 and primary murine macrophages.

A. Fold Proliferation of *Salmonella* Typhimurium within RAW 264.7 macrophages in transfected and un-transfected conditions. Data is representative of N=3, n=3. Unpaired two tailed Student's t test was performed to obtain the p values. (** p<0.01, * p<0.05)

B. Fold Proliferation of *Salmonella* Typhimurium within infected peritoneal macrophages isolated from adult male C57BL/6 mice upon SIRT1 (EX-527) or SIRT3 (3TYP) inhibitor treatment. Unpaired two tailed Student's t test was performed to obtain the p values. (** $p<0.01$, * $p<0.05$)

Fig.3- *Salmonella* Typhimurium skews the polarization state of the macrophage toward an immunosuppressive M2 state along the course of infection

A. nanoString gene expression profiling data of *S*. Typhimurium infected RAW 264.7 macrophages versus uninfected control data sets at 2hr, 6hr and 16hr time points of infection. Data is representative of N=2,n=2.

B. Quantitative representation of flow cytometric analysis of alteration in M1 CD86 positive population in *S*. Typhimurium (STM) infected samples in comparison to uninfected (UI) and Paraformaldehyde Fixed (PFA) bacteria at the indicated time post-infection. Data is representative of N=2, n=3. Two-way ANOVA and Bonferroni post-t-test was used to obtain p values. (*** $p < 0.001$)

C. Quantitative representation of flow cytometric analysis of M2 surface marker CD206 in *S*. Typhimurium (STM) infected SIRT1 or SIRT3 knockdown RAW264.7 macrophages in comparison to the scrambled control at the indicated time post-infection. UI-Uninfected sample. Data is representative of N=3, n=3. Two-way ANOVA and Bonferroni post-t-test was used to obtain p values. (*** $p < 0.001$)

Fig.4- SIRT1 mediates modulation of immune functions via deacetylation of p65 subunit of NF-κB in *S*.Typhimurium infected macrophages.

A. Immunoblot depicting p65 NF-κB interaction with SIRT1 post immunoprecipitation of SIRT1 in uninfected (UI) or *S*. Typhimurium (STM) infected RAW264.7 macrophages at 16hr post-infection. Data is representative of N=3, n=1

B. An immunoblot depicting p65 NF-κB interaction with SIRT1 as well as the p65 NF-κB acetylation status post immunoprecipitation of p65 (IP: p65) or with control IgG (IP: IgG) in uninfected (UI) or *S.* Typhimurium (STM) infected RAW264.7 macrophages upon knockdown with SIRT1 shRNA or scrambled control.

C. Densitometric plot depicting the band intensities of Acetylated p65 over total p65 in blot B.

D. An immunoblot depicting p65 NF-κB interaction with SIRT1 as well as the p65 NF-κB acetylation status post immunoprecipitation of p65 (IP: p65) or with control IgG (IP: IgG) in uninfected (UI) or *S.* Typhimurium (STM) infected RAW264.7 macrophages upon SIRT1 inhibitor (EX-527, 1μM) treatment at 16hr post-infection. UT- Untreated.

E. Densitometric plot depicting the band intensities of Acetylated p65 subunit of NF-κ B over total p65 NF-κB in blot D.

Fig.5- *Salmonella* Typhimurium drives the metabolism of the infected macrophage toward fatty acid oxidation

A. Metabolic gene expression data of *S.* Typhimurium infected RAW 264.7 macrophages at 2hr, 6hr and 16hr time points of infection through nanoString. Data is representative of N=2, n=1.

B. *PPARδ* qPCR expression data in *S.* Typhimurium infected RAW 264.7 macrophages at the indicated time points of infection. Data is representative of N=3, n=2.

C. Lactate estimation assay of *S.*Typhimurium infected RAW264.7 macrophages at the initial time point of 2hr and at the late time point of 16hr post infection. Data is representative of N=3, n=3. Unpaired two-tailed Student's t test was performed to obtain the p values. (** $p<0.01$, * $p<0.05$)

D-E-Lactate estimation assay of *S.*Typhimurium infected RAW264.7 macrophages upon SIRT1 (D) or SIRT3 (E) knockdown condition at16h post-infection. Data is representative of N=3 , n=3. Unpaired two-tailed Student's t test was performed to obtain the p values.

F. Immunoblotting of host glycolytic (PGK), TCA cycle (PDHA1) and fatty acid oxidation (HADHA, ACOX-1) proteins under SIRT1 and SIRT3 knockdown condition of *S.* Typhimurium infected RAW264.7 macrophages at 16h post-infection.

G. Fatty Acid Oxidation (FAO) Assay of uninfected (UI) and infected (STM) RAW264.7 macrophages under SIRT1 or SIRT3 knockdown or inhibitor treatment. N=2, n=2. (** $p<0.01$, * $p<0.05$)

H. Fatty Acid Oxidation (FAO) Assay of uninfected (UI) and infected RAW264.7 macrophages under infection with wildtype *S*. Typhimurium (STM WT), SPI-1 (Δ*invC*)or SPI-2 (Δ*ssaV* and Δ*steE*) *m*utants of *S*. Typhimurium. Data is representative of N=2,n=2. (** $p<0.01$, * $p<0.05$)

Fig.6- *Salmonella* Typhimurium infection proceeds with increased glycolysis and glucose uptake inside the infected RAW 264.7 macrophages

A. *Salmonella* gene expression profiling data of *S*. Typhimurium infected RAW 264.7 macrophages at 2hr, 6hr and 16hr time points of infection through nanoString. SI- *S*. Typhimurium infected, PI- PFA fixed *S*. Typhimurium infected. SPI-1 genes- *Inv, PrgH* , SPI-2 genes- *ssaV,stfF, glk*- glucokinase, *pfkA*-phosphofrucktose kinase A, *ptsG*-Phosphophenolpyruvate-dependent sugar phosphotransferase system (PTS). Data is representative of N=2, n=2.

B. qRT PCR gene expression profiling of *Salmonella* metabolic genes within infected RAW264.7 macrophages in knockdown condition of either SIRT1 or SIRT3 at 6hr post infection. Data is representative of N=3, n=3.

C-D. qRT PCR gene expression profiling of *Salmonella* metabolic genes within infected female C57BL/6 mice spleen (C) and liver (D) under SIRT1 or SIRT3 inhibitor treatment harvested at 5th day post infection of *S.*Typhimurium (10^7 cfu units/animal). Unpaired two-tailed Student's t test was performed to obtain the p values. Data is representative of N=3, n=3. (****p<0.0001, *** p < 0.001, ** p<0.01, * p<0.05)

Fig.7- SIRT1 inhibition triggers hyperacetylation of glycolytic master regulator HIF-1α within *S*. Typhimurium infected macrophages while SIRT3 skews metabolism of *S.* Typhimurium-infected macrophages via interaction with PDHA1.

A. An immunoblot depicting HIF-1α interaction with SIRT1 post immunoprecipitation of SIRT1 in uninfected (UI) or *S.* Typhimurium (STM) infected RAW264.7 macrophages at 16hr post-infection. (Derived from same SIRT1 IP blot as in Fig. 4A)

B. Immunoblotting of SIRT1 in SIRT1 knockdown uninfected (UI) or *S.* Typhimurium (STM) infected RAW 264.7 cells at 16hr post-infection to assess the acetylation status of HIF-1α.

C . Densitometric plot depicting the band intensities of Acetylated HIF-1α over total HIF-1α in blot B. Data is representative of N=3.

D. An immunoblot depicting HIF-1α interaction with SIRT1 as well as the HIF-1α acetylation status post immunoprecipitation of HIF-1$^{\alpha}$ (IP:HIF-1α or with control IgG (IP:IgG) in uninfected (UI) or *S.* Typhimurium (STM) infected RAW264.7 macrophages upon SIRT1 inhibitor (EX-527, 1μM) treatment at 16hr post-infection. UT-untreated.

E. Densitometric plot depicting the band intensities of Acetylated HIF-1α over total HIF-1α in blot D. Data is representative of N=3.

F. Densitometric plot depicting the band intensities of SIRT1 in blot D.

G. Lactate estimation assay of *S.*Typhimurium infected RAW264.7 macrophages upon SIRT1 and SIRT3 knockdown condition in the presence of HIF-1α inhibitor, chetomine (50nM) at16h post-infection. Data is representative of N=3 , n=3. Unpaired two-tailed Student's t test was performed to obtain the p values. (****p<0.0001, *** p < 0.001, ** p<0.01, * p<0.05)

H. An immunoblot depicting PDHA1 interaction with SIRT1 or SIRT3 post immunoprecipitation of PDHA1 in uninfected (UI) or *S.* Typhimurium (STM) infected RAW264.7 macrophages in SIRT3 knockdown condition at 16hr post-infection.

I. Densitometric plot depicting the band intensities of SIRT3 interaction over total input in blot. Data is representative of N=3.

J. An immunoblot depicting PDHA1 interaction with SIRT3 post immunoprecipitation of PDHA1 in uninfected (UI) or *S.* Typhimurium (STM) infected RAW264.7 macrophages at 16hr post-infection under SIRT3 inhibitor (3-TYP, 1μM) treatment at 16hr post-infection. UT-untreated.

K. Densitometric plot depicting the band intensities of Acetylated PDHA1 over total PDHA1 in blot I. Data is representative of N=3.

L. Densitometric plot depicting the band intensities of SIRT3 interaction over total input in blot I. Data is representative of N=3.

Fig.8- Effect of SIRT1 or SIRT3 inhibition on *S.* Typhimurium infected C57BL/6 mice

A**.** The schematic representation of the experimental strategy for studying the effect of SIRT1 and SIRT3 on the *in vivo* pathogenesis of STM (WT).

B. *In-vivo* organ burden of *S.* Typhimurium upon SIRT1 or SIRT3 inhibition in C57BL/6 mice at day 5 post-infection under specified dosage of inhibitor treatment. Data is representative of

N=4, n=8. Mann-Whitney Test was performed to obtain the p values.(****p<0.0001, *** p < 0.001, ** p<0.01, * p<0.05).

C. Percent survival of *S.* Typhimurium infected C57BL/6 mice upon SIRT1 or SIRT3 inhibitor treatment at a specific dose of inhibitor treatment. Data is representative of N=4, n=5.

D. Representation of splenic length of *S.* Typhimurium infected spleen tissue harvested from C57BL/6 mice (males) at day 5 post-infection upon SIRT1 or SIRT3 inhibition at 1mg/kg dosage. Data is representative of N=4, n=8. (** p<0.01, * p<0.05).

E. Bacterial load in blood at different days post-infection upon SIRT1 or SIRT3 inhibition at 1mg/kg dosage in C57BL/6 mice (males). Data is representative of N=3, n>5. (** p<0.01, * p<0.05) Mann-Whitney Test was performed to obtain the p values. (** p<0.01, * p<0.05).

F. Bacterial load in blood at day 5 post-infection upon SIRT1 or SIRT3 inhibition at 1mg/kg dosage in C57BL/6 WT mice (males) and *gp91phox*-/- (males) mice. Data is representative of N=3, n>5. Mann-Whitney Test was performed to obtain the p values. (** p<0.01, * p<0.05).

G. Serum IL-6 levels of *S.* Typhimurium infected C57BL/6 WT mice (males) mice treated with SIRT1(EX-527) or SIRT3 (3TYP) inhibitors or SRT1720 (SIRT1 activator) at 1mg/kg dosage at 5th day post-infection. Data is representative of N=3, n>5. Unpaired two-tailed Student's t test was performed to obtain the p values.(** p<0.01, * p<0.05).

H. Quantitative analysis of percentage population of cells within liver showing DCFDA positive staining shown in Fig. S9, A. Data is representative of N=3, n>5. Unpaired two-tailed Student's t- test was performed to obtain the p values. (** p < 0.01).

I. Enumeration of GFP positive bacterial cells through flow cytometry in splenic tissues homogenate harvested from adult male 6-8 week old C57BL/6 mice (subjected to different chemical treatment-Vehicle treated or SIRT1 (EX-527) or SIRT3 (3-TYP) inhibitor or SIRT1

activator SRT1720 treated at a dose of 1mg/kg) at 5th day post *S.* Typhimurium (expressing GFP) infection (10^{7} CFU orally). Data is representative of N=3, n>5. Unpaired two-tailed Student's t test was performed to obtain the p values. (** $p < 0.01$).

J. Quantitative analysis of the percentage population of splenic cells harboring GFP+ bacterial cells shown in I. Unpaired two-tailed Student's t test was performed. (** $p<0.01$, * $p<0.05$).

K. Enumeration of GFP positive bacterial cells through flow cytometry within F4/80 positive splenic macrophages present within splenic tissues homogenate harvested from adult male 6-8 week old C57BL/6 mice (subjected to different chemical treatment-Vehicle treated or SIRT1 (EX-527) or SIRT3 (3-TYP) inhibitor or SIRT1 activator SRT1720 treated aa t dose of 1mg/kg) at 5th day post *S.* Typhimurium infection. Data is representative of N=3, n>5.

L. Quantitative analysis of percentage population of F4/80 positive macrophage cells harboring GFP+ bacteria shown in K . Unpaired two-tailed Student's t test was performed to obtain the p values. Data is representative of N=3, n>5.(* $p < 0.05$).

M-S. Quantitative analysis of different mCherry-*S.*Typhimurium-infected splenic populations harboring mCherry+bacteria via flow cytometry depicted in Fig. S8. Unpaired two-tailed Student's t test was performed. (*** $p < 0.001$,** $p<0.01$, * $p<0.05$).

T. Representative image of haematoxylin-eosin-stained liver sections to assess the liver tissue architecture upon *Salmonella* infection at 5th days post-infection in different mice cohorts. (UI-Uninfected, STM- *S.* Typhimurium infected, EX-527-SIRT1 inhibitor, 3TYP-SIRT3 inhibitor, SRT1720- SIRT1 activator, Vehicle Control-(PBS containing 0.1% DMSO). Scale bar-50µm. **Scoring system:-** according to pathological changes the tissue sections are scored as 0 for normal pathology, 1 for mild/ minor pathology, 2 for moderate pathology, and 3 for severe pathological changes.

U. Graph representing the histopathological scoring of the liver sections depicted in L. Unpaired two-tailed Student's t test was performed to obtain the p values. (* $p < 0.05$)(****$p<0.0001$, *** $p < 0.001$, ** $p<0.01$, * $p<0.05$).

V. *In-vivo* organ burden of *S.* Typhimurium upon SIRT1 or SIRT3 adenovirus-mediated *in vivo* knockdown in C57BL/6 mice at day 5 post-infection. Data is representative of N=3, n>3. Mann-Whitney Test was performed to obtain the p values. (****$p<0.0001$, *** $p < 0.001$, ** $p<0.01$, * $p<0.05$).

W. Serum IL-6 levels of *S.* Typhimurium infected C57BL/6 WT mice (males) upon *in vivo* adenovirus-mediated SIRT1 or SIRT3 knockdown. Data is representative of N=3, n>3. Unpaired two-tailed Student's t test was performed to obtain the p values. (** $p<0.01$, * $p<0.05$).

X. Percent survival of *S.* Typhimurium infected C57BL/6 mice upon *in vivo* adenovirus-mediated SIRT1 or SIRT3 knockdown. Data is representative of N=3, n>3.

Y. Representative image of haematoxylin-eosin-stained liver sections upon *Salmonella* infection at 5th days post-infection in different mice cohorts. (Scrambled STM, shSIRT1 STM, shSIRT3 STM). Scale bar-50µm. **Scoring system:-** according to pathological changes the tissue sections are scored as 0 for normal pathology, 1 for mild/ minor pathology, 2 for moderate pathology, and 3 for severe pathological changes.

SUPPLEMENTARY FIGURE LEGENDS

Fig.S1- *Salmonella* modulates the expression of SIRT1 and SIRT3 along its course of infection

A. Expression studies of SIRT1 and SIRT3 through immunoblotting in RAW 264.7 macrophages.

B. Representative immunoblot showing SIRT1 and SIRT3 expression at 16hr post-infection with wildtype *S*. Typhimurium, SPI-1 mutant- Δ*invC* and SPI-2 mutants-Δ*ssaV*, Δ*steE*.

C. *SIRT1* and *SIRT3* transcript level expression in M1 polarized RAW264.7 macrophages at 16h post-infection. Data is representative of N=3, n=3. . Un-paired t-test were performed to obtain p-values. (****p<0.0001,***p < 0.001, ** p<0.01, *p<0.05)

D. Expression profile of *SIRT1* and *SIRT3* in M2 polarized RAW264.7 macrophages at 16h post-infection. Data is representative of N=3, n=3. Un-paired t-test were performed to obtain p-values. (****p<0.0001,***p < 0.001, ** p<0.01, *p<0.05)

E. Intracellular fold proliferation of *S*. Typhimurium within non-polarized, M1 and M2 polarized RAW264.7 macrophages. Data is representative of N=3, n=3. Un-paired t-test were performed to obtain p-values. (****p<0.0001,***p < 0.001, ** p<0.01, *p<0.05)

F. Validation of M1 and M2 polarized status of RAW264.7 macrophages by estimation of IL-6 and IL-10 production via ELISA 24h post-polarization. Data is representative of N=3, n=3. Un-paired t-test were performed to obtain p-values. (****p<0.0001,***p < 0.001, ** p<0.01, *p<0.05)

Fig.S2- Validation of SIRT1 and SIRT3 knockdown in RAW 264.7 macrophages

A. Knockdown confirmation of *SIRT1* at transcript level through qPCR.

B. qPCR expression of *SIRT3* in order to validate knockdown efficiency.

C. Immunoblotting of SIRT1 for verification of knockdown. Scr=Scrambled, Mix=transfection with equimolar concentration of both SIRT1 shRNA construct C4 and C12.

D. SIRT3 knockdown validation through western blotting. Scr=Scrambled, Mix=transfection with equimolar concentration of both SIRT3 shRNA construct E8 and E12

Fig. S3- SIRT1 and SIRT3 modulates cytokine production in *Salmonella* infection scenario

A. Estimation of pro-inflammatory IL-6 cytokine production upon *S.* Typhimurium infection in SIRT1 and SIRT3 knockdown RAW 264.7 macrophages through ELISA. Data is representative of N=2, n=2. Unpaired two tailed Student's t test was performed to obtain the p values. (** $p<0.01$, * $p<0.05$).

B. Estimation of anti-inflammatory IL-10 cytokine production upon *S.* Typhimurium infection in SIRT1 and SIRT3 knockdown RAW 264.7 macrophages through ELISA. Data is representative of N=2, n=2. Unpaired two tailed Student's t test was performed to obtain the p values. (*** $p < 0.001$, * $p<0.05$)

C. Estimation of IL-1β cytokine production upon *S.* Typhimurium infection in SIRT1 and SIRT3 knockdown RAW 264.7 macrophages through ELISA at 20hr post-infection. Data is representative of N=2, n=2. Unpaired two-tailed Student's t test was performed to obtain the p values. (*** $p < 0.001$, * $p<0.05$) Uninfected (UI) samples values were below the detection level (ND-Not detectable).

D. Estimation of pro-inflammatory IL-6 cytokine production within uninfected or *S.* Typhimurium infected peritoneal macrophages in presence or absence of SIRT1 or SIRT3 inhibitor treatment at 6hr post-infection. Data is representative of N=2, n=2. Unpaired two tailed Student's t test was performed to obtain the p values. (** $p<0.01$, * $p<0.05$)

E. Estimation of pro-inflammatory IL-1β cytokine production within uninfected or *S.* Typhimurium infected peritoneal macrophages in presence or absence of SIRT1 or SIRT3 inhibitor treatment at 6hr post-infection. Data is representative of N=2, n=2. Unpaired two tailed Student's t test was performed to obtain the p values. (** $p<0.01$, * $p<0.05$). Uninfected (UI) samples values were below the detection level (ND-Not detectable).

F. Serum IL-1β levels of *S.* Typhimurium infected C57BL/6 WT mice (males) upon SIRT1 or SIRT3 inhibitor treatment at 5th day post-infection. Data is representative of N=3, n>3. Unpaired two-tailed Student's t test was performed to obtain the p values. (** $p<0.01$, * $p<0.05$).

G. Intestinal (ileal) IL-1β levels of *S.* Typhimurium infected C57BL/6 WT mice (males) upon SIRT1 or SIRT3 inhibitor treatment at 5th day post-infection. Data is representative of N=3, n>3. Unpaired two-tailed Student's t test was performed to obtain the p values. (** $p<0.01$, * $p<0.05$).

Fig.S4- *Salmonella* Typhimurium skews the polarization state of the macrophage toward an immunosuppressive M2 state along the course of infection

A- Flow cytometric analysis of alteration in M1 CD86 (PE) positive population in *S.* Typhimurium (STM) infected samples in comparison to uninfected (UI) and Paraformaldehyde Fixed (PFA) bacteria at the indicated time post-infection.

B- Flow cytometric analysis of M2 surface marker CD206 (APC) in *S.* Typhimurium (STM) infected SIRT1 or SIRT3 knockdown RAW264.7 macrophages in comparison to the scrambled control at the indicated time post-infection. UI-Uninfected sample.

Fig.S5- SIRT1 and SIRT3 play a role in maintaining ROS balance within *Salmonella* infected macrophages.

A. DCFDA fluorescence measured through Flow cytometry in shSIRT1, shSIRT3 or scrambled shRNA transfected and un-transfected RAW 264.7 macrophages at 16hr post *S.* Typhimurium infection. Data is representative of N=3, n=2.

B. Quantitative analysis of percentage population of DCFDA positive cells shown in Fig.6, A. Unpaired two-tailed Student's t test was performed. Data is statistically non-significant. (** $p<0.01$, * $p<0.05$)

C. Detection of extracellular H_2O_2 production through Phenol Red Hydrogen peroxidase assay at 610nm absorbance. Two-way ANOVA and Bonferroni post-t-test was used to obtain p values. (** $p < 0.01$, * $p < 0.05$, ns-not significant) Data is representative of N=2, n=2. (** $p<0.01$, * $p<0.05$)

Fig.S6- Effect of SIRT1 and SIRT3 knockdown or inhibition in intracellular bacterial proliferation within RAW 264.7 macrophages or peritoneal macrophages in presence of ROS scavenger N-Acetyl Cysteine (NAC).

A.Fold Proliferation of *Salmonella* Typhimurium within RAW 264.7 macrophages in transfected and un-transfected conditions in presence or absence of NAC (1mM). Data are representative of N=3, n=3. Unpaired two tailed Student's t test was performed to obtain the p values. (****$p<0.0001$,*** $p < 0.001$, ** $p<0.01$, * $p<0.05$)

B.Fold Proliferation of *Salmonella* Typhimurium within peritoneal macrophages isolated from 6-8 week old adult male C57BL/6 mice upon SIRT1 (EX-527, 1µM) or SIRT3 (3TYP, 1µM) inhibitor treatment in presence or absence of NAC (1mM). Data are representative of N=3, n=3. Unpaired two tailed Student's t test was performed to obtain the p values. (****$p<0.0001$,*** $p < 0.001$, ** $p<0.01$, * $p<0.05$)

Fig.S7 SIRT1 and SIRT3 knockdown or inhibitor treatment led to decrease in fatty acid oxidation and promoted host glycolysis in *S*. Typhimurium infected peritoneal macrophages

A-qRT PCR mediated gene expression analysis of several host metabolic genes in SIRT1 or SIRT3 knockdown RAW264.7 macrophages at 6 hr post-infection. Data is representative of N=3,n=3. Unpaired two-tailed Student's t test was performed to obtain the p values. (* $p<0.05$)

B- qRT PCR mediated gene expression analysis of several host metabolic genes in SIRT1 or SIRT3 inhibitor-treated (1µM) peritoneal macrophages isolated from 6-8 week old C57BL/6 male mice liver harvested at 5th day post thioglycolate injection. Data is representative of N=3,n=3. Unpaired two-tailed Student's t test was performed to obtain the p values. (****$p<0.0001$, *** $p < 0.001$, ** $p<0.01$, * $p<0.05$)

C-Lactate estimation assay of *S.*Typhimurium infected peritoneal macrophages upon SIRT1 or SIRT3 catalytic inhibition at 2h, 6h and 16h post-infection. Data is representative of N=3,n=3. Unpaired two-tailed Student's t test was performed to obtain the p values. (****$p<0.0001$, *** $p < 0.001$, ** $p<0.01$, * $p<0.05$)

D-Immunoblotting of host glycolytic (PGK, PFK) and fatty acid oxidation (HADHA, ACOX-1) proteins under SIRT1 (EX-527) and SIRT3 (3TYP) catalytic inhibitor treated condition in *S.* Typhimurium infected peritoneal macrophages (isolated from thioglycolate treated adult male C57BL/6 mice) at 16h post-infection. Data is representative of N=2, n=1.

E- qRT PCR mediated gene expression profiling of several host metabolic genes in SIRT1 or SIRT3 inhibitor treated 6-8 week old C57BL/6 male mice liver harvested at 5-day post infection of *S.*Typhimurium (10^7 CFU units/animal). Unpaired two-tailed Student's t test was performed to obtain the p values. Data is representative of N=3, n=3. (****$p<0.0001$, *** $p < 0.001$, ** $p<0.01$, * $p<0.05$)

F-qRT PCR mediated gene expression profiling of several host metabolic genes in SIRT1 or SIRT3 inhibitor treated 6-8 week old C57BL/6 male mice spleen harvested at 5 day post-infection of *S.*Typhimurium (10^7 CFU units/animal). Unpaired two-tailed Student's t test was

performed to obtain the p values. Data is representative of N=3, n=3. (****$p<0.0001$, *** $p < 0.001$, ** $p<0.01$, * $p<0.05$)

Fig. S8-Flow cytometric analysis of different splenic populations within mCherry-labelled *S.* Typhimurium infected mice cohorts upon SIRT1 or SIRT3 inhibitor treatment

A-Enumeration of mCherry positive bacterial cells through flow cytometry in splenic tissues homogenate harvested from adult male 6–8-week-old C57BL/6 mice (subjected to different chemical treatment-Vehicle treated or SIRT1 (EX-527) or SIRT3 (3-TYP) inhibitor or SIRT1 activator SRT1720 treated at a dose of 1mg/kg) at 5th day post-*S*. Typhimurium infection (10^7 CFU orally).

B-Flow cytometric analysis of eFluor450 conjugated CD11c+ population within single cell splenic suspension isolated from adult male 6–8-week-old C57BL/6 mice (subjected to different chemical treatment-Vehicle treated or SIRT1 (EX-527) or SIRT3 (3-TYP) inhibitor or SIRT1 activator SRT1720 treated at a dose of 1mg/kg) at 5th day post-mCherry-labelled *S*. Typhimurium infection (10^7 CFU orally).

C-Flow cytometric analysis of FITC conjugated Ly6C+ population within single cell splenic suspension isolated from adult male 6–8-week-old C57BL/6 mice (subjected to different chemical treatment-Vehicle treated or SIRT1 (EX-527) or SIRT3 (3-TYP) inhibitor or SIRT1 activator SRT1720 treated at a dose of 1mg/kg) at 5th day post-mCherry-labelled *S*. Typhimurium infection (10^7 CFU orally).

D- Flow cytometric analysis of Alexa 647-conjugated CD45+ population within single cell splenic suspension isolated from adult male 6–8-week-old C57BL/6 mice (subjected to different chemical treatment-Vehicle treated or SIRT1 (EX-527) or SIRT3 (3-TYP) inhibitor or SIRT1 activator SRT1720 treated at a dose of 1mg/kg) at 5th day post-mCherry-labelled *S*. Typhimurium infection (10^7 CFU orally).

E-G-Alexa 647-conjugated CD45+ population (as shown in D) was gated as per granularity (Side Scatter versus Alexa 647 plot) into P6 population with high granularity (granulocytes), P5 (monocytes), and P4 population with low granularity (lymphocytes). Flow cytometric analysis of Alexa 647-conjugated CD45+ (E) P6 (granulocyte), (F) P5 (monocyte), and (G) P4 (lymphocyte) population within single cell splenic suspension isolated from adult male 6–8-week-old C57BL/6 mice (subjected to different chemical treatment-Vehicle treated or SIRT1 (EX-527) or SIRT3 (3-TYP) inhibitor or SIRT1 activator SRT1720 treated at a dose of 1mg/kg) at 5th day post-mCherry-labelled *S*. Typhimurium infection (10^{7} CFU orally).

Fig.S9- SIRT1 and SIRT3 inhibition led to enhanced ROS production within *Salmonella*-infected mice liver and spleen tissues.

A-DCFDA fluorescence measured through flow cytometry in liver tissues homogenate harvested from adult male 6-8 week old C57BL/6 mice (subjected to different chemical treatment- Vehicle treated or SIRT1 (EX-527) or SIRT3 (3-TYP) inhibitor or SIRT1 activator SRT1720 treated at dose of 1mg/kg) at 5th day post *S.* Typhimurium infection (10^{8} CFU orally). Data is representative of N=3, n=2.

B- DCFDA fluorescence measured through Flow cytometry in splenic tissues homogenate harvested from adult male 6-8 week old C57BL/6 mice (subjected to different chemical treatment-Vehicle treated or SIRT1 (EX-527) or SIRT3 (3-TYP) inhibitor or SIRT1 activator SRT1720 treated at dose of 1mg/kg) at 5th day post *S.* Typhimurium infection. Data is representative of N=3, n=2.

C- Quantitative analysis of percentage population of splenocytes showing DCFDA positive staining shown in splenic tissues homogenate harvested from adult male 6-8 week old C57BL/6 mice as shown in B. Unpaired two-tailed Student's t test was performed to obtain the p values. (** $p < 0.01$)

Fig. S10 *In vivo* knockdown validation by Western blotting and qPCR in liver

A-Immunoblotting of SIRT1 and SIRT3 in harvested liver samples upon AAV- mediated *in vivo* knockdown in mice.

B- qPCR mediated gene expression of *SIRT1* in harvested liver samples upon *in vivo* AAV-mediated gene inhibition in mice. Data is representative of N=3,n=3. Unpaired two-tailed Student's t test was performed to obtain the p values. (****$p<0.0001$,***$p < 0.001$, ** $p<0.01$, *$p<0.05$)

C-qPCR mediated gene expression of *SIRT3* in harvested liver samples upon *in vivo* AAV-mediated gene inhibition in mice. Data is representative of N=3,n=3.Unpaired two-tailed Student's t test was performed to obtain the p values. (****$p<0.0001$,***$p < 0.001$, ** $p<0.01$, *$p<0.05$)

Fig. S11-Schematic Diagram-In murine macrophages, *Salmonella* infection drives an immuno-metabolic shift toward an immunosuppressive state with an increase in host fatty acid oxidation rate by modulating SIRT1 and SIRT3. SIRT1 and SIRT3 regulate the acetylation status of NFκB p65 subunit, HIF-1α, PDHA1 thereby influencing host metabolism which in turn impacts the intracellular *Salmonella* metabolism. Inhibition or knockdown of SIRT1 or SIRT3 triggers increased ROS, pro-inflammatory cytokine burst with a concomitant decline in host fatty acid oxidation and a corresponding increase in bacterial fatty acid oxidation together amounting to decreased intracellular bacterial replication. Contrastingly, in *in vivo* mice model of infection, SIRT1 and SIRT3 cause increased bacterial dissemination owing to increased ROS, IL-6 and IL-1β production.

1402

MANUSCRIPT_1 TITLE:
***Salmonella*-induced SIRT1 and SIRT3 are crucial for maintaining the metabolic switch in bacteria and host for successful pathogenesis**

MAIN FIGURES

Fig.1

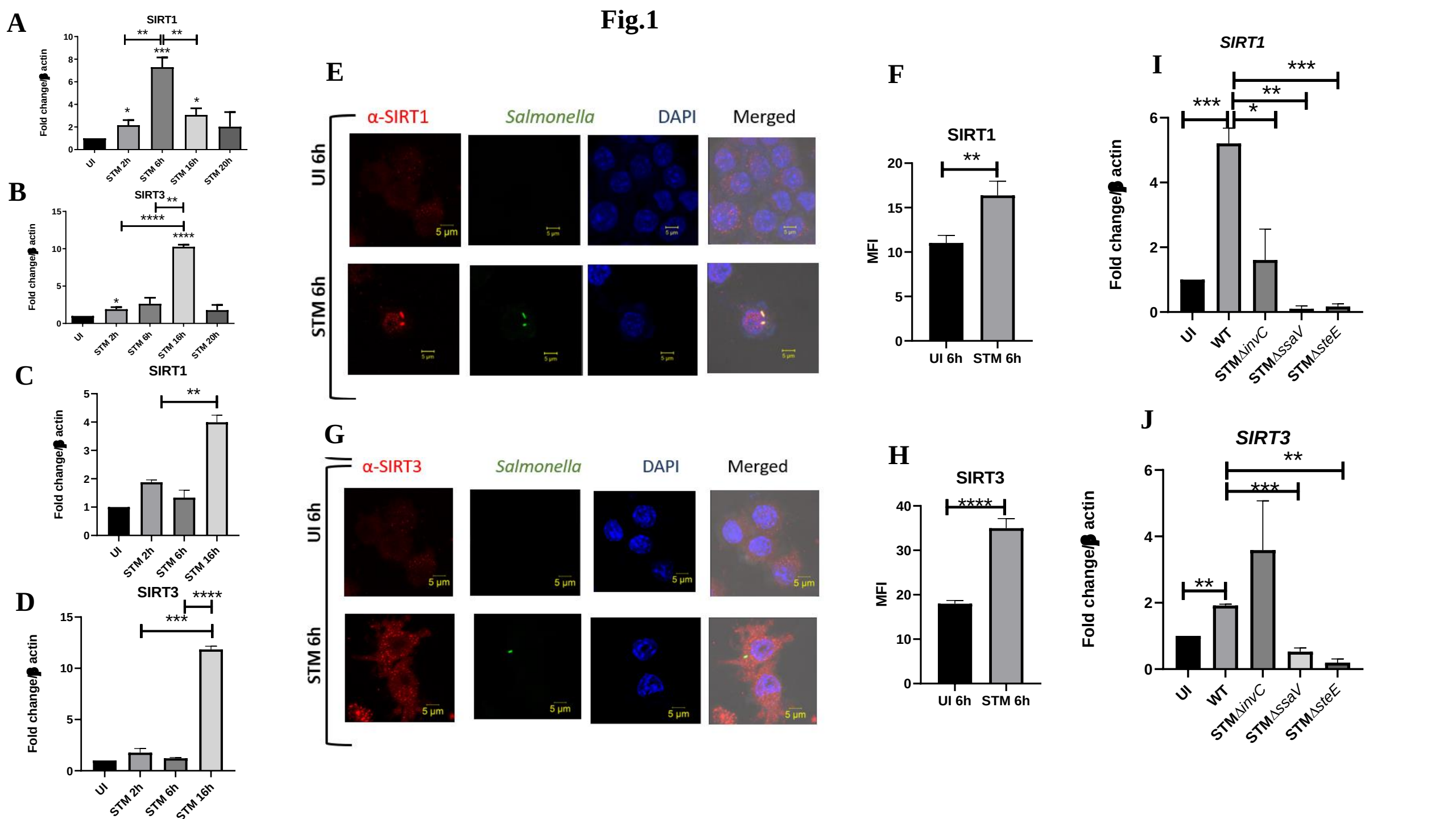
A
SIRT1
Fold change/β actin
UI
STM 2h
STM 6h
STM 16h
STM 20h
B
SIRT3
C
SIRT1
D
SIRT3
E
α-SIRT1
Salmonella
DAPI
Merged
UI 6h
STM 6h
5 µm
F
SIRT1
MFI
UI 6h
STM 6h
G
α-SIRT3
H
SIRT3
I
SIRT1
WT
STMΔinvC
STMΔssaV
STMΔsteE
J
SIRT3

Fig.2

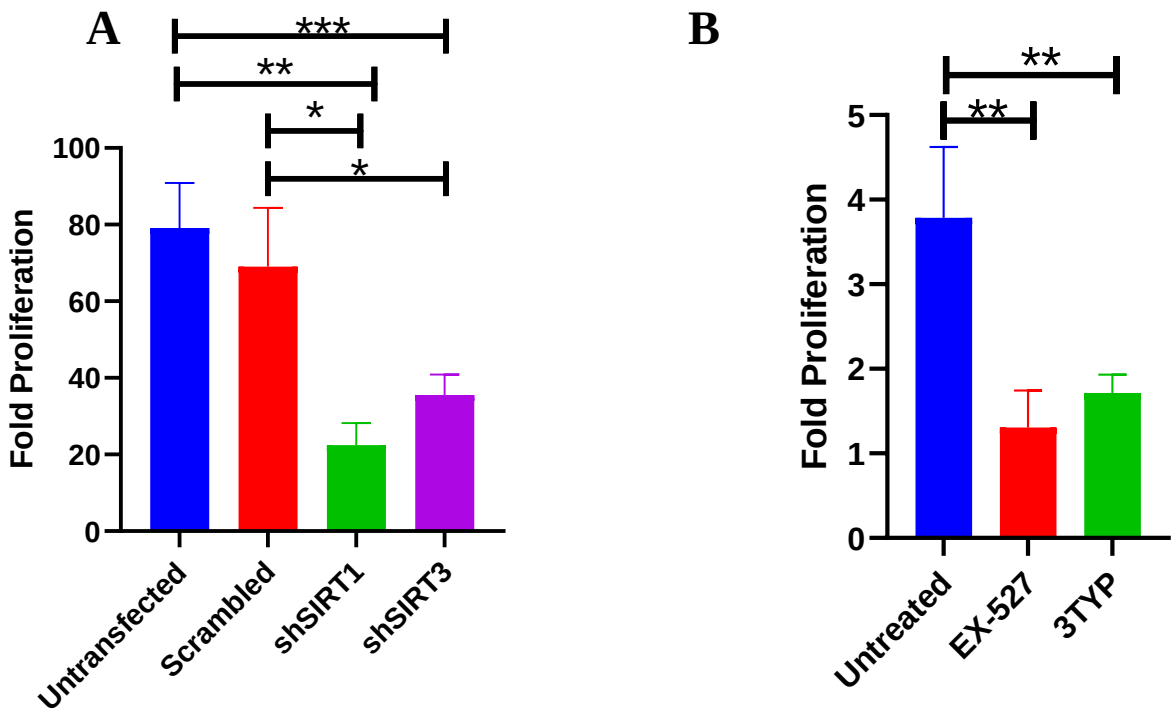
A
***
**
*
*
100
80
60
40
20
0
Fold Proliferation
Untransfected
Scrambled
shSIRT1
shSIRT3
B
**
**
5
4
3
2
1
0
Fold Proliferation
Untreated
EX-527
3TYP

Fig.3

A

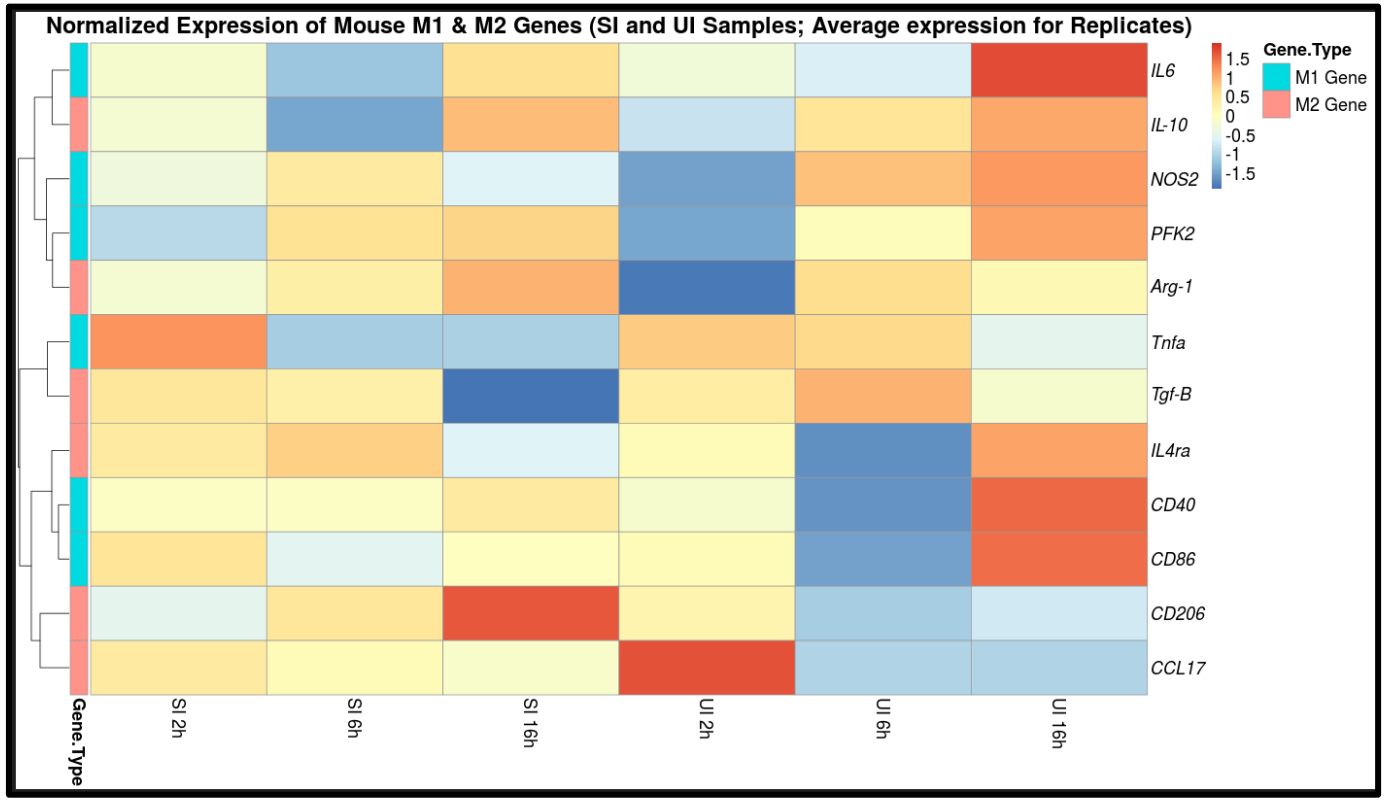
Normalized Expression of Mouse M1 & M2 Genes (SI and UI Samples; Average expression for Replicates)
Gene.Type
M1 Gene
M2 Gene
1.5
1
0.5
0
-0.5
-1
-1.5
IL6
IL-10
NOS2
PFK2
Arg-1
Tnfa
Tgf-B
IL4ra
CD40
CD86
CD206
CCL17
Gene.Type
SI 2h
SI 6h
SI 16h
UI 2h
UI 6h
UI 16h

B

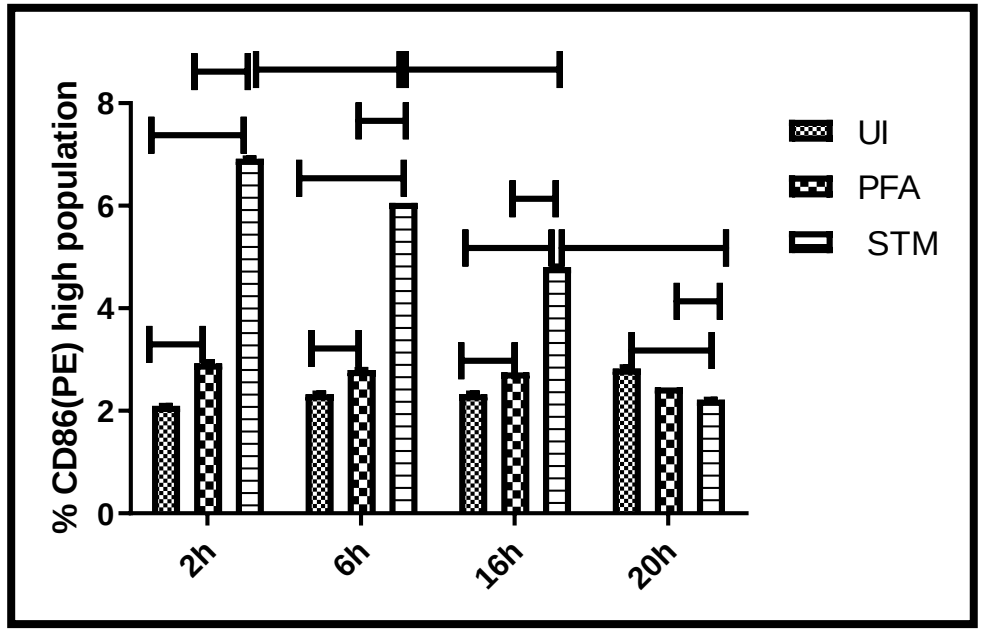
% CD86(PE) high population
0
2
4
6
8
2h
6h
16h
20h
UI
PFA
STM

C

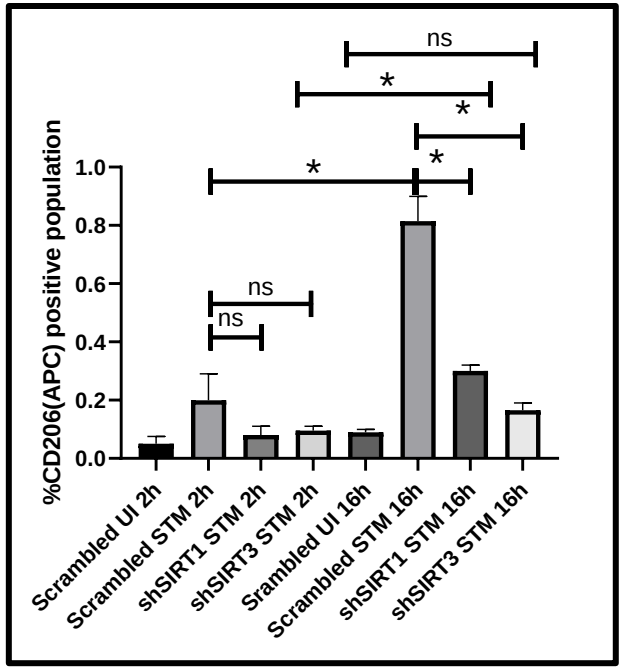
%CD206(APC) positive population
0.0
0.2
0.4
0.6
0.8
1.0
ns
ns
ns
*
*
*
*
Scrambled UI 2h
Scrambled STM 2h
shSIRT1 STM 2h
shSIRT3 STM 2h
Srambled UI 16h
Scrambled STM 16h
shSIRT1 STM 16h
shSIRT3 STM 16h

Fig.4

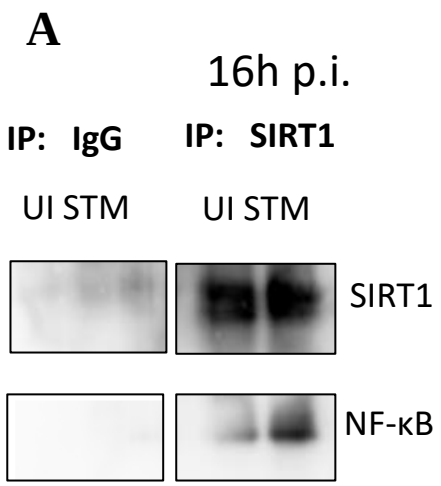
A
16h p.i.
IP: IgG
IP: SIRT1
UI STM
UI STM
SIRT1
NF-κB

INPUT

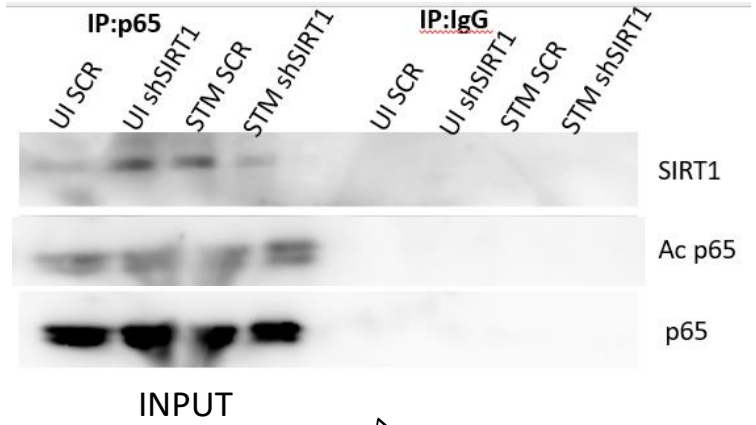
B
IP:p65
IP:IgG
UI SCR
UI shSIRT1
STM SCR
STM shSIRT1
UI SCR
UI shSIRT1
STM SCR
STM shSIRT1
SIRT1
Ac p65
p65

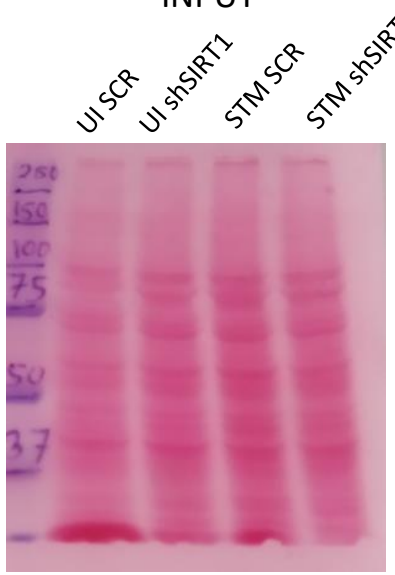
INPUT
UI SCR
UI shSIRT1
STM SCR
STM shSIRT1

shSIRT1
SCR
SIRT1

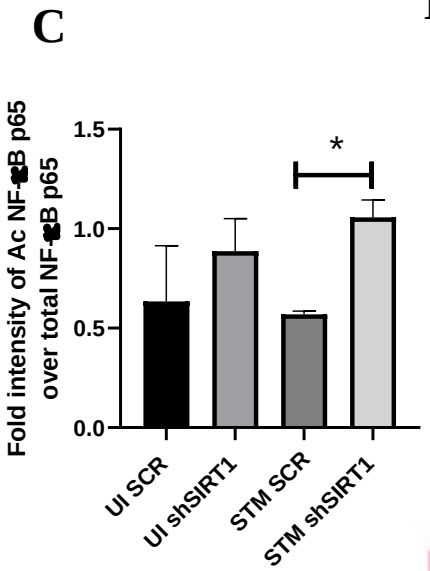
C
Fold intensity of Ac NF-κB p65 over total NF-κB p65
1.5
1.0
0.5
0.0
*
UI SCR
UI shSIRT1
STM SCR
STM shSIRT1

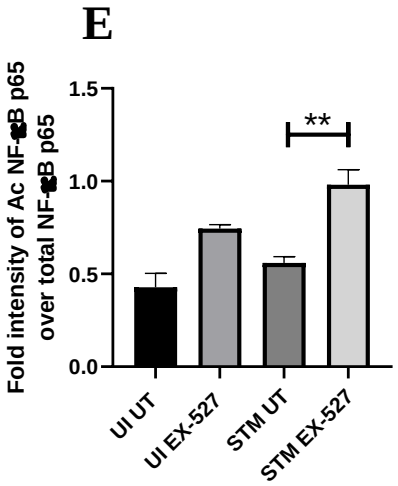
E
Fold intensity of Ac NF-κB p65 over total NF-κB p65
1.5
1.0
0.5
0.0
**
UI UT
UI EX-527
STM UT
STM EX-527

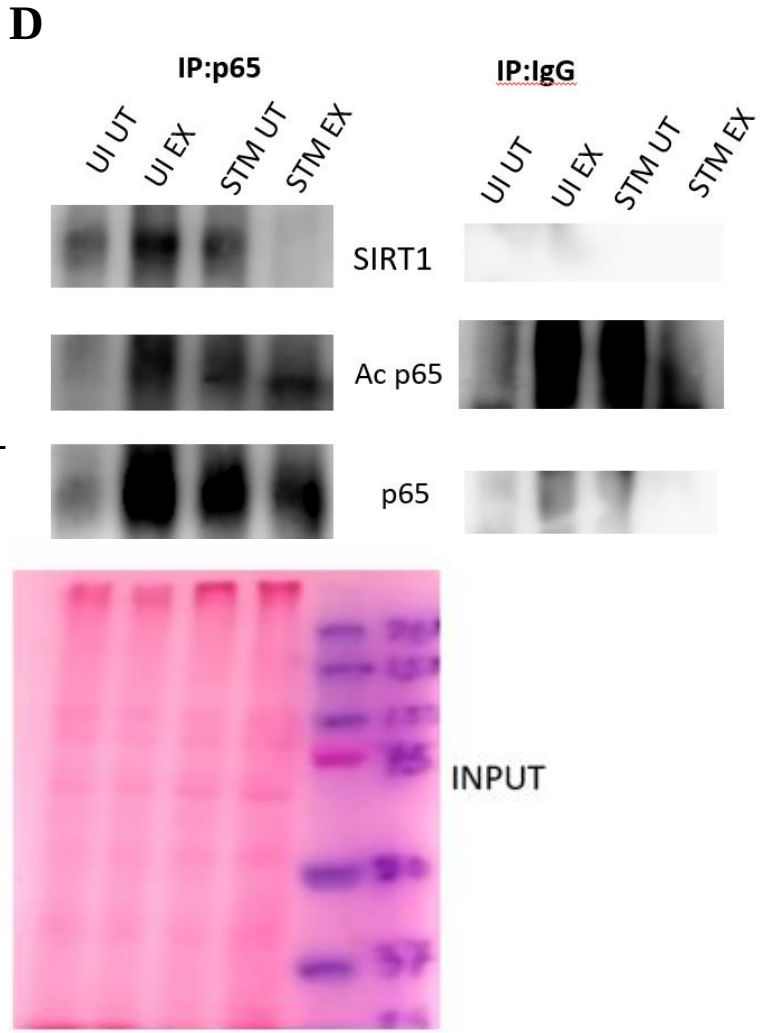
D
IP:p65
IP:IgG
UI UT
UI EX
STM UT
STM EX
UI UT
UI EX
STM UT
STM EX
SIRT1
Ac p65
p65
INPUT

Fig.5

RAW 264.7

A

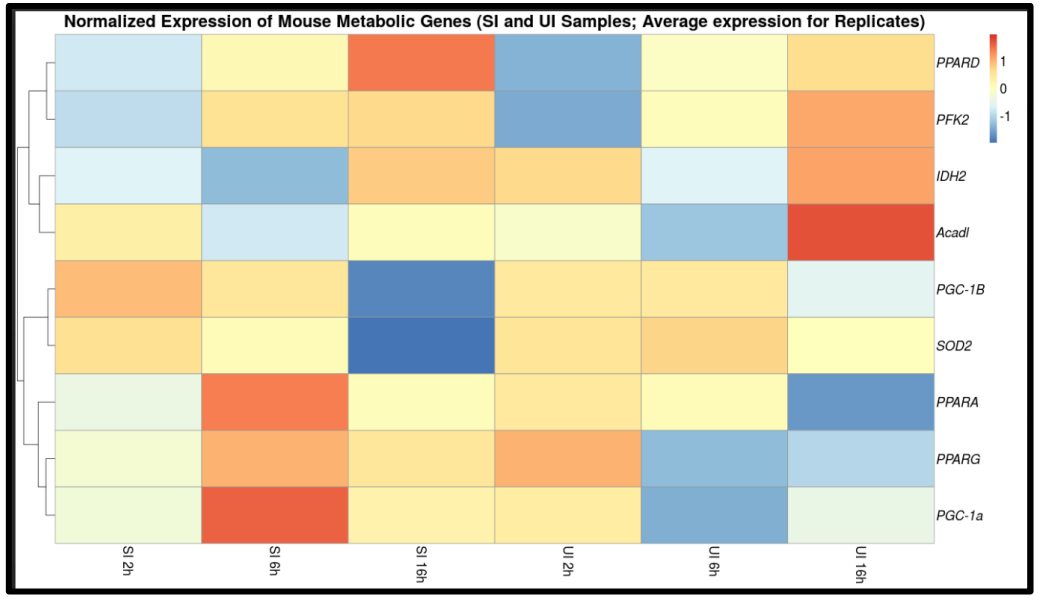

B

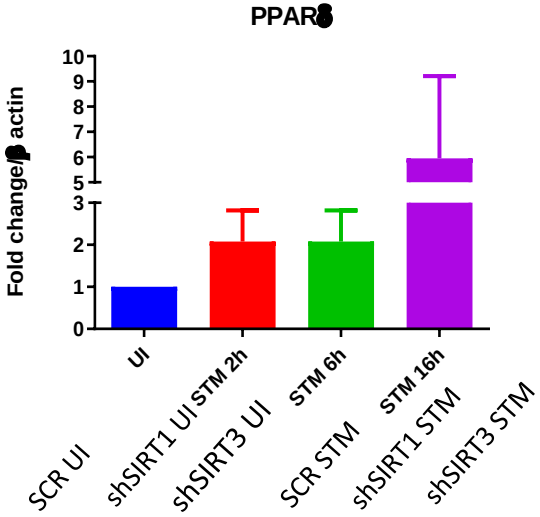

C

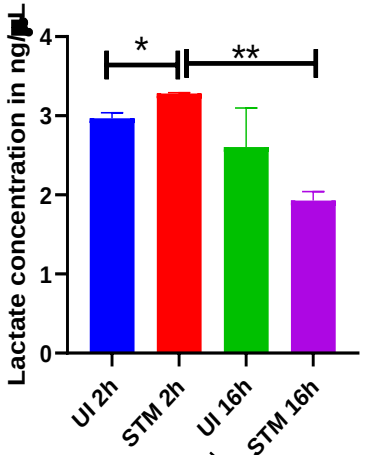

G

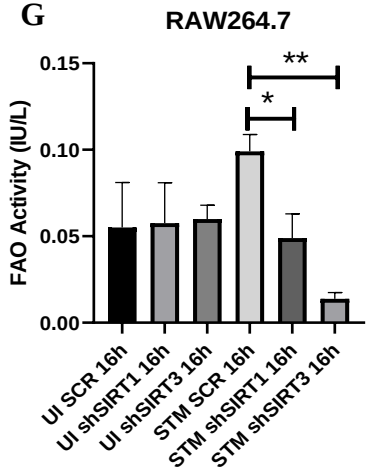

F

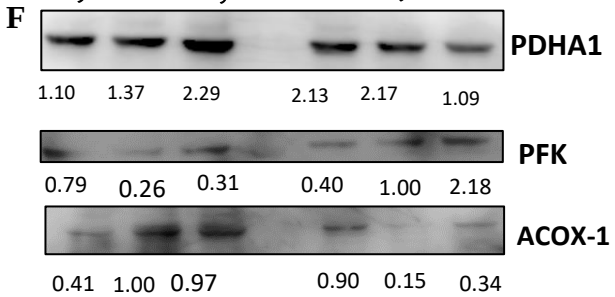

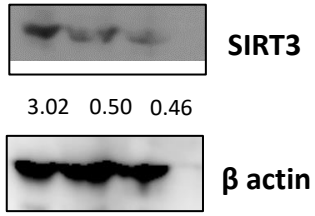

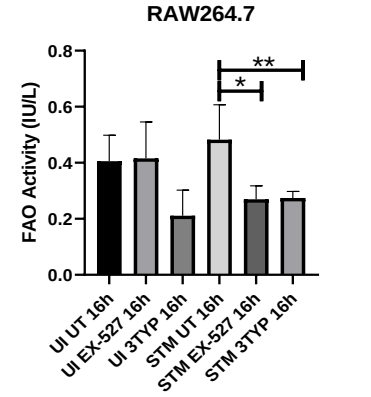

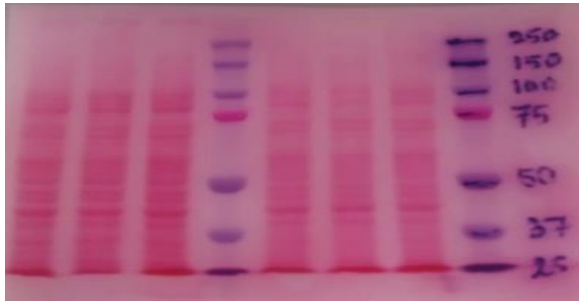

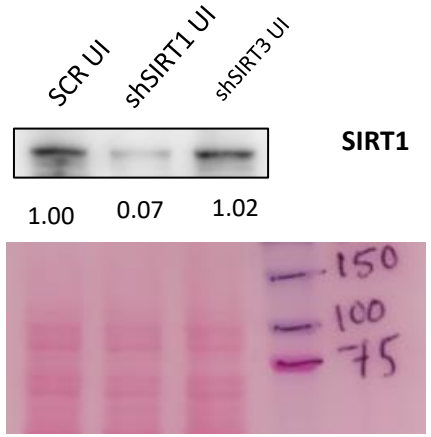

D

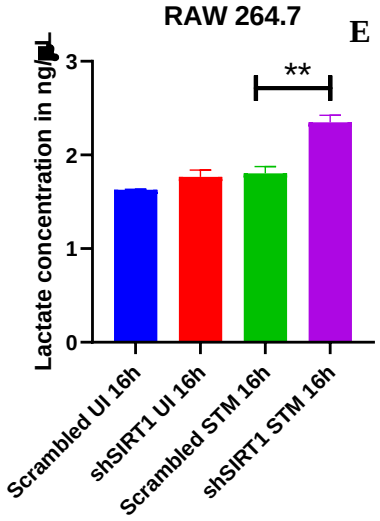

E

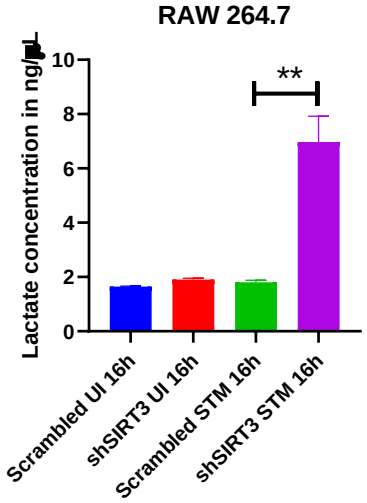

H

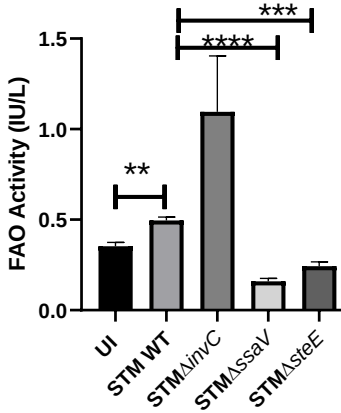

Fig.6

A

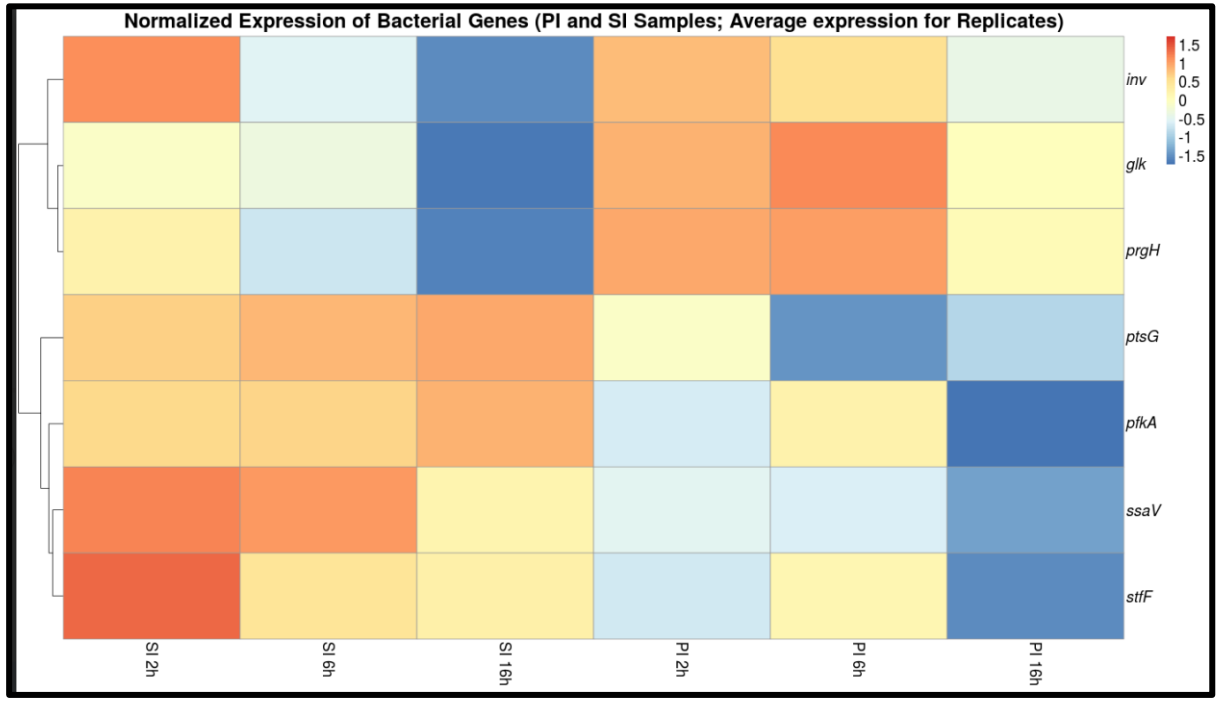
Normalized Expression of Bacterial Genes (PI and SI Samples; Average expression for Replicates)
1.5
1
0.5
0
-0.5
-1
-1.5
inv
glk
prgH
ptsG
pfkA
ssaV
stfF
SI 2h
SI 6h
SI 16h
PI 2h
PI 6h
PI 16h

B

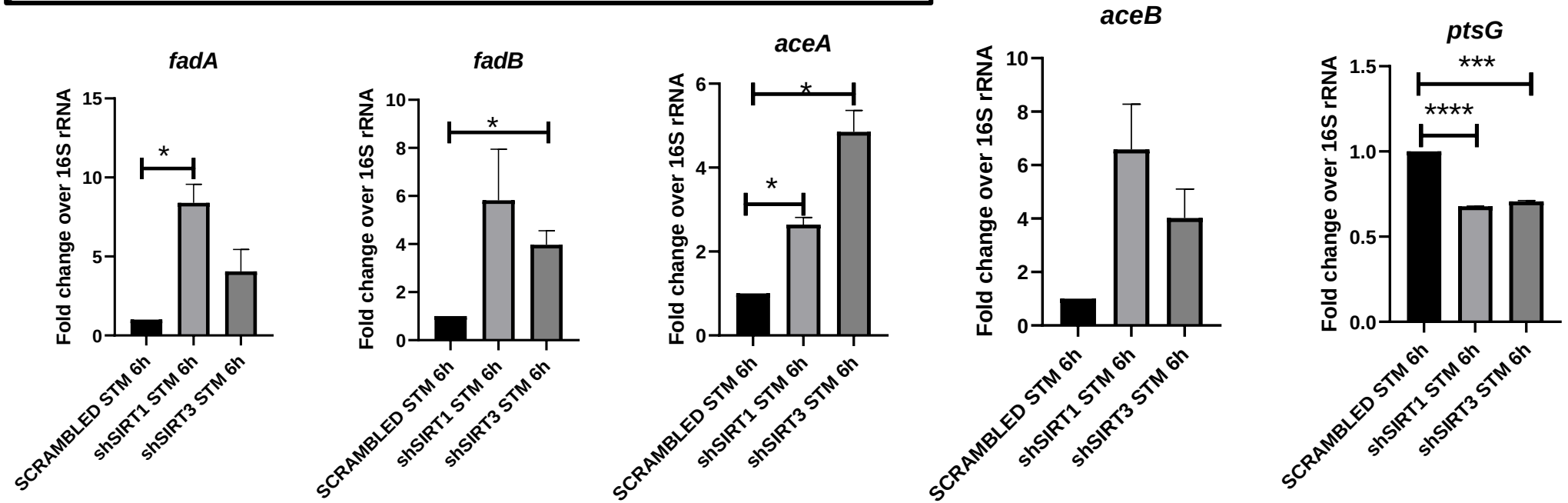
fadA
fadB
aceA
aceB
ptsG
Fold change over 16S rRNA
*
***
****
SCRAMBLED STM 6h
shSIRT1 STM 6h
shSIRT3 STM 6h

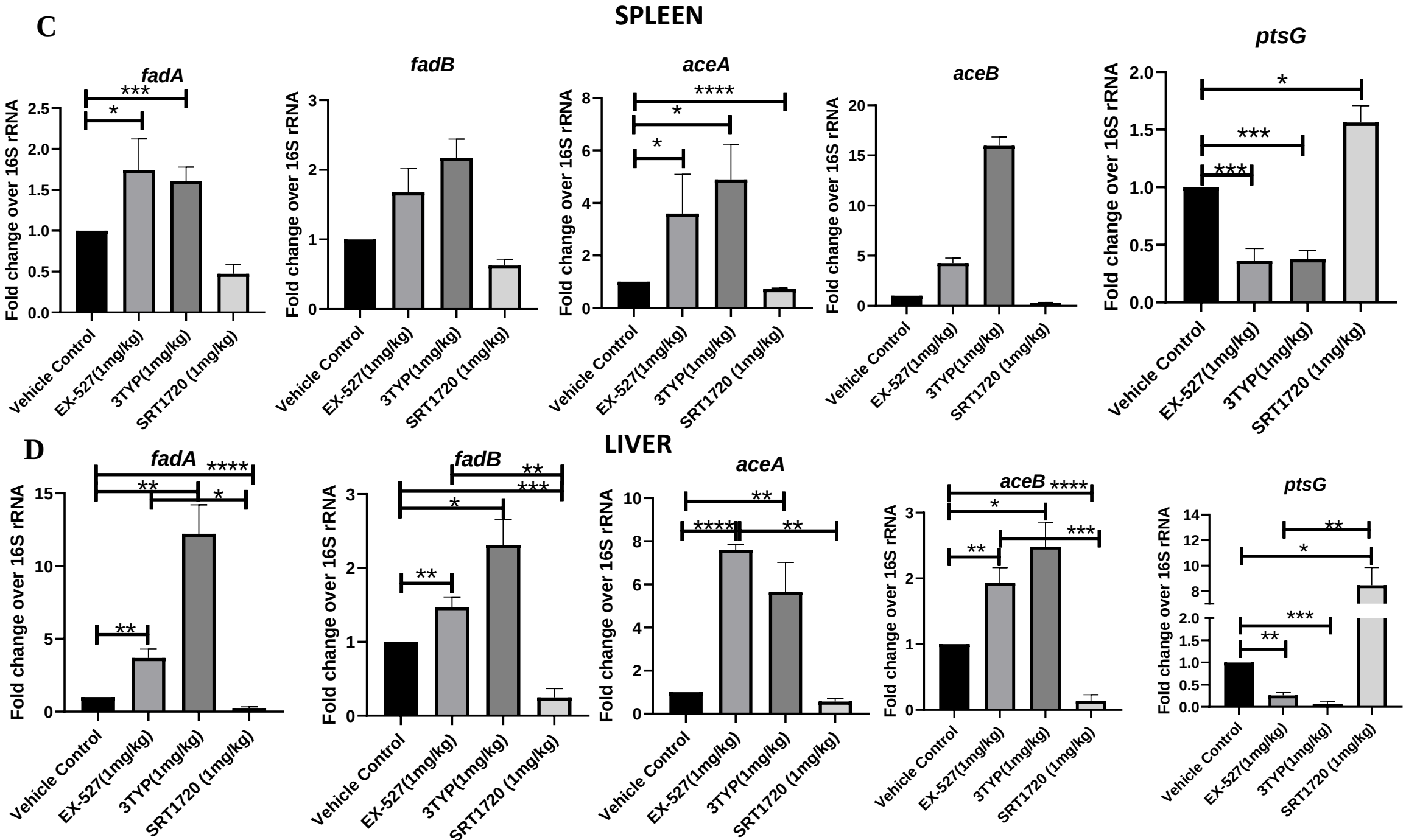
C
SPLEEN
fadA
fadB
aceA
aceB
ptsG
Fold change over 16S rRNA
Vehicle Control
EX-527(1mg/kg)
3TYP(1mg/kg)
SRT1720 (1mg/kg)
D
LIVER
fadA
fadB
aceA
aceB
ptsG
Fold change over 16S rRNA
Vehicle Control
EX-527(1mg/kg)
3TYP(1mg/kg)
SRT1720 (1mg/kg)

Fig.7

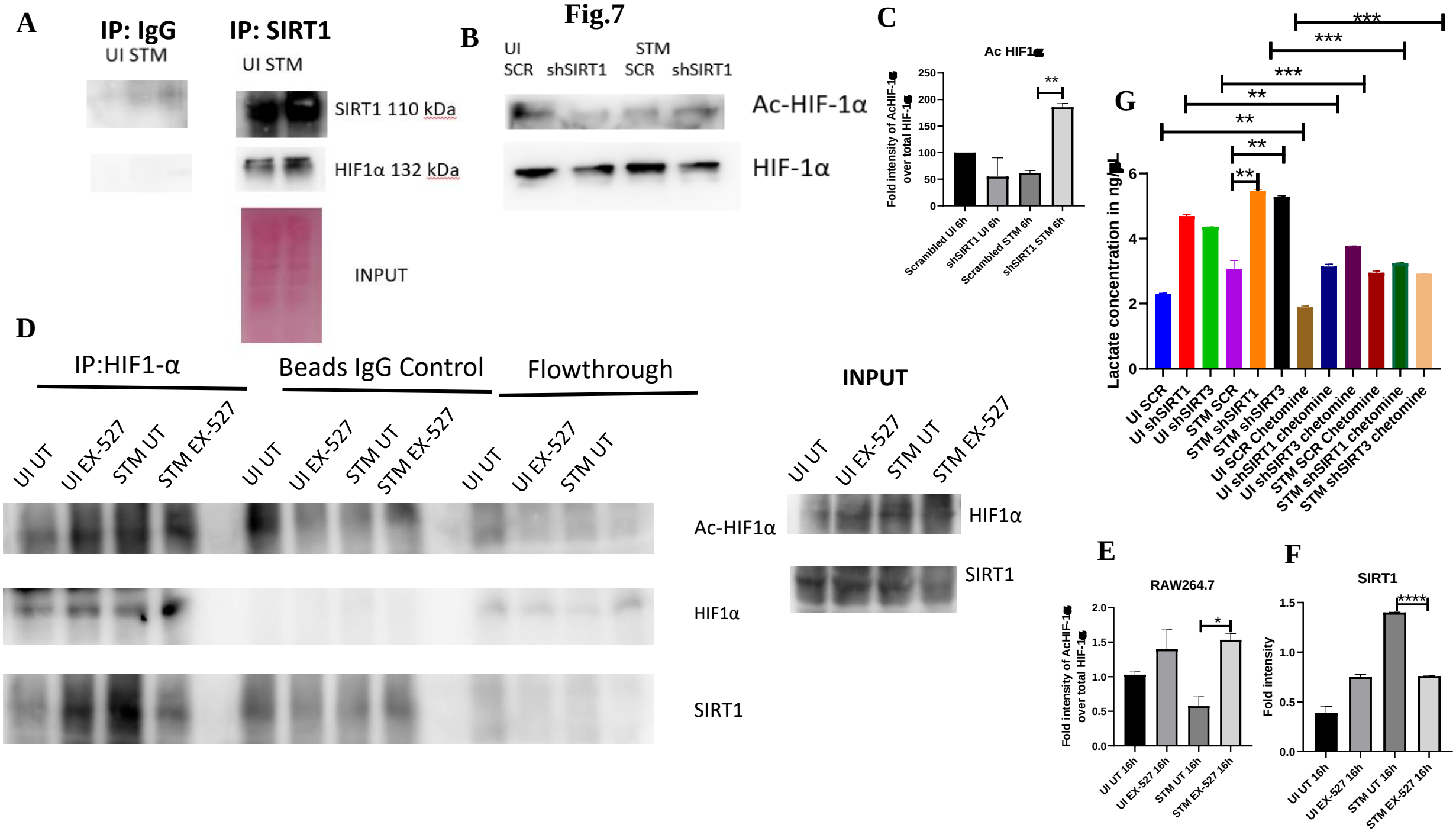
A
IP: IgG
UI STM
IP: SIRT1
UI STM
SIRT1 110 kDa
HIF1α 132 kDa
INPUT
B
UI
STM
SCR shSIRT1 SCR shSIRT1
Ac-HIF-1α
HIF-1α
C
Ac HIF1α
Fold intensity of AcHIF-1α over total HIF-1α
Scrambled UI 6h
shSIRT1 UI 6h
Scrambled STM 6h
shSIRT1 STM 6h
G
Lactate concentration in ng/mL
UI SCR
UI shSIRT1
UI shSIRT3
STM SCR
STM shSIRT1
STM shSIRT3
UI SCR Chetomine
UI shSIRT1 chetomine
UI shSIRT3 chetomine
STM SCR Chetomine
STM shSIRT1 chetomine
STM shSIRT3 chetomine
D
IP:HIF1-α
Beads IgG Control
Flowthrough
UI UT
UI EX-527
STM UT
STM EX-527
Ac-HIF1α
HIF1α
SIRT1
INPUT
HIF1α
SIRT1
E
RAW264.7
Fold intensity of AcHIF-1α over total HIF-1α
UI UT 16h
UI EX-527 16h
STM UT 16h
STM EX-527 16h
F
SIRT1
Fold intensity

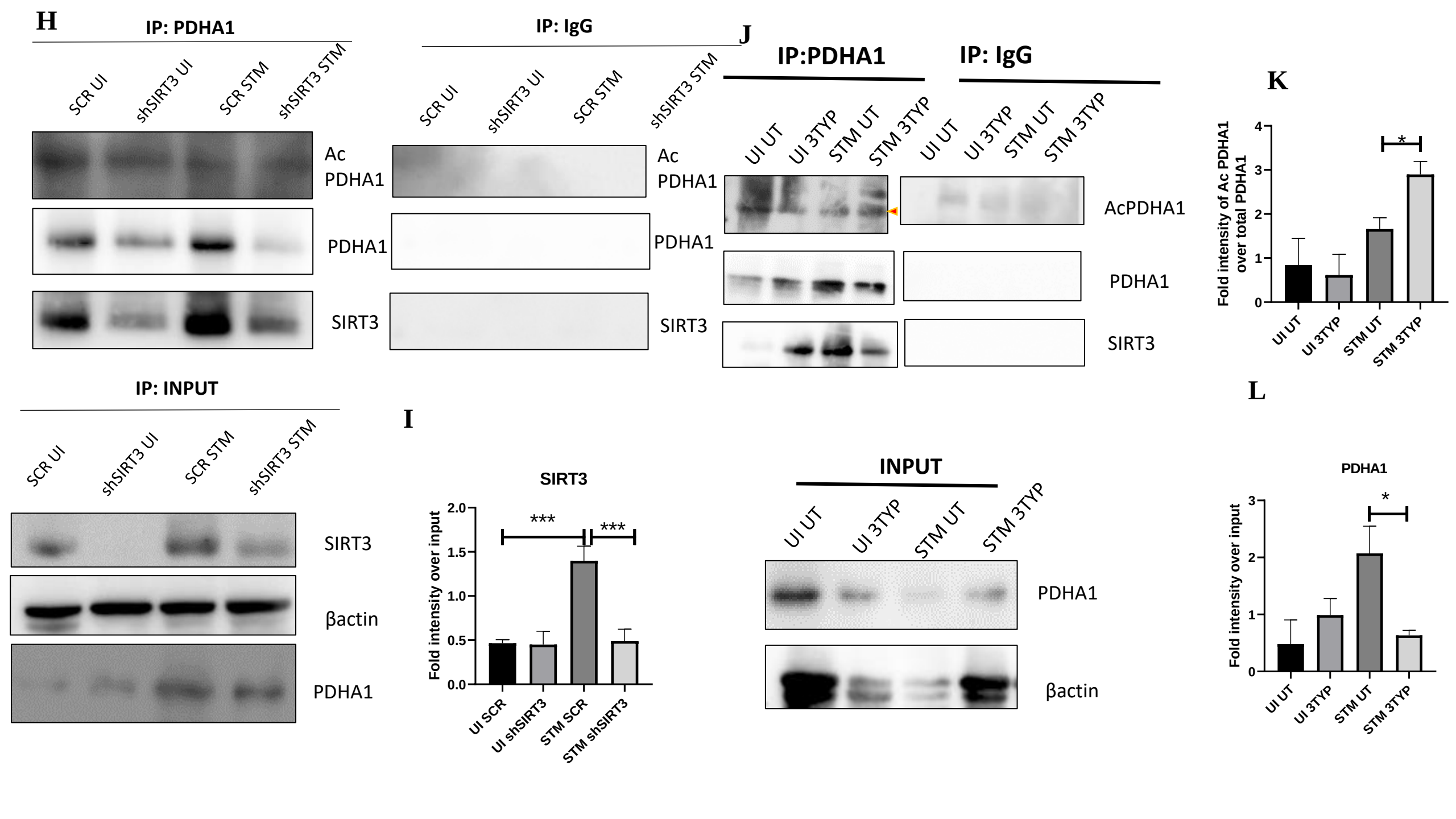
H
IP: PDHA1
SCR UI
shSIRT3 UI
SCR STM
shSIRT3 STM
Ac PDHA1
PDHA1
SIRT3
IP: IgG
SCR UI
shSIRT3 UI
SCR STM
shSIRT3 STM
Ac PDHA1
PDHA1
SIRT3
J
IP:PDHA1
IP: IgG
UI UT
UI 3TYP
STM UT
STM 3TYP
UI UT
UI 3TYP
STM UT
STM 3TYP
AcPDHA1
PDHA1
SIRT3
K
Fold intensity of Ac PDHA1 over total PDHA1
4
3
2
1
0
*
UI UT
UI 3TYP
STM UT
STM 3TYP
IP: INPUT
SCR UI
shSIRT3 UI
SCR STM
shSIRT3 STM
SIRT3
βactin
PDHA1
I
SIRT3
Fold intensity over input
2.0
1.5
1.0
0.5
0.0
***
***
UI SCR
UI shSIRT3
STM SCR
STM shSIRT3
INPUT
UI UT
UI 3TYP
STM UT
STM 3TYP
PDHA1
βactin
L
PDHA1
Fold intensity over input
3
2
1
0
*
UI UT
UI 3TYP
STM UT
STM 3TYP

Fig.8

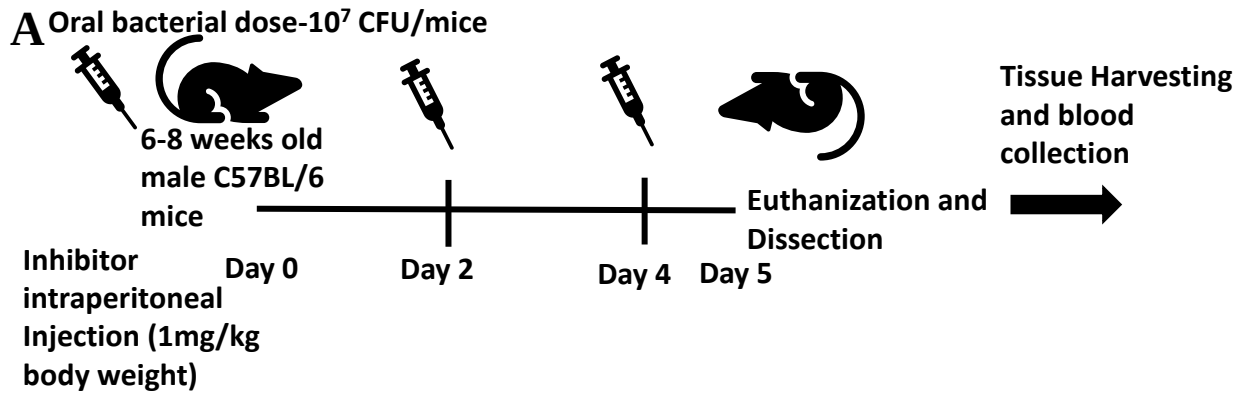
A
Oral bacterial dose-10⁷ CFU/mice
6-8 weeks old male C57BL/6 mice
Inhibitor intraperitoneal Injection (1mg/kg body weight)
Day 0
Day 2
Day 4
Day 5
Euthanization and Dissection
Tissue Harvesting and blood collection

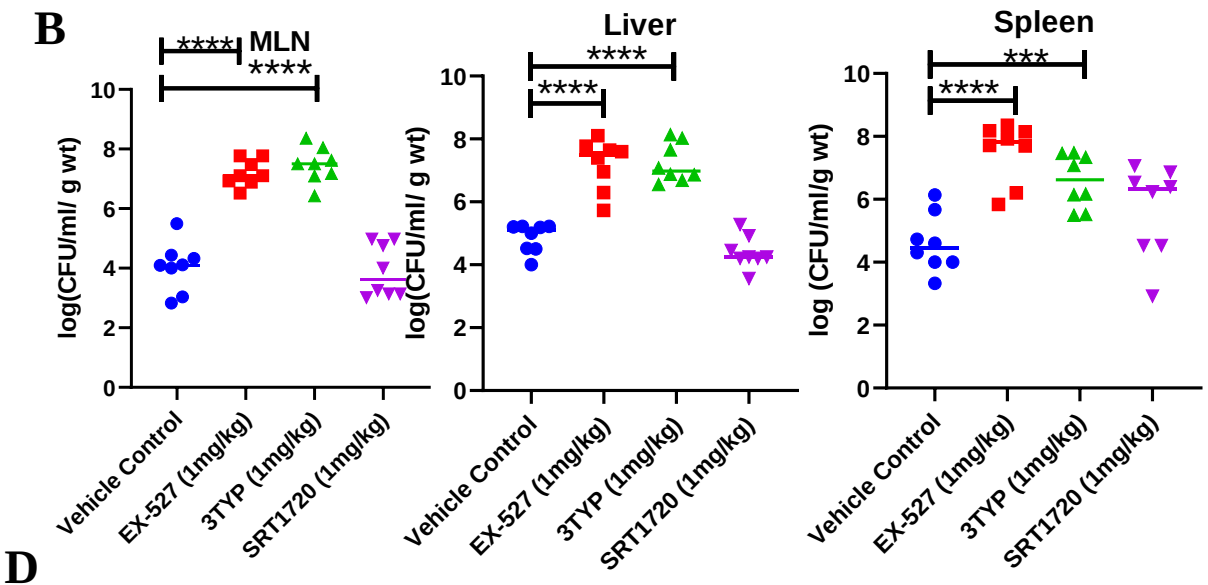
B
MLN
Liver
Spleen
log(CFU/ml/ g wt)
log (CFU/ml/g wt)
Vehicle Control
EX-527 (1mg/kg)
3TYP (1mg/kg)
SRT1720 (1mg/kg)

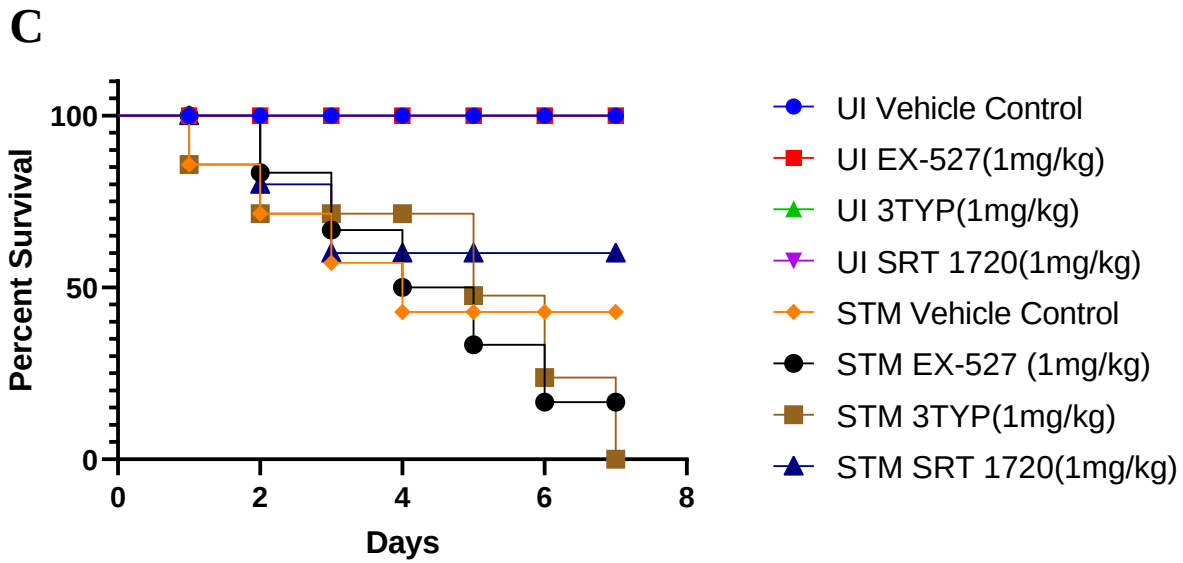
C
Percent Survival
Days
UI Vehicle Control
UI EX-527(1mg/kg)
UI 3TYP(1mg/kg)
UI SRT 1720(1mg/kg)
STM Vehicle Control
STM EX-527 (1mg/kg)
STM 3TYP(1mg/kg)
STM SRT 1720(1mg/kg)

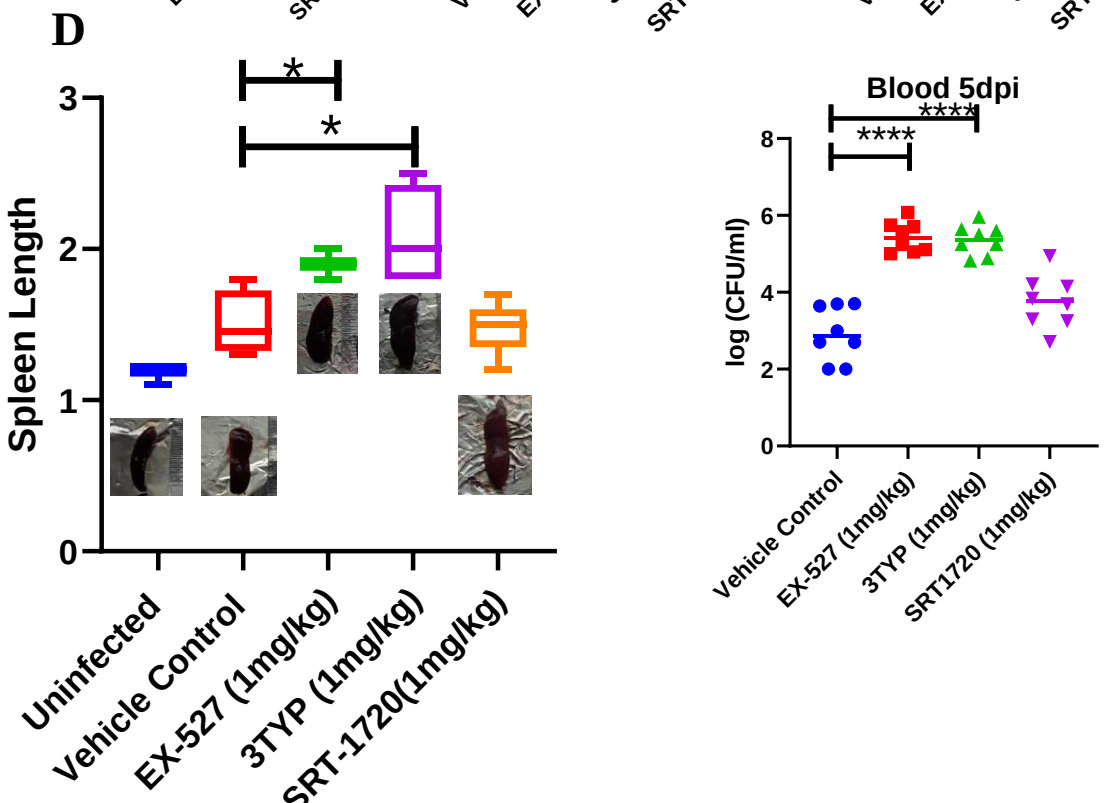
D
Spleen Length
Uninfected
Vehicle Control
EX-527 (1mg/kg)
3TYP (1mg/kg)
SRT-1720(1mg/kg)
Blood 5dpi
log (CFU/ml)

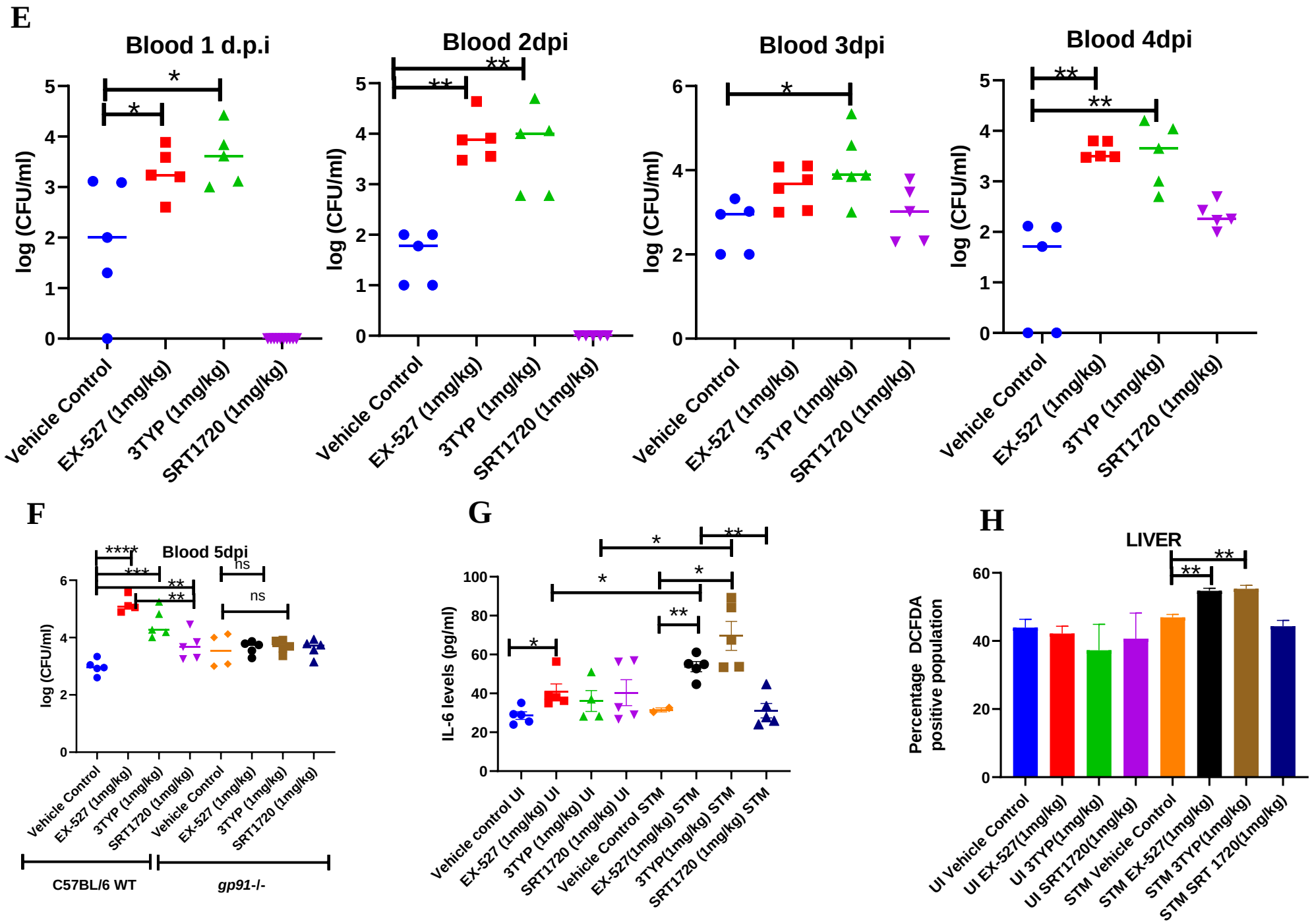
E
Blood 1 d.p.i
Blood 2dpi
Blood 3dpi
Blood 4dpi
log (CFU/ml)
Vehicle Control
EX-527 (1mg/kg)
3TYP (1mg/kg)
SRT1720 (1mg/kg)
F
Blood 5dpi
****
***
**
ns
C57BL/6 WT
gp91-/-
G
IL-6 levels (pg/ml)
Vehicle control UI
EX-527 (1mg/kg) UI
3TYP (1mg/kg) UI
SRT1720 (1mg/kg) UI
Vehicle Control STM
EX-527(1mg/kg) STM
3TYP(1mg/kg) STM
SRT1720 (1mg/kg) STM
H
LIVER
Percentage DCFDA positive population
UI Vehicle Control
UI EX-527(1mg/kg)
UI 3TYP(1mg/kg)
UI SRT1720(1mg/kg)
STM Vehicle Control
STM EX-527(1mg/kg)
STM 3TYP(1mg/kg)
STM SRT 1720(1mg/kg)

I

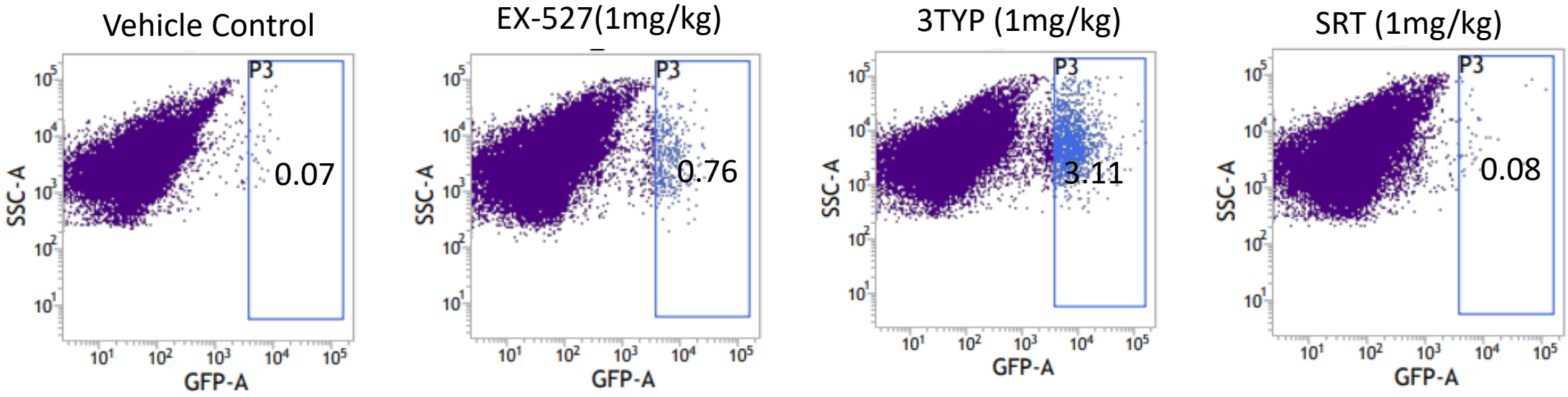
Vehicle Control
EX-527(1mg/kg)
3TYP (1mg/kg)
SRT (1mg/kg)
P3
0.07
0.76
3.11
0.08
SSC-A
GFP-A

J

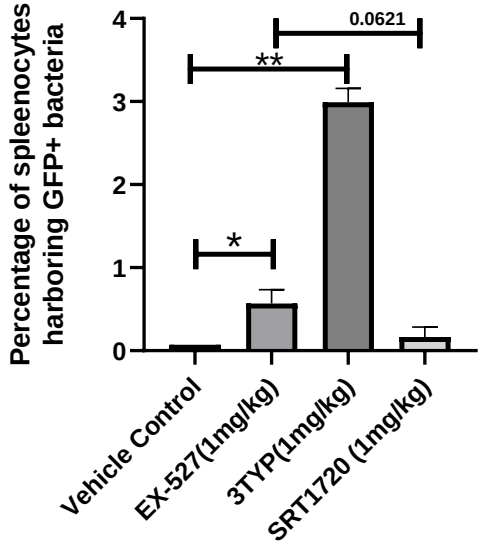
Percentage of spleenocytes harboring GFP+ bacteria
0.0621
**
*
Vehicle Control
EX-527(1mg/kg)
3TYP(1mg/kg)
SRT1720 (1mg/kg)

K

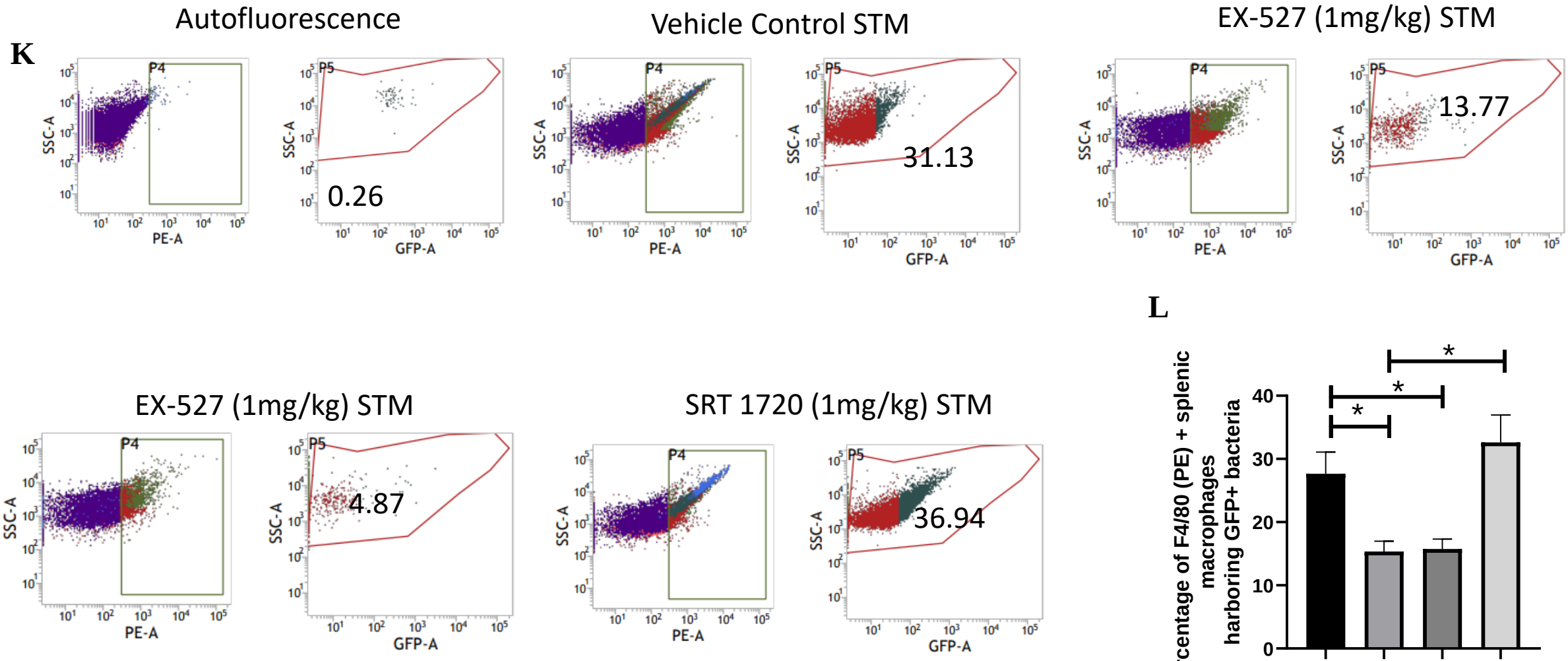
Autofluorescence
Vehicle Control STM
EX-527 (1mg/kg) STM
EX-527 (1mg/kg) STM
SRT 1720 (1mg/kg) STM
P4
P5
SSC-A
PE-A
GFP-A
0.26
31.13
13.77
4.87
36.94

L

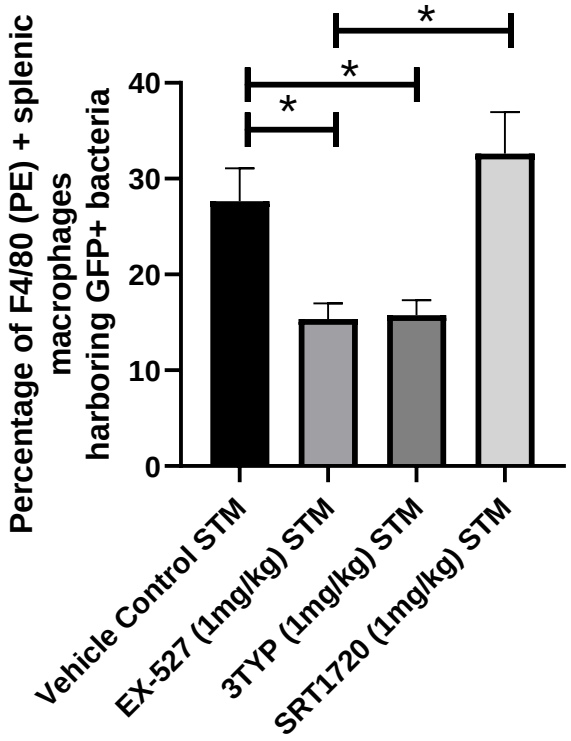
Percentage of F4/80 (PE) + splenic macrophages harboring GFP+ bacteria
0
10
20
30
40
*
*
*
Vehicle Control STM
EX-527 (1mg/kg) STM
3TYP (1mg/kg) STM
SRT1720 (1mg/kg) STM

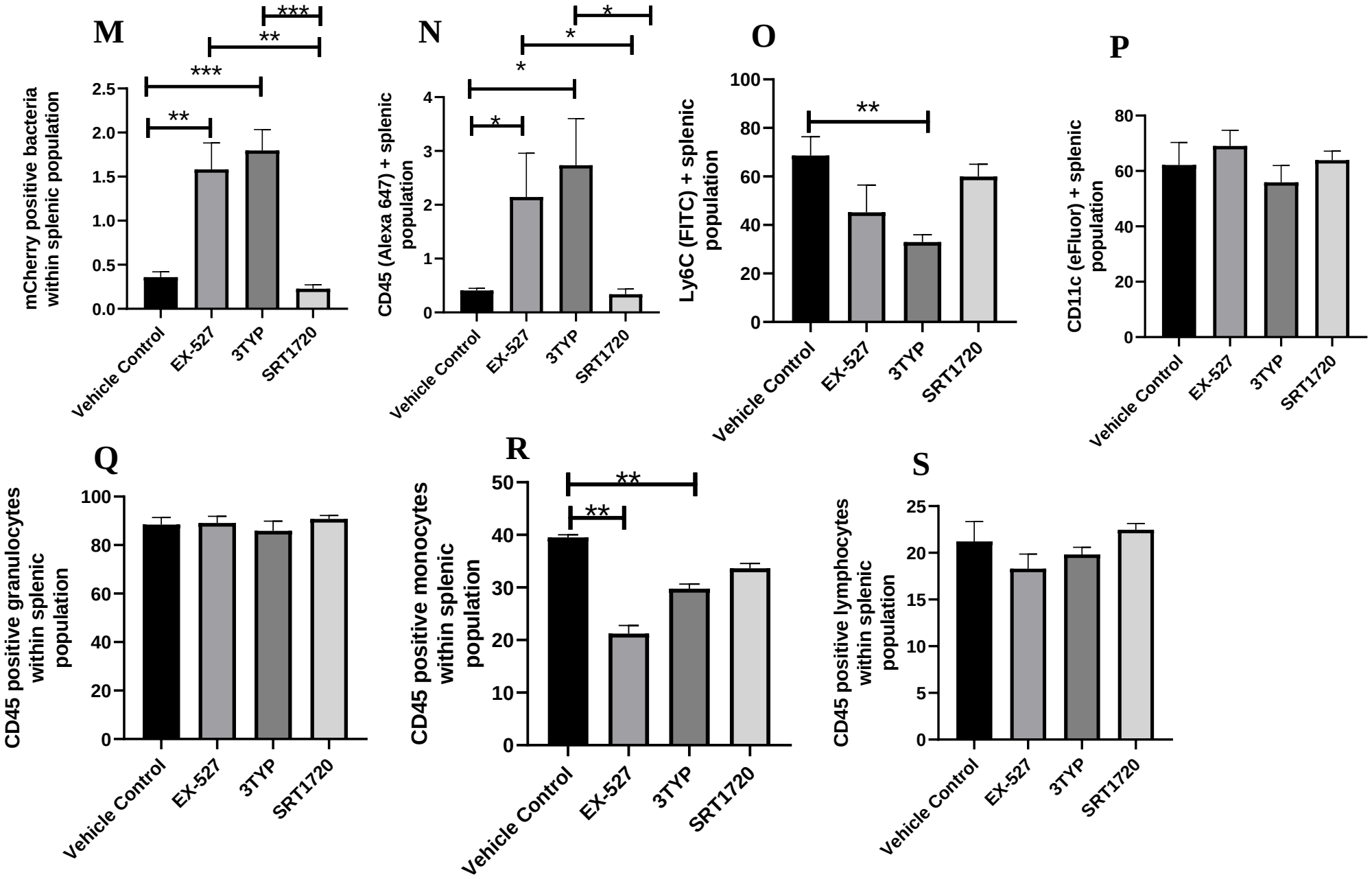
M
mCherry positive bacteria within splenic population
2.5
2.0
1.5
1.0
0.5
0.0
***
**
***
**
Vehicle Control
EX-527
3TYP
SRT1720
N
CD45 (Alexa 647) + splenic population
4
3
2
1
0
*
*
*
*
Vehicle Control
EX-527
3TYP
SRT1720
O
Ly6C (FITC) + splenic population
100
80
60
40
20
0
**
Vehicle Control
EX-527
3TYP
SRT1720
P
CD11c (eFluor) + splenic population
80
60
40
20
0
Vehicle Control
EX-527
3TYP
SRT1720
Q
CD45 positive granulocytes within splenic population
100
80
60
40
20
0
Vehicle Control
EX-527
3TYP
SRT1720
R
CD45 positive monocytes within splenic population
50
40
30
20
10
0
**
**
Vehicle Control
EX-527
3TYP
SRT1720
S
CD45 positive lymphocytes within splenic population
25
20
15
10
5
0
Vehicle Control
EX-527
3TYP
SRT1720

T

STM Vehicle Control

Score:1

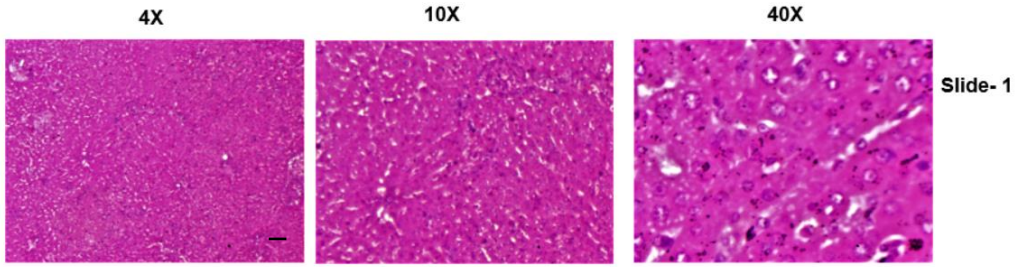

Showing minimal/ mild focal inflammatory cell collections in lobular parenchyma

STM SRT1720 (1mg/kg)

Score-1

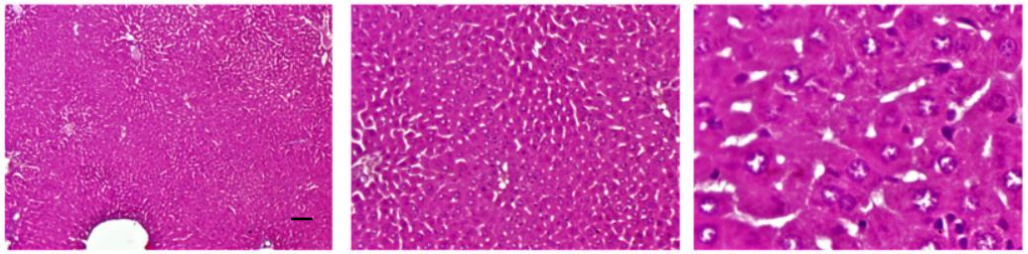

Showing minimal/ mild pathology in lobular parenchyma with normal hepatic architecture

STM EX-527(1mg/kg)

Score : 3

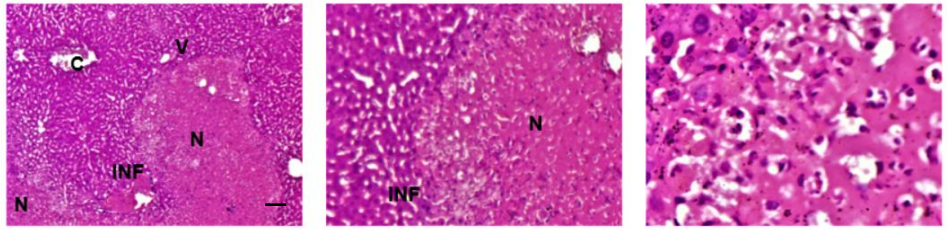

Showing multiple (small and big areas) severe acute hepatic necrosis (N), with complete loss of hepatic architecture due to loss of hepatic cells, the necrotic area filled with edema and surrounded by inflammatory cells, hepatocytes with cytoplasmic vacuolation (V), inflammatory cells (INF), and damage of the endothelial lining of central vein (C)

STM 3TYP (1mg/kg)

Score-3

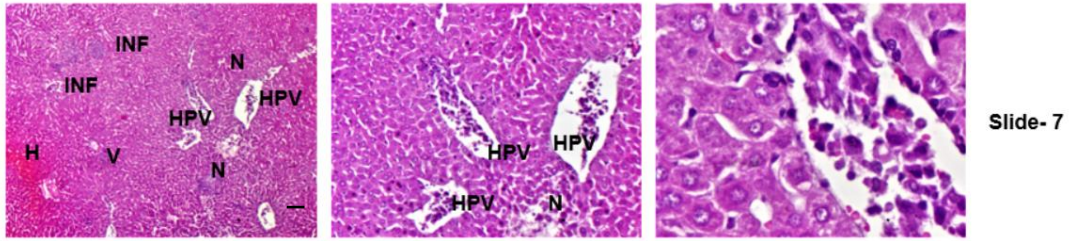

Showing small multiple necrotic foci (N), severe blood hemorrhage (H) congested hepatic portal veins of liver clogged with clumps and inflammatory cell infiltrates (HPV) vacuolar degeneration (V). Multiple Microgranuloma formation with the aggregation of inflammatory cells (INF)

Score-0 UI Vehicle Control

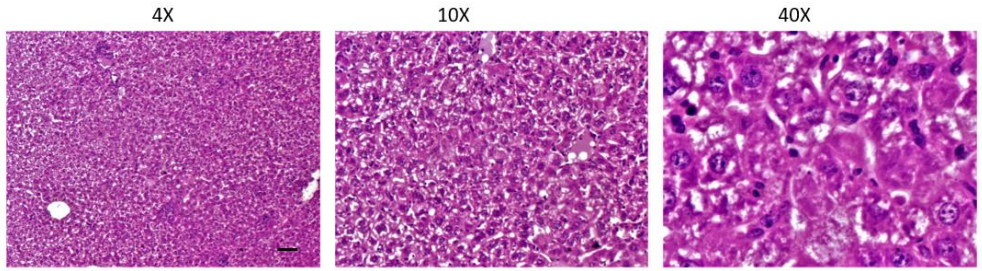

normal pathology with normal hepatic architecture

Score-0 UI SRT1720 (1mg/kg)

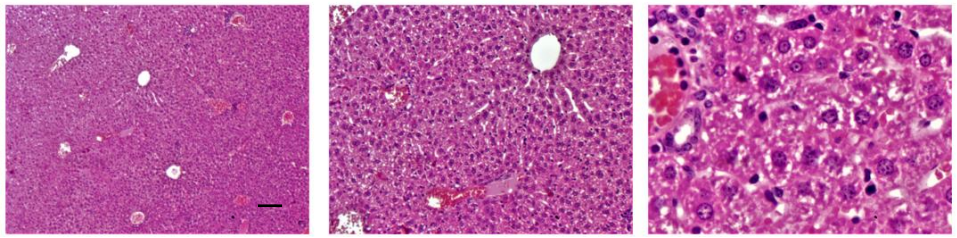

normal pathology with normal hepatic architecture

Score-1 UI EX-527(1mg/kg)

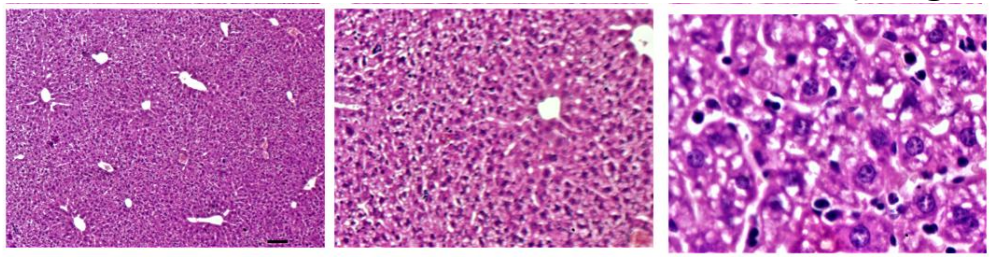

Showing minimal/ mild focal inflammatory cell collections in lobular parenchyma

Score-1 UI 3TYP (1mg/kg)

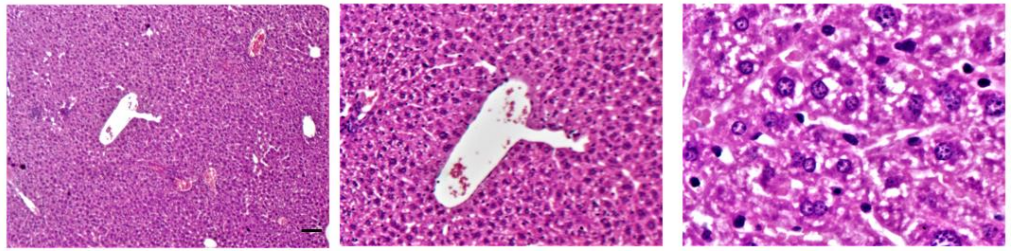

Showing minimal/ mild focal inflammatory cell collections in lobular parenchyma

U

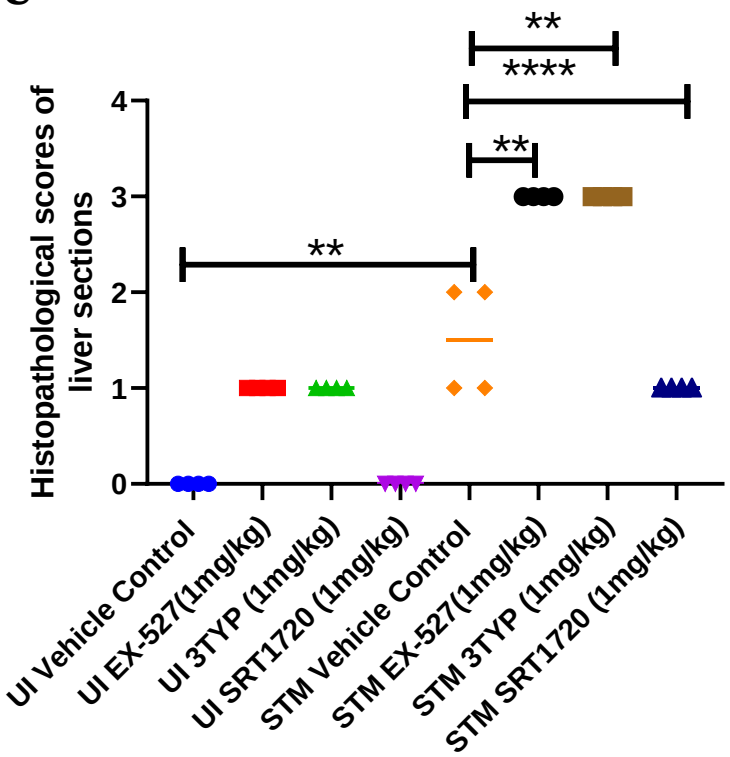

V

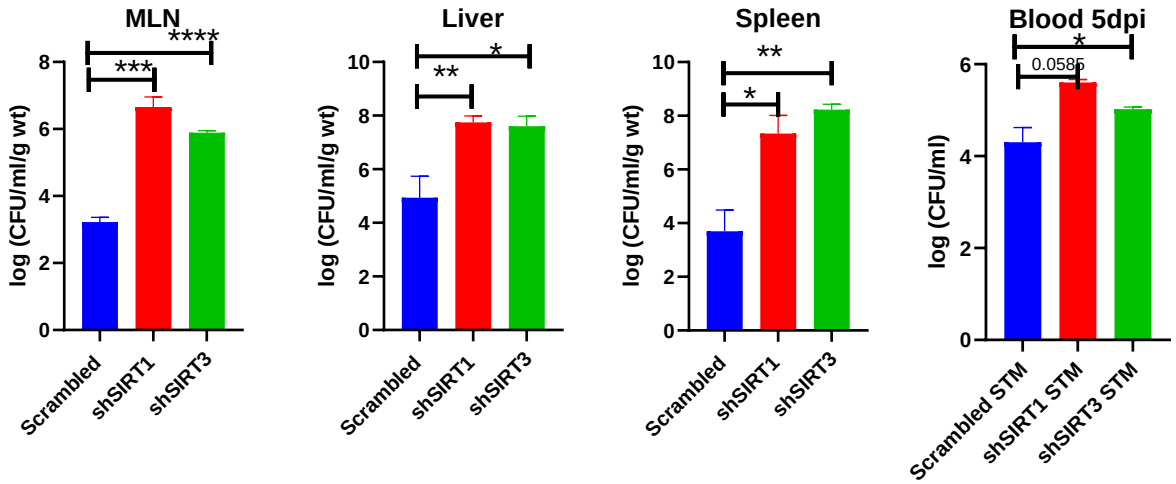

W

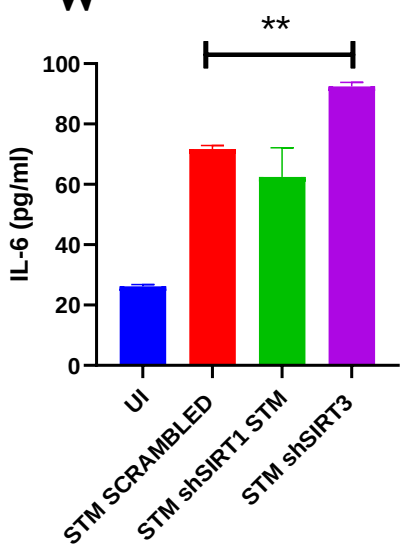

X

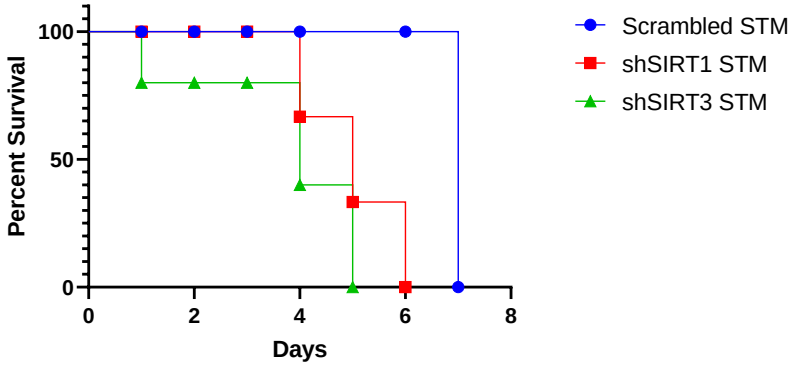

Y

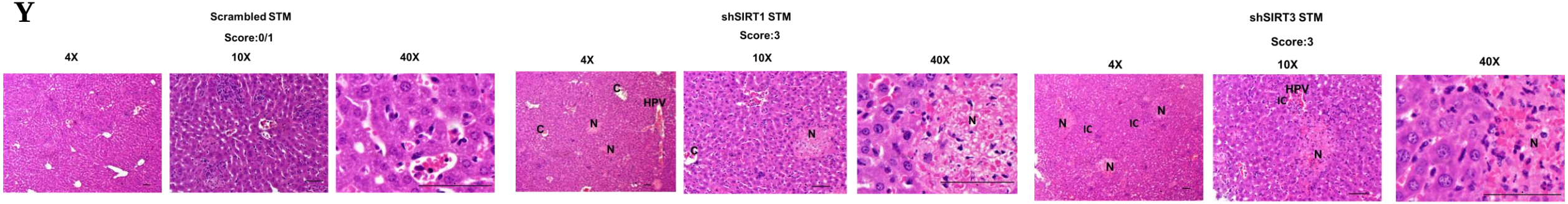

Showing normal hepatic architecture with some area immune cell accumulation

Showing multiple necrotic areas (N), congestion and damage to the endothelial lining of the central vein (C), congestion of the hepatic portal vein (HPV), and severe infiltration of inflammatory immune cells(IC),

Showing multiple necrotic areas (N), congestion of the hepatic portal vein (HPV) and severe infiltration of inflammatory immune cells(IC),

MANUSCRIPT_1 TITLE:

***Salmonella*-induced SIRT1 and SIRT3 are crucial for maintaining the metabolic switch in bacteria and host for successful pathogenesis**

SUPPLEMENTARY FIGURES

Fig. S1

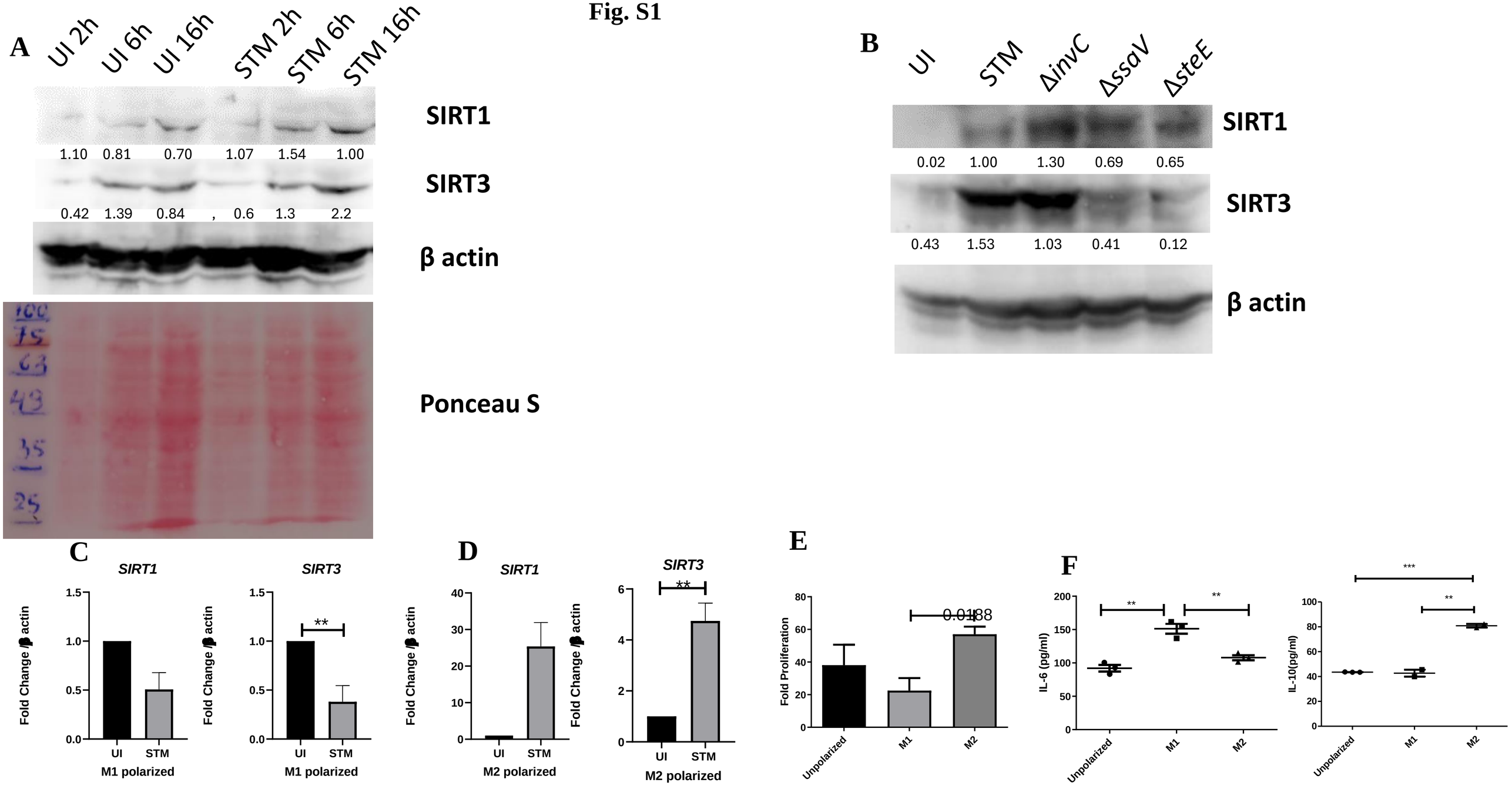
A
UI 2h
UI 6h
UI 16h
STM 2h
STM 6h
STM 16h
SIRT1
1.10 0.81 0.70 1.07 1.54 1.00
SIRT3
0.42 1.39 0.84 , 0.6 1.3 2.2
β actin
Ponceau S
B
UI
STM
ΔinvC
ΔssaV
ΔsteE
SIRT1
0.02 1.00 1.30 0.69 0.65
SIRT3
0.43 1.53 1.03 0.41 0.12
β actin
C
SIRT1
SIRT3
Fold Change /β actin
UI
STM
M1 polarized
**
D
SIRT1
SIRT3
M2 polarized
E
Fold Proliferation
0.0188
Unpolarized
M1
M2
F
IL-6 (pg/ml)
IL-10(pg/ml)
***

Fig. S2

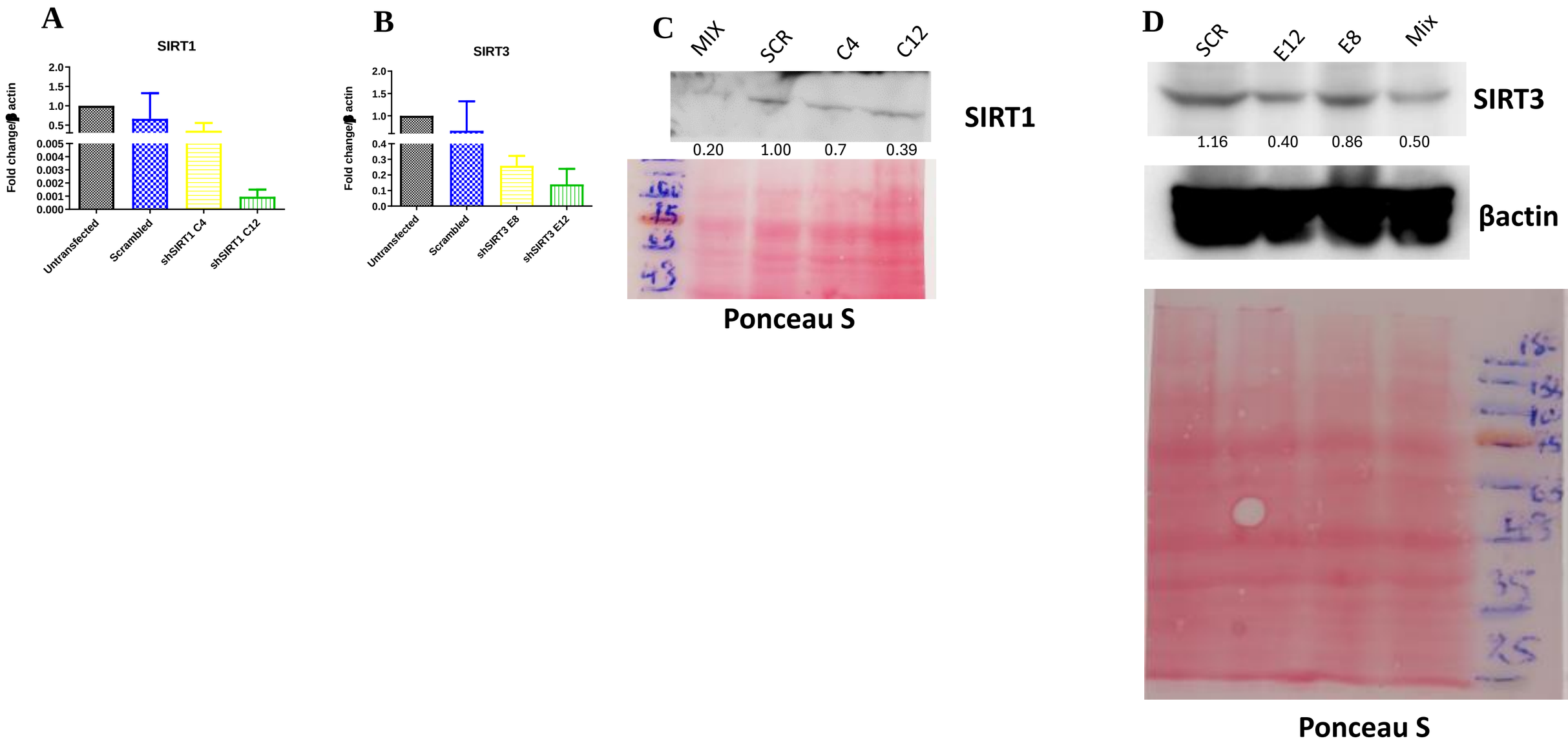
A
SIRT1
Fold change/β actin
2.0
1.5
1.0
0.5
0.005
0.004
0.003
0.002
0.001
0.000
Untransfected
Scrambled
shSIRT1 C4
shSIRT1 C12
B
SIRT3
Fold change/β actin
2.0
1.5
1.0
0.4
0.3
0.2
0.1
0.0
Untransfected
Scrambled
shSIRT3 E8
shSIRT3 E12
C
MIX
SCR
C4
C12
0.20
1.00
0.7
0.39
SIRT1
Ponceau S
D
SCR
E12
E8
Mix
1.16
0.40
0.86
0.50
SIRT3
βactin
Ponceau S

Fig. S3

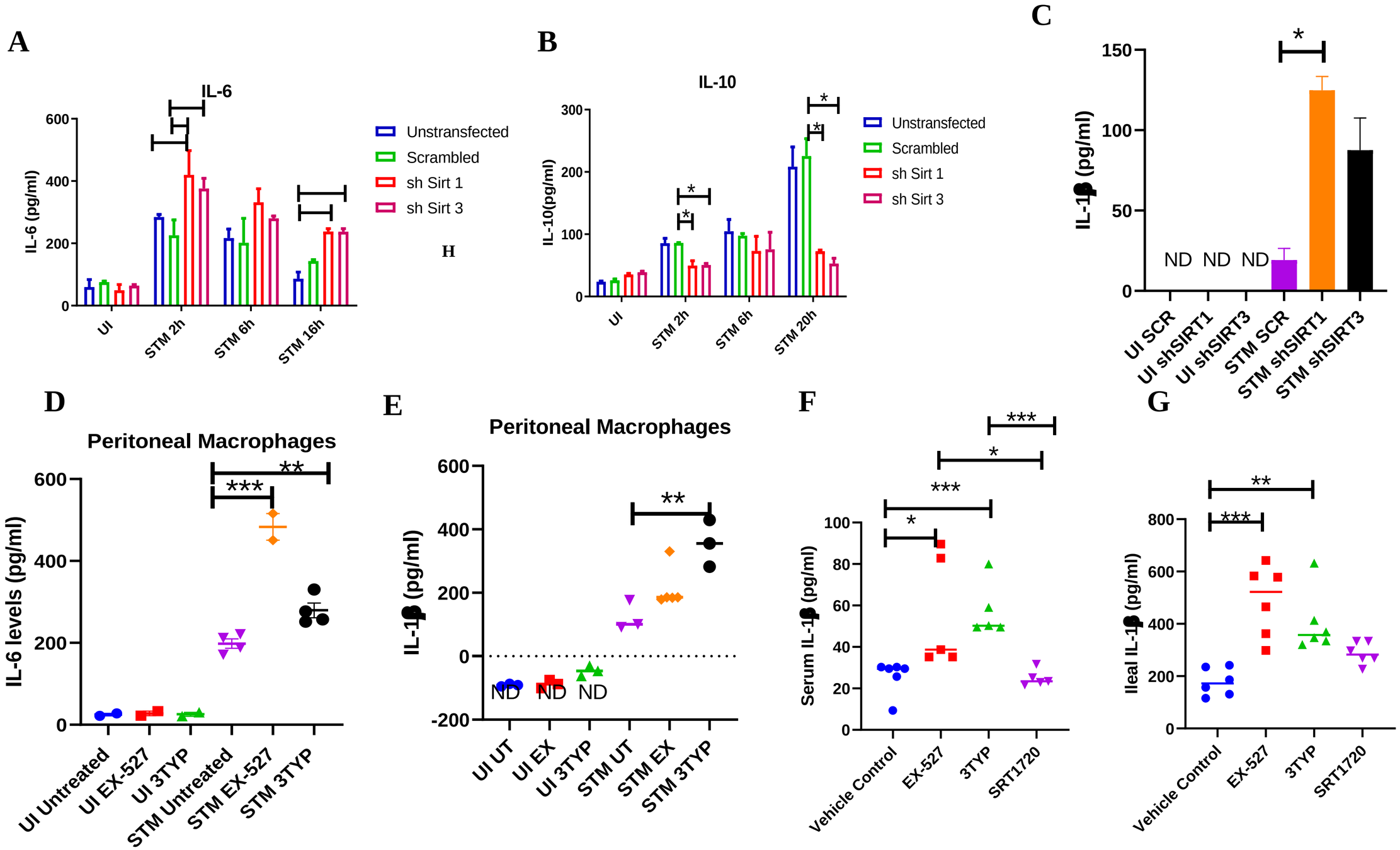
A
IL-6
IL-6 (pg/ml)
600
400
200
0
UI
STM 2h
STM 6h
STM 16h
Unstransfected
Scrambled
sh Sirt 1
sh Sirt 3
H
B
IL-10
IL-10(pg/ml)
300
200
100
0
UI
STM 2h
STM 6h
STM 20h
Unstransfected
Scrambled
sh Sirt 1
sh Sirt 3
C
IL-1β (pg/ml)
150
100
50
0
ND ND ND
UI SCR
UI shSIRT1
UI shSIRT3
STM SCR
STM shSIRT1
STM shSIRT3
D
Peritoneal Macrophages
IL-6 levels (pg/ml)
600
400
200
0
UI Untreated
UI EX-527
UI 3TYP
STM Untreated
STM EX-527
STM 3TYP
E
Peritoneal Macrophages
IL-1β (pg/ml)
600
400
200
0
-200
ND ND ND
UI UT
UI EX
UI 3TYP
STM UT
STM EX
STM 3TYP
F
Serum IL-1β (pg/ml)
100
80
60
40
20
0
Vehicle Control
EX-527
3TYP
SRT1720
G
Ileal IL-1β (pg/ml)
800
600
400
200
0
Vehicle Control
EX-527
3TYP
SRT1720

Fig. S4

A

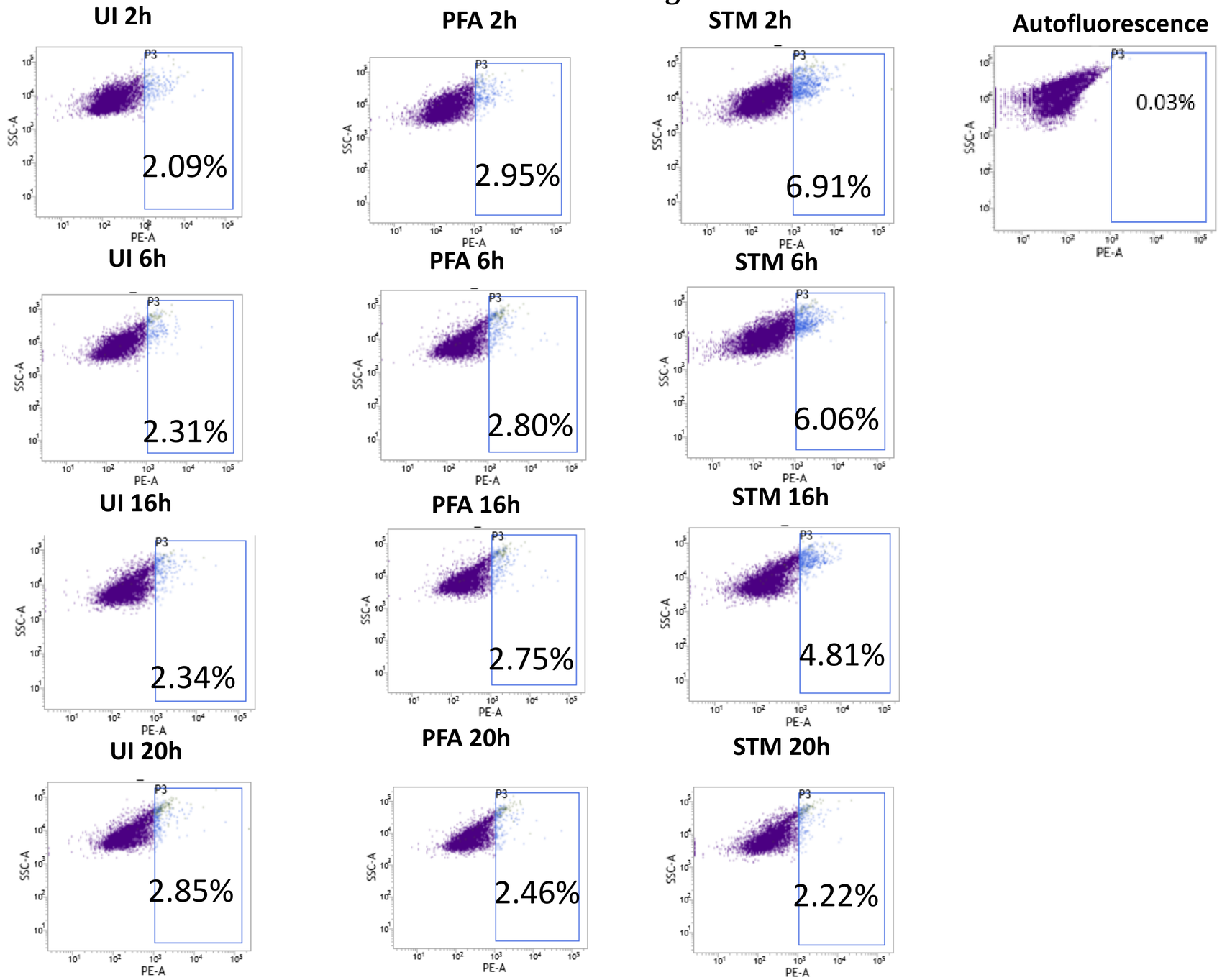
UI 2h
2.09%
PFA 2h
2.95%
STM 2h
6.91%
Autofluorescence
0.03%
UI 6h
2.31%
PFA 6h
2.80%
STM 6h
6.06%
UI 16h
2.34%
PFA 16h
2.75%
STM 16h
4.81%
UI 20h
2.85%
PFA 20h
2.46%
STM 20h
2.22%
P3
SSC-A
PE-A

B

UI SCRAMBLED 2h

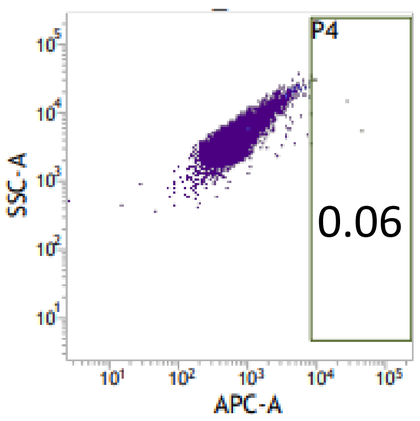

STM SCRAMBLED 2h

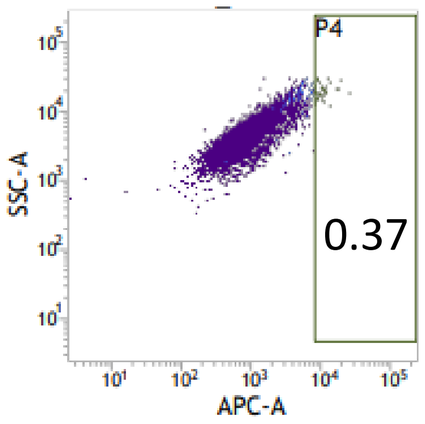

STM shSIRT1 2h

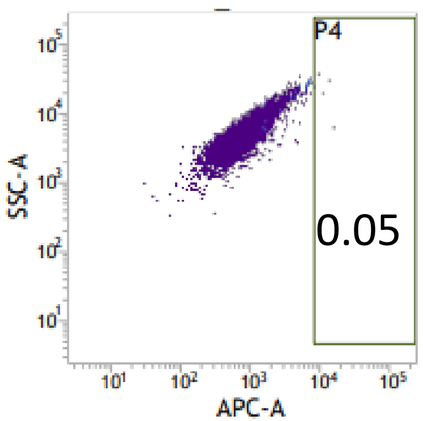

STM shSIRT3 2h

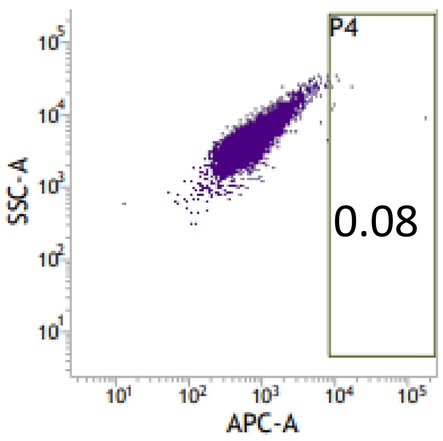

Autofluorescence

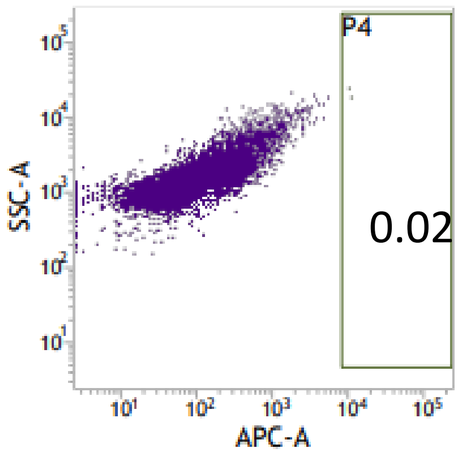

UI SCRAMBLED 16h

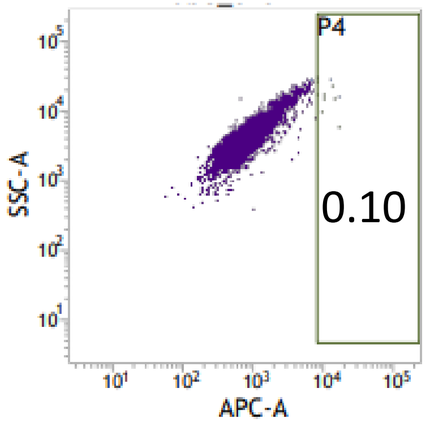

STM SCRAMBLED 16h

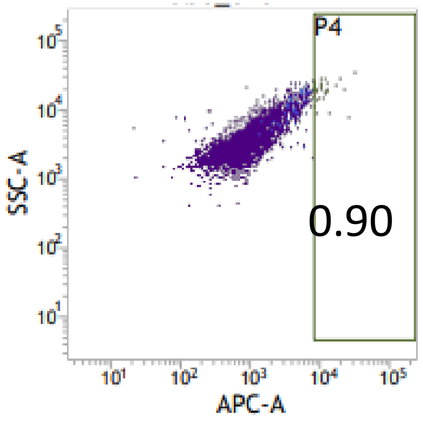

STM shSIRT1 16h

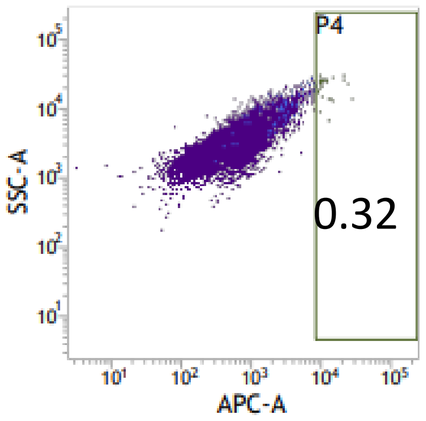

STM shSIRT3 16h

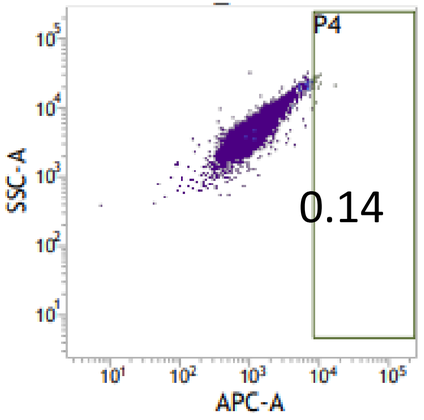

Fig.S5

A

Untransfected STM 16h

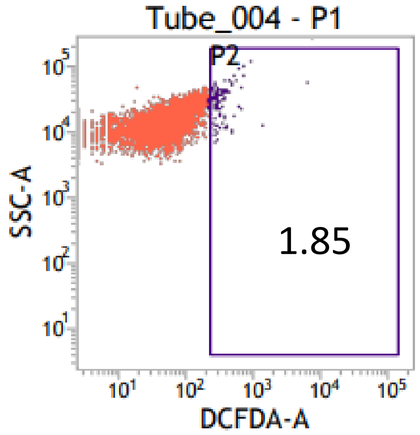

Scrambled STM 16h

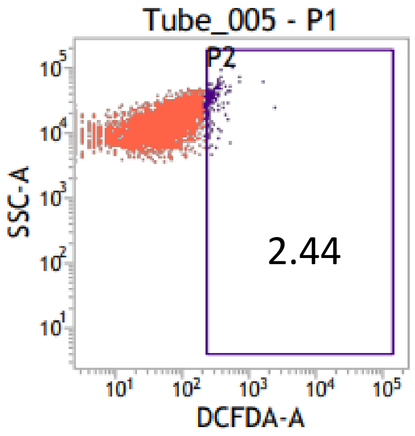

Uninfected 16h

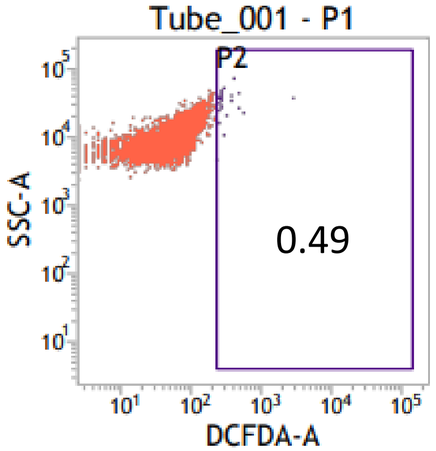

shSIRT1 STM 16h

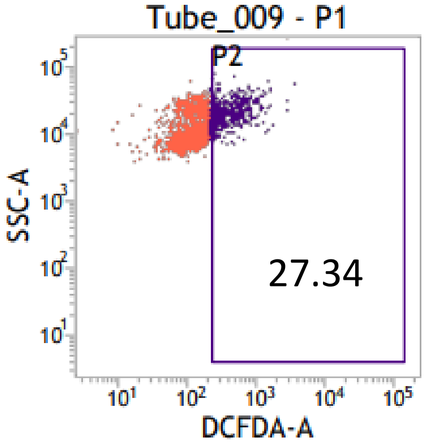

shSIRT3 STM 16h

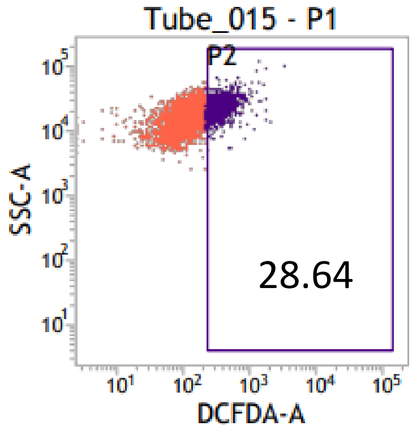

B

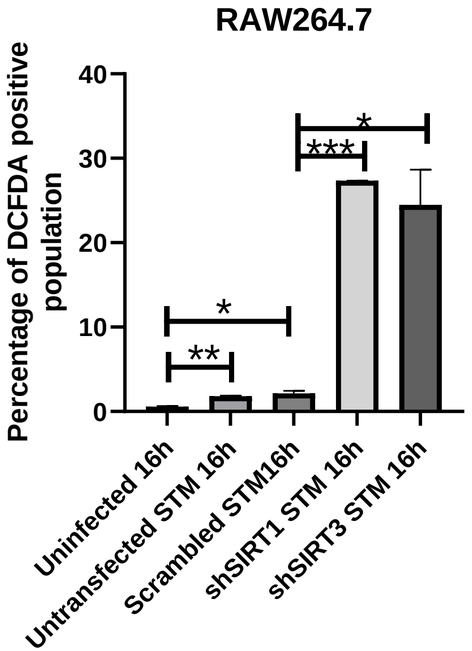

C

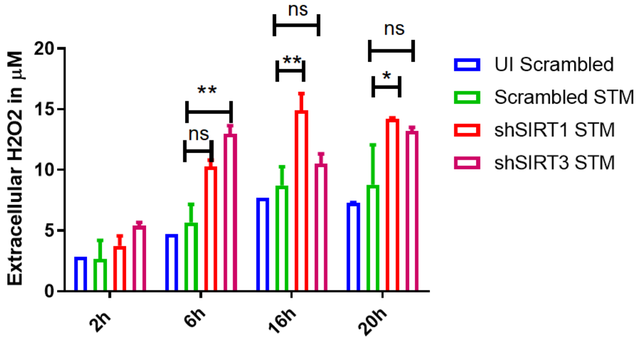

Fig.S6

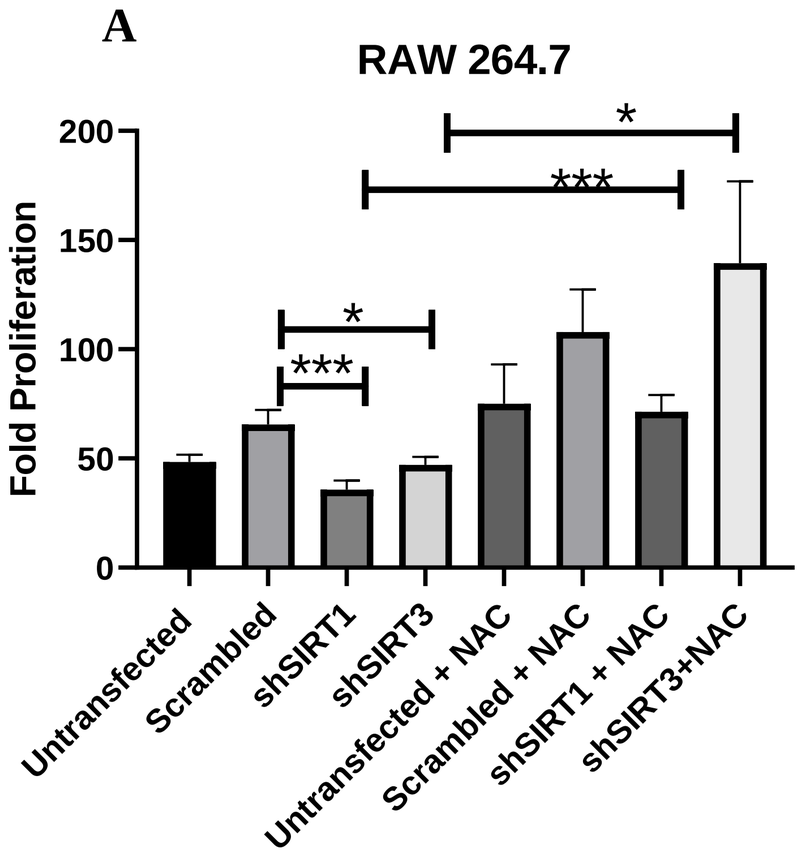
A
RAW 264.7
Fold Proliferation
200
150
100
50
0
*
***
*
***
Untransfected
Scrambled
shSIRT1
shSIRT3
Untransfected + NAC
Scrambled + NAC
shSIRT1 + NAC
shSIRT3+NAC

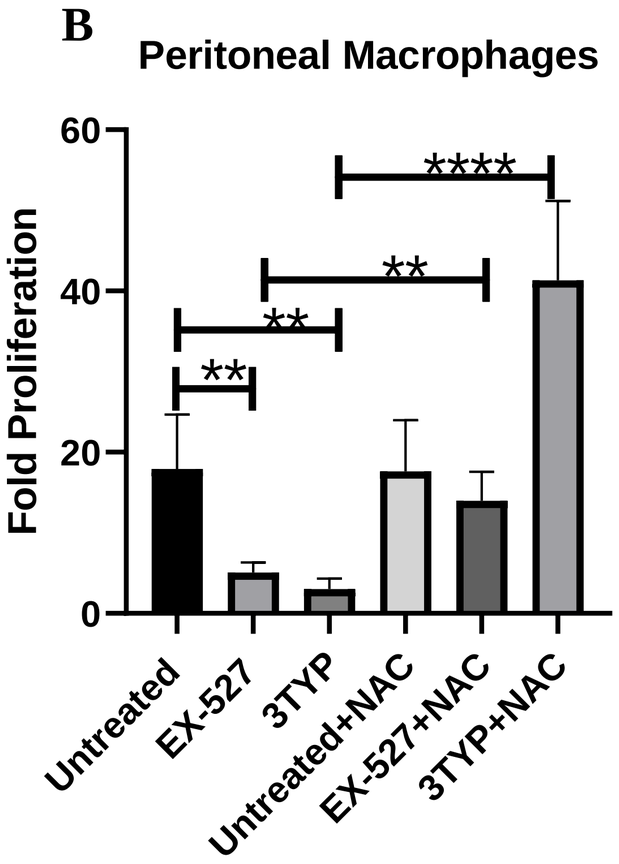
B
Peritoneal Macrophages
Fold Proliferation
60
40
20
0
****
**
**
**
Untreated
EX-527
3TYP
Untreated+NAC
EX-527+NAC
3TYP+NAC

Fig.S7

A

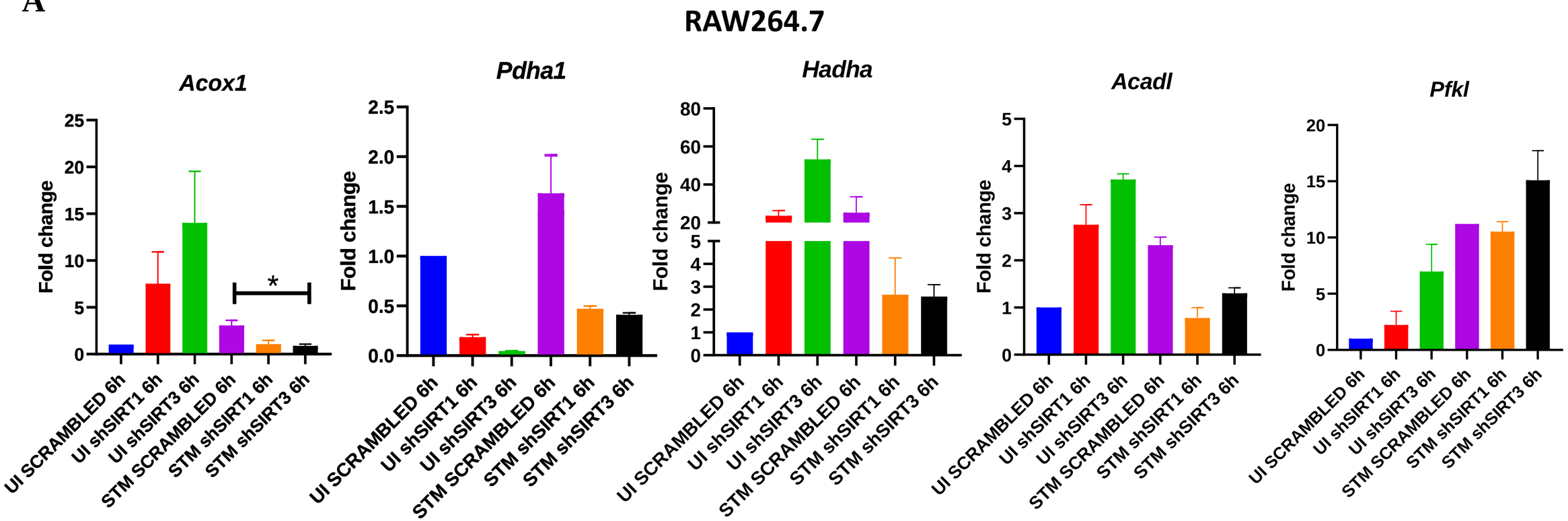
RAW264.7
Acox1
Pdha1
Hadha
Acadl
Pfkl
Fold change
*
UI SCRAMBLED 6h
UI shSIRT1 6h
UI shSIRT3 6h
STM SCRAMBLED 6h
STM shSIRT1 6h
STM shSIRT3 6h

Peritoneal Macrophages

B

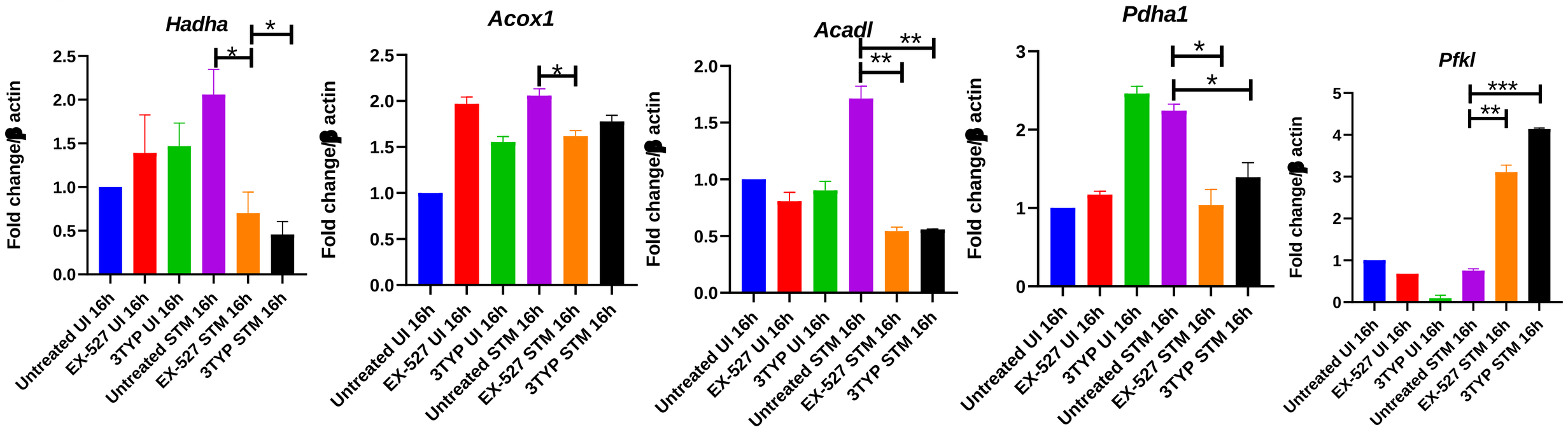

C

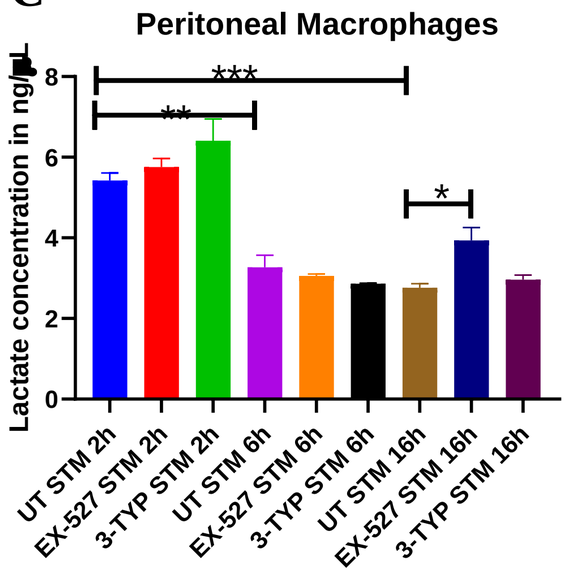

D

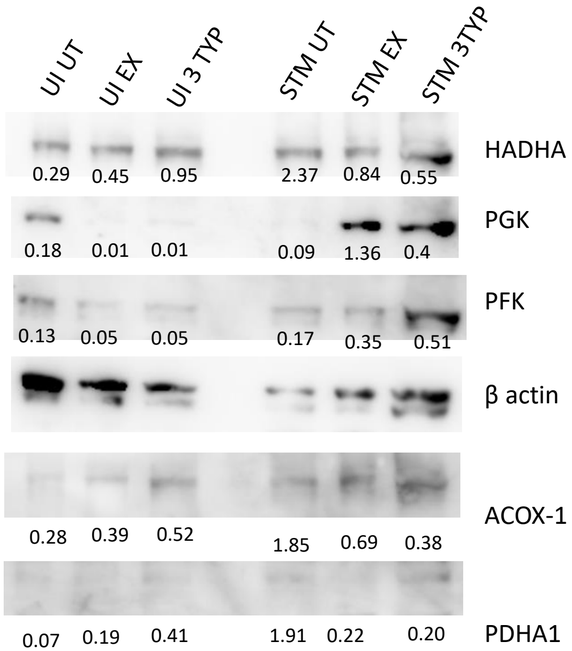

E

LIVER

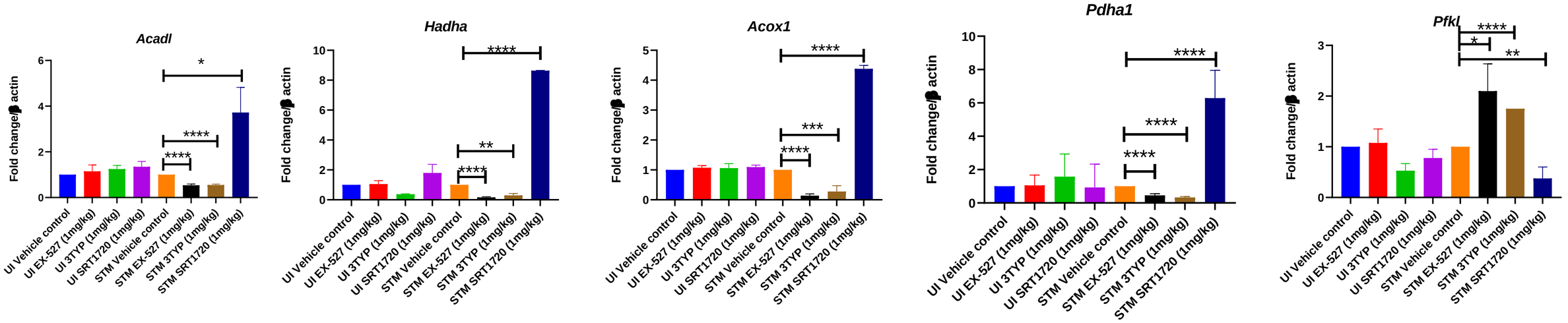

F

SPLEEN

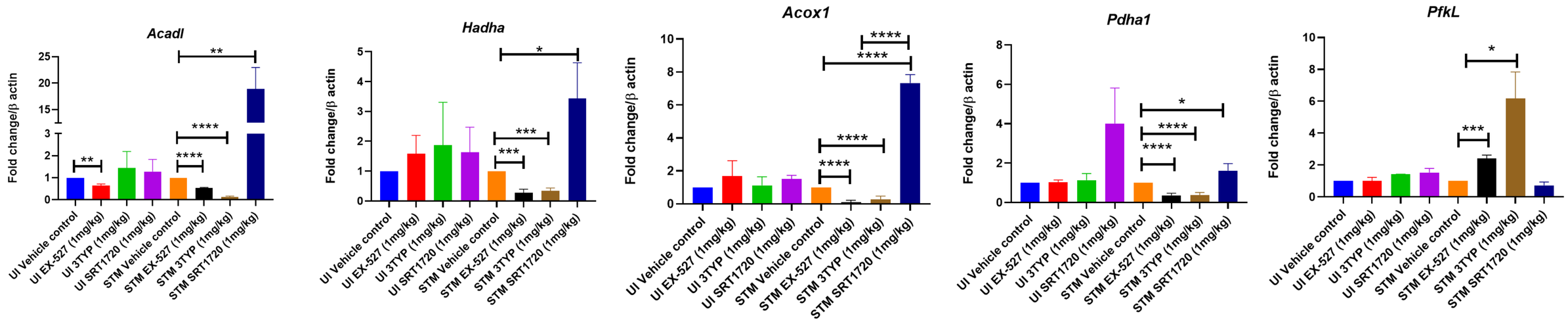

Fig.S8

A

Vehicle Control STM

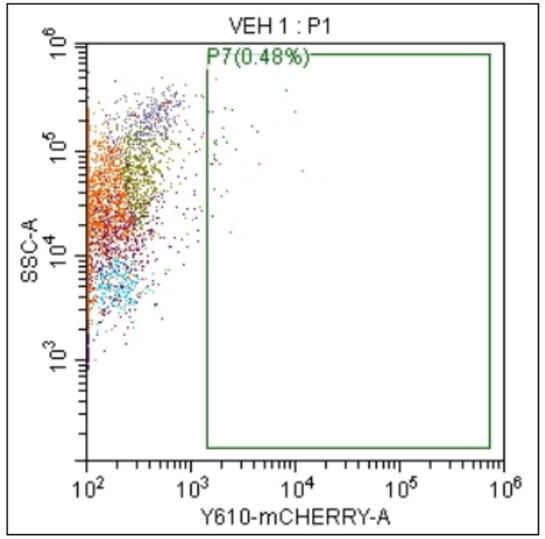

EX-527

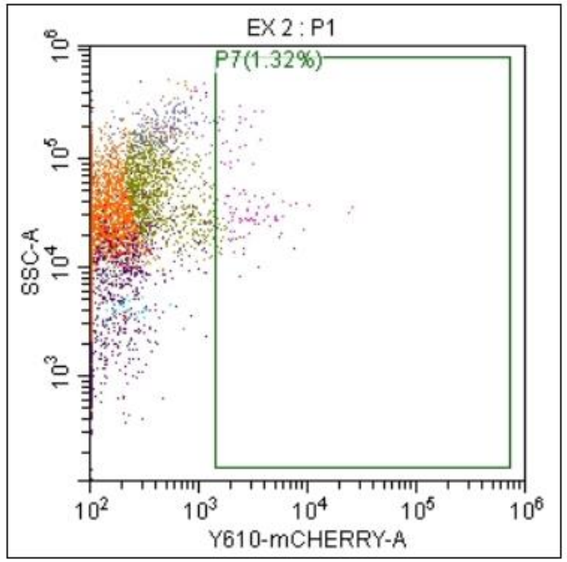

3TYP

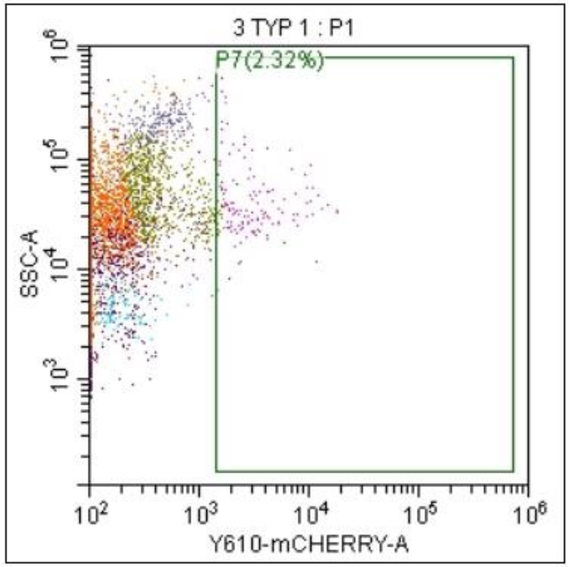

SRT1720

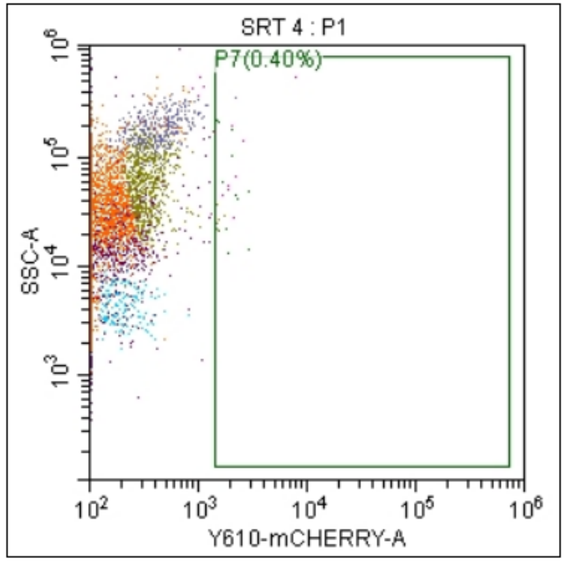

B

Vehicle Control STM

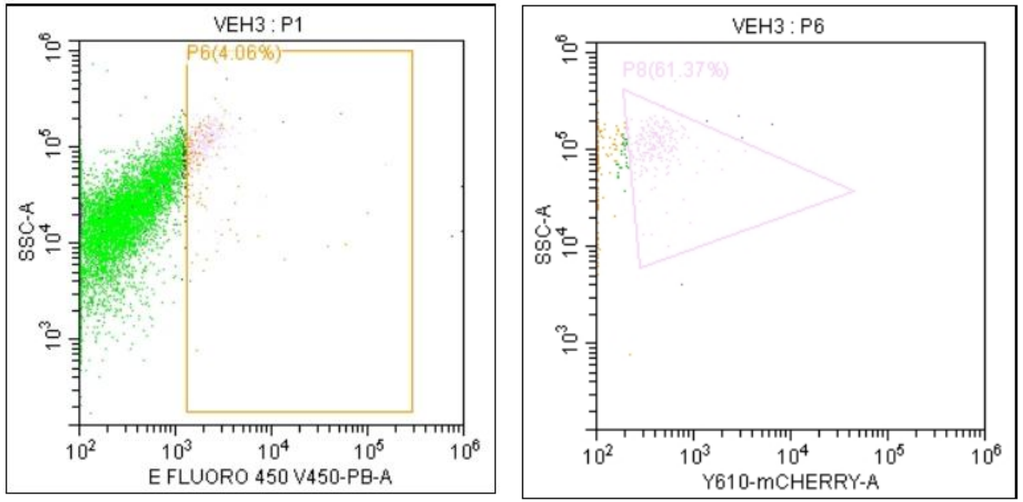

EX-527

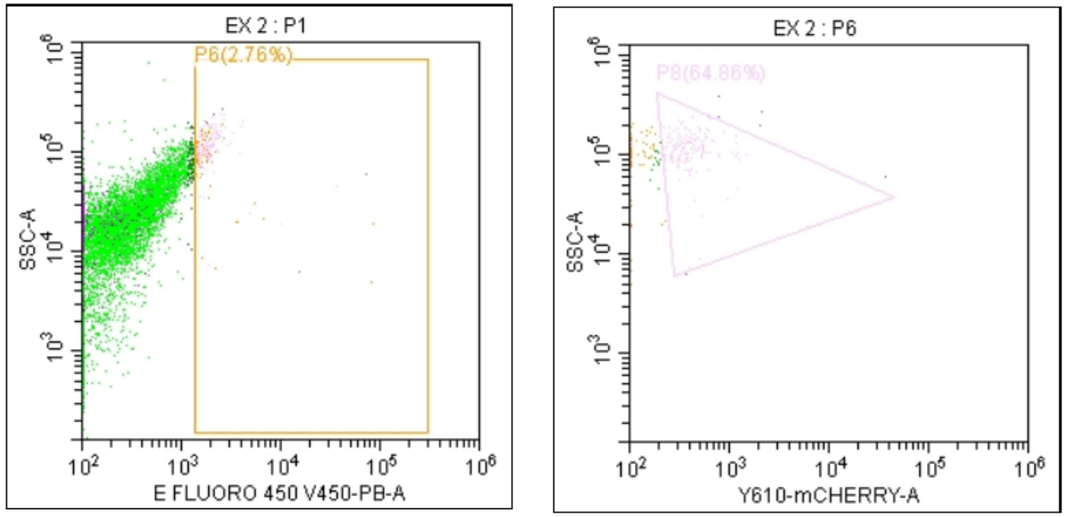

3TYP

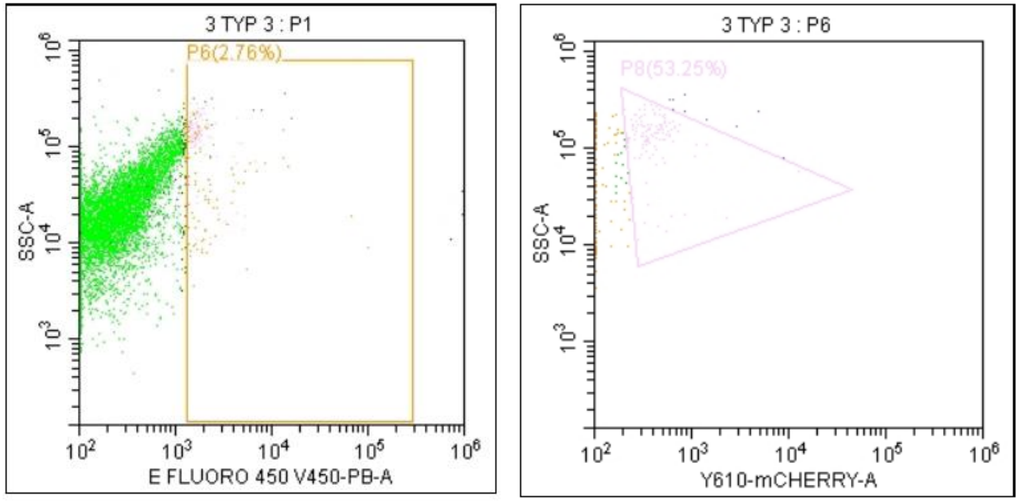

SRT1720

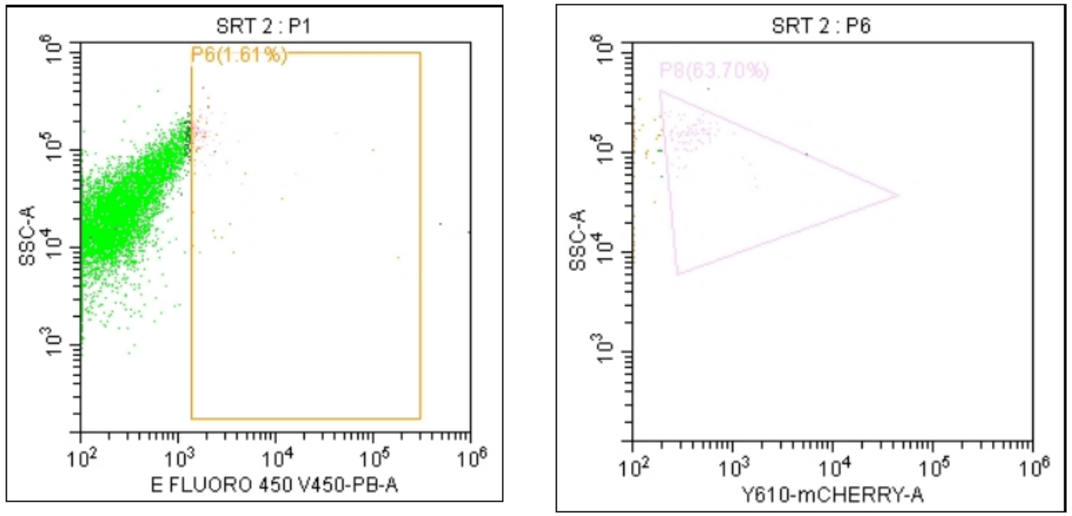

eFluor 450 CD11c+ population

C

Vehicle Control STM

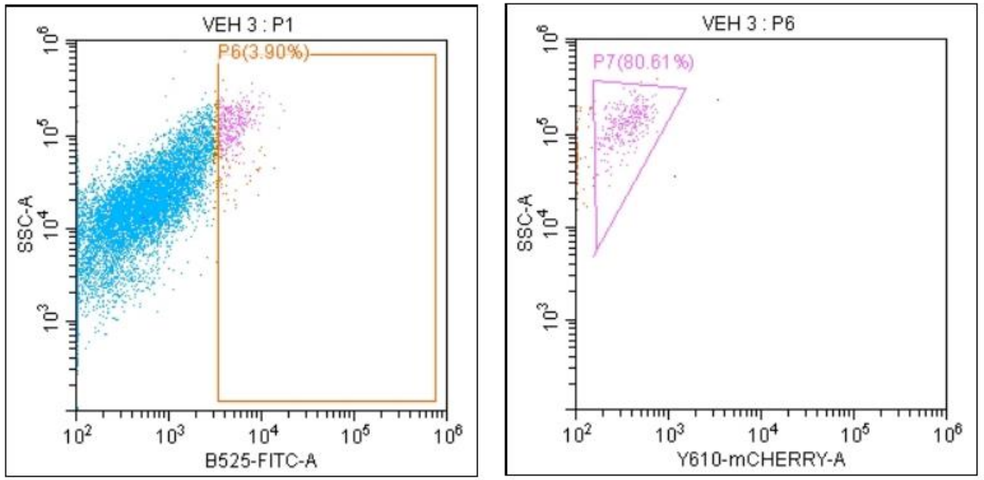

EX-527

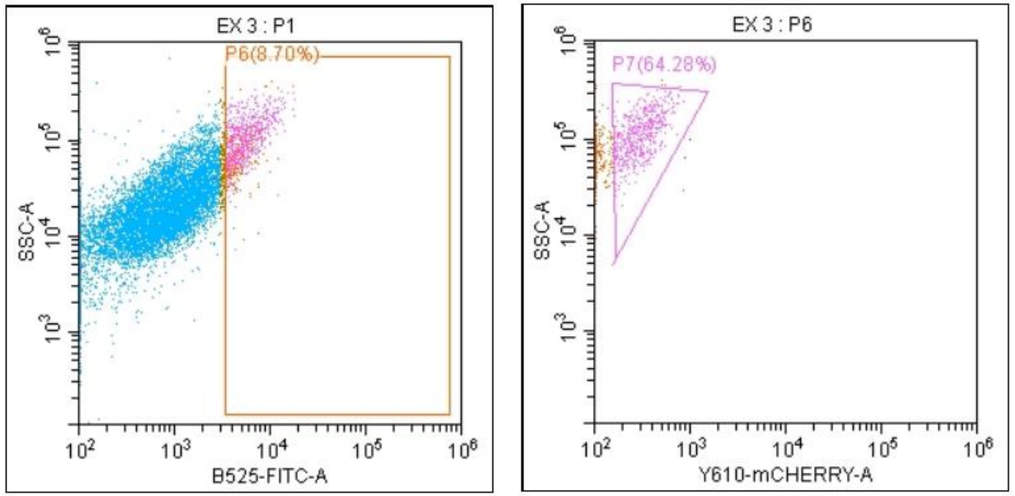

3TYP

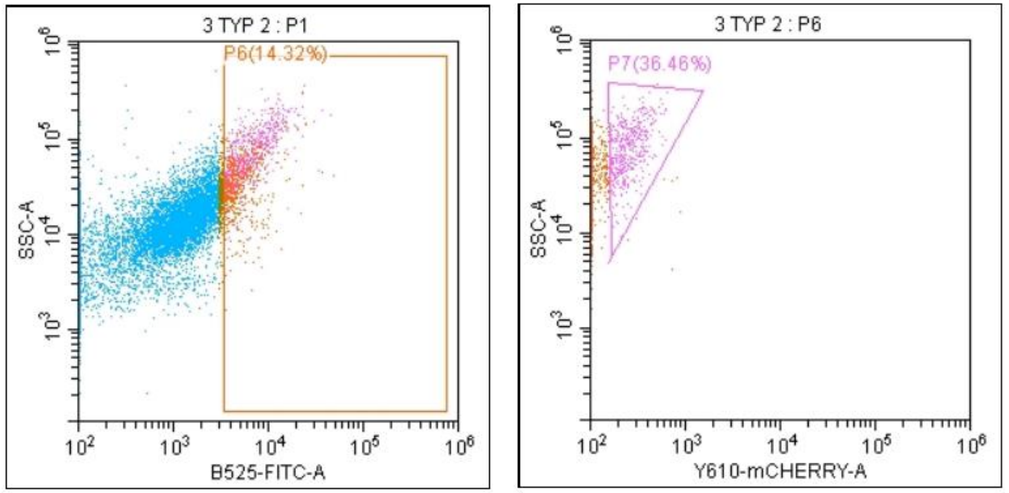

SRT1720

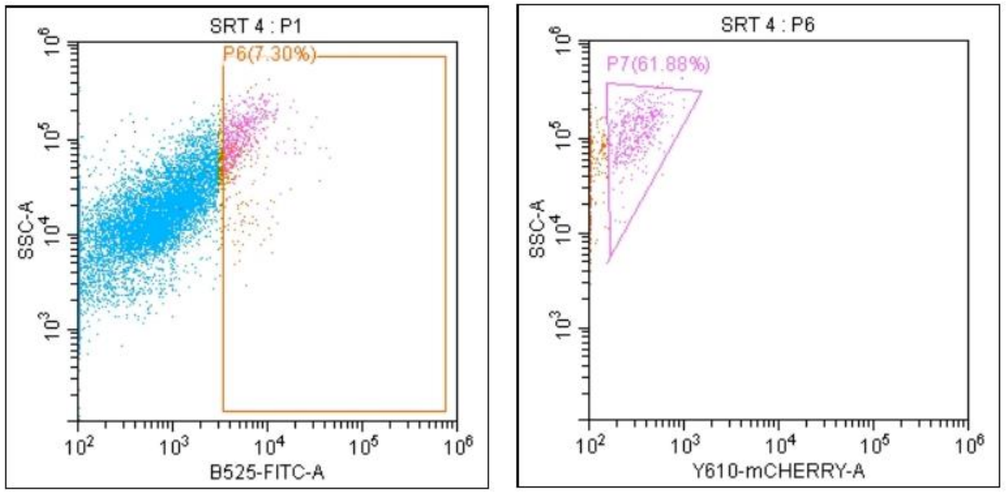

FITC Ly6C+ population

D

Vehicle Control STM

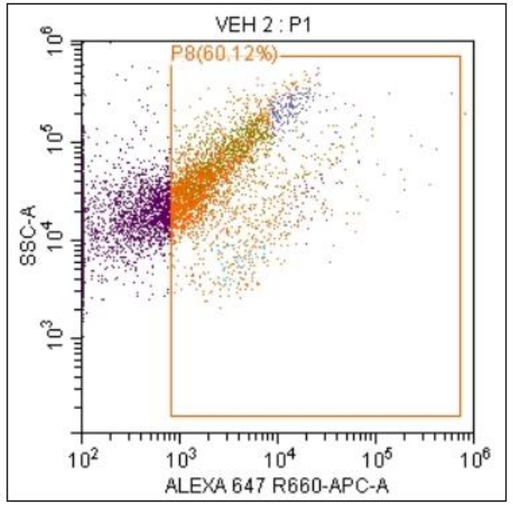

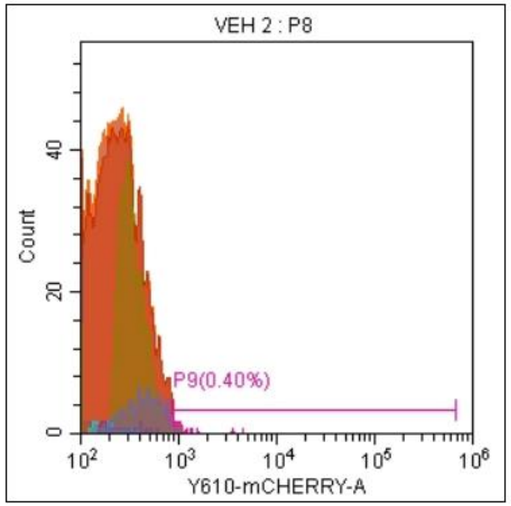

EX-527

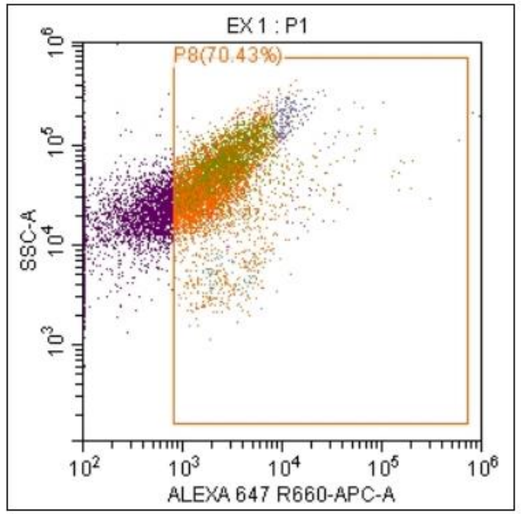

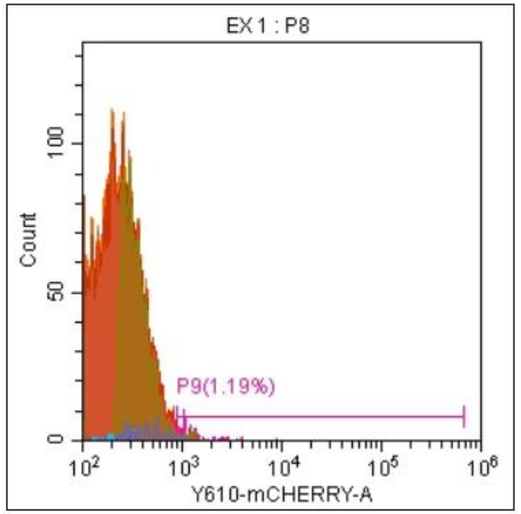

3TYP

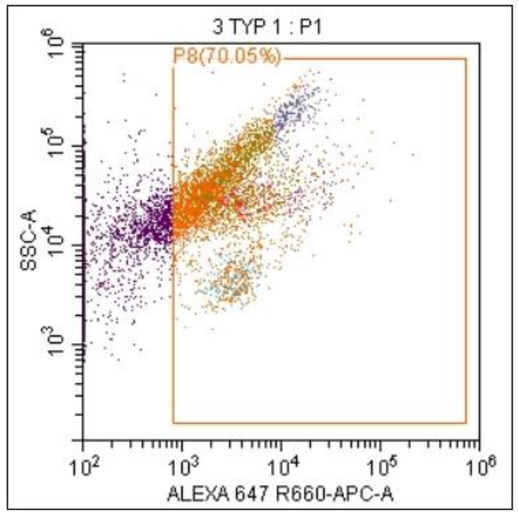

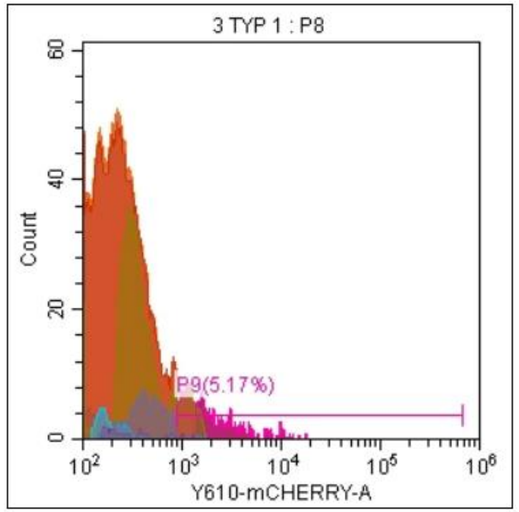

SRT1720

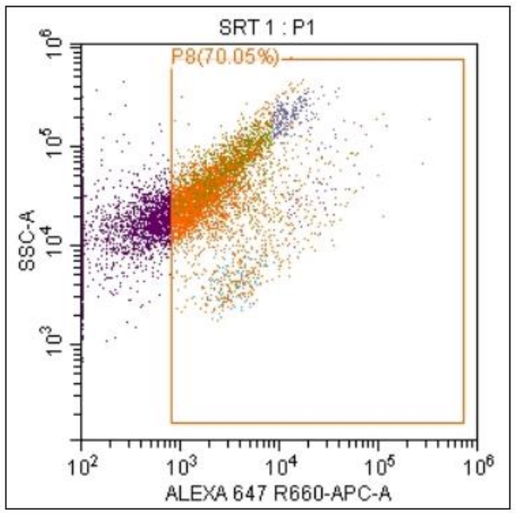

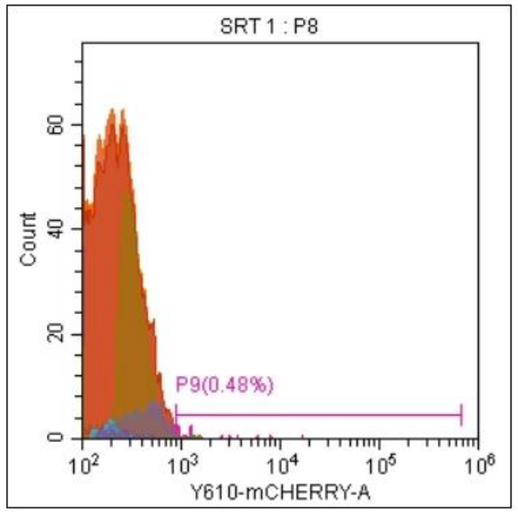

Alexa 647 CD45+ population

E

Vehicle Control STM

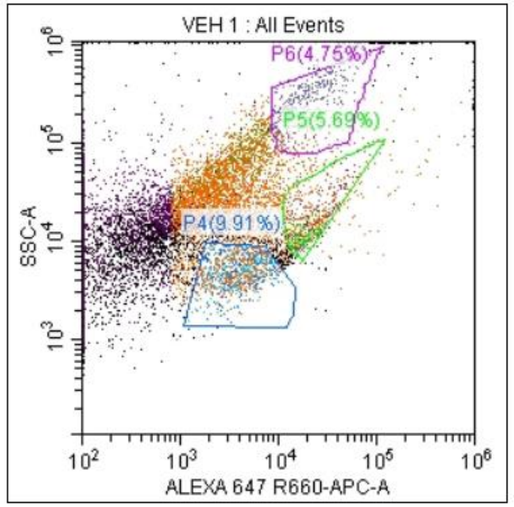

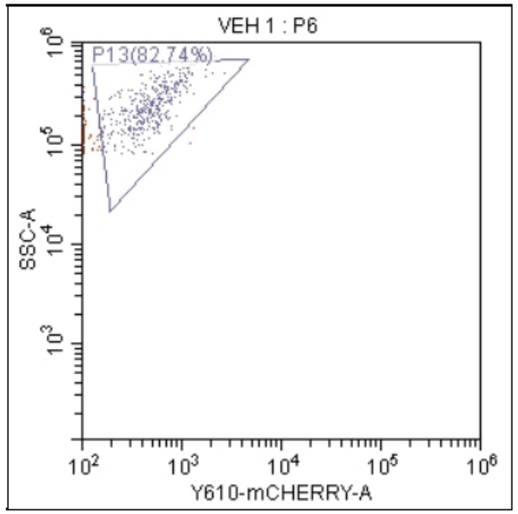

EX-527

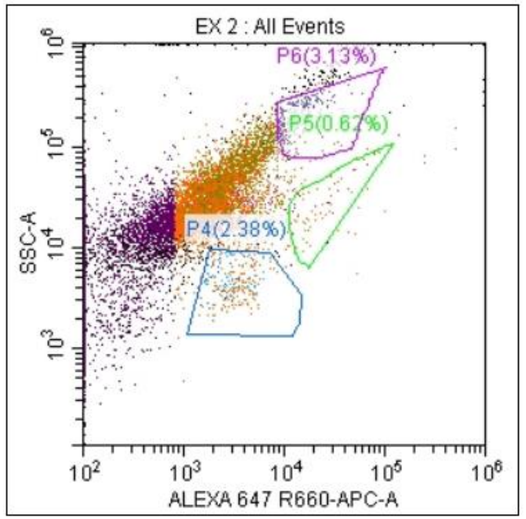

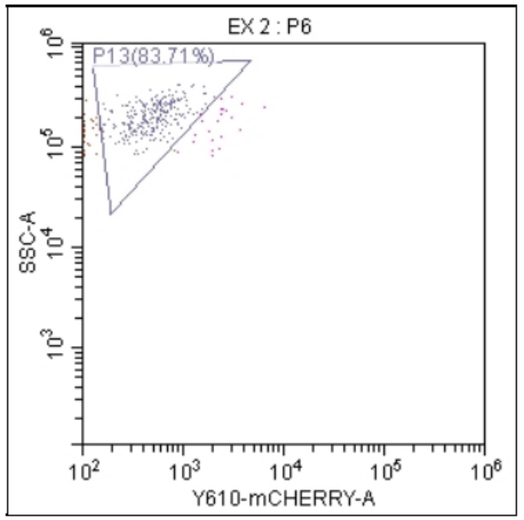

3TYP

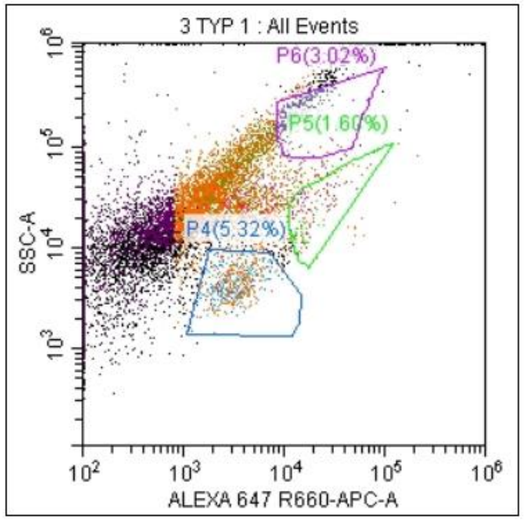

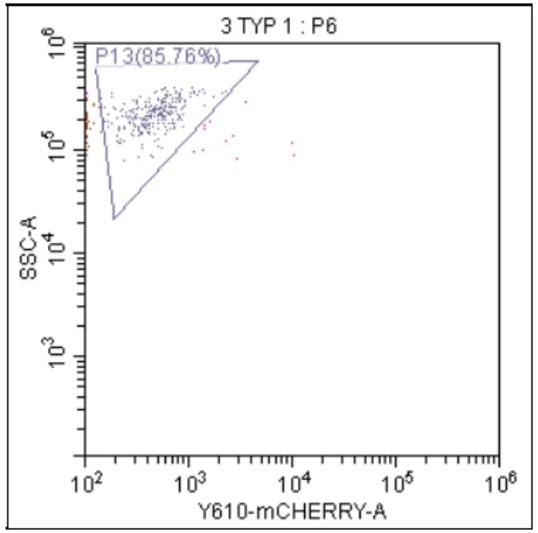

SRT1720

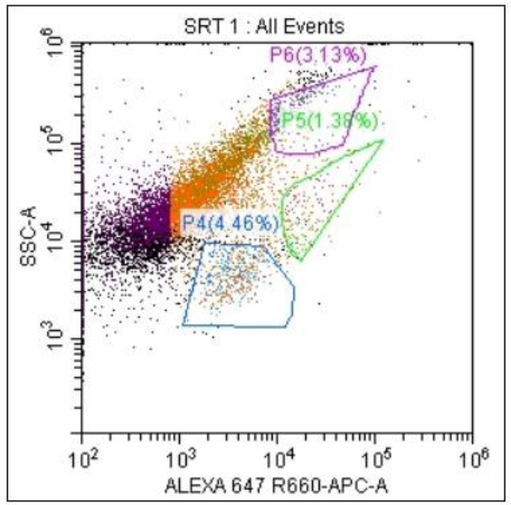

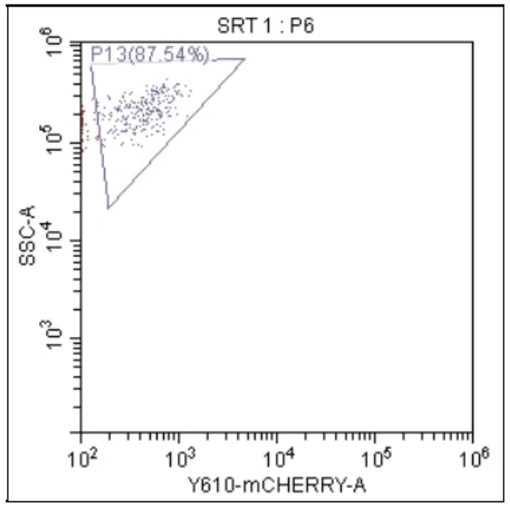

Alexa 647 CD45+ granulocytes P6 population

F

Vehicle Control STM

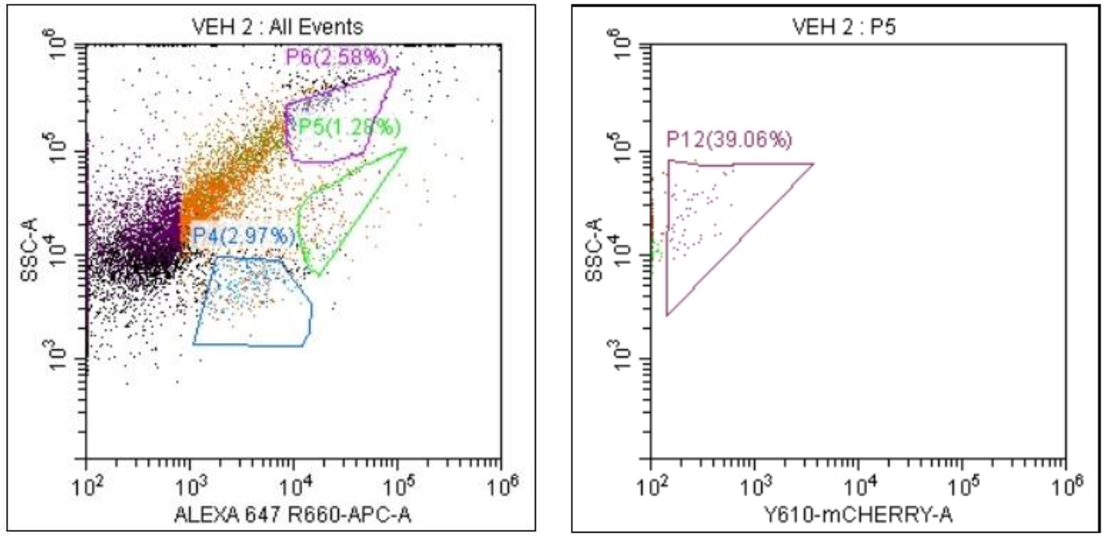

EX-527

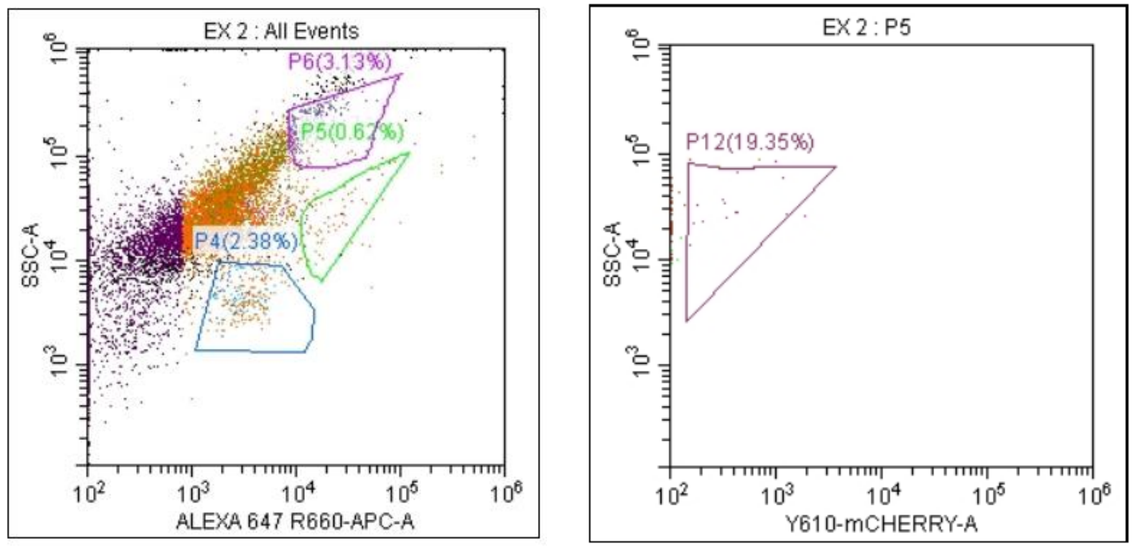

3TYP

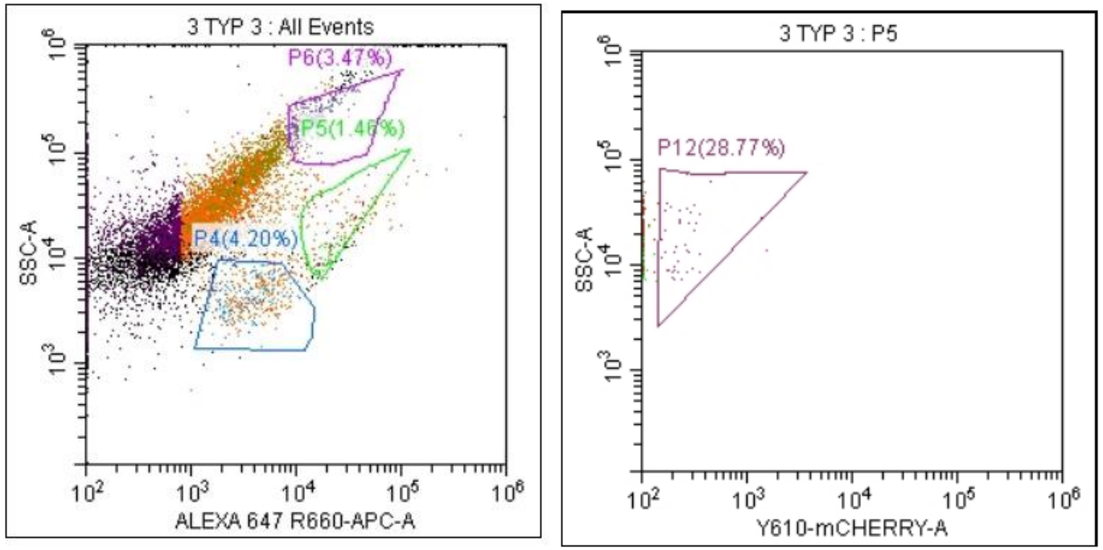

SRT1720

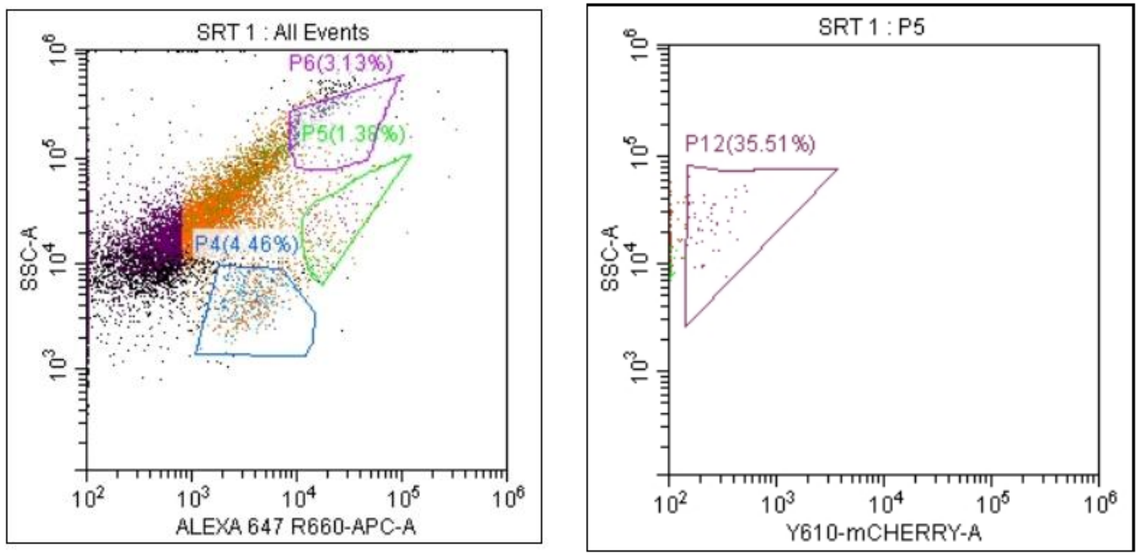

Alexa 647 CD45+ monocytes P5 population

G

Vehicle Control STM

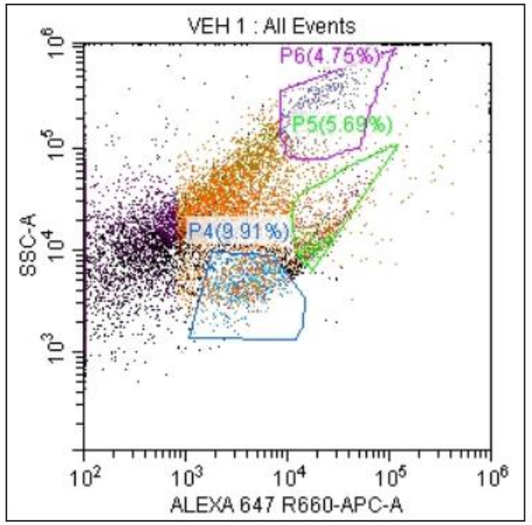

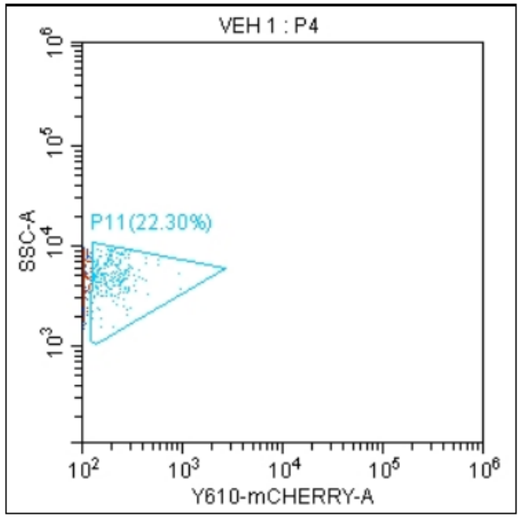

EX-527

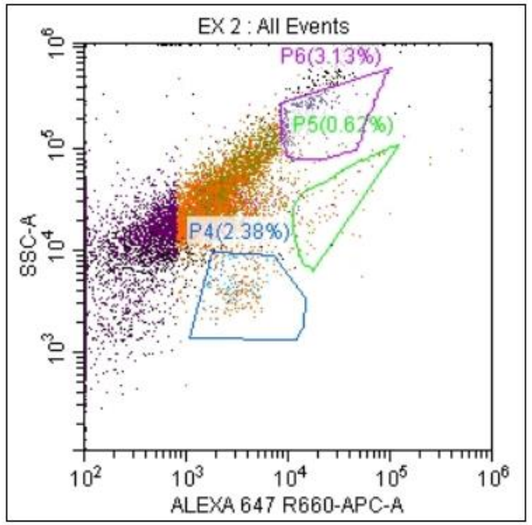

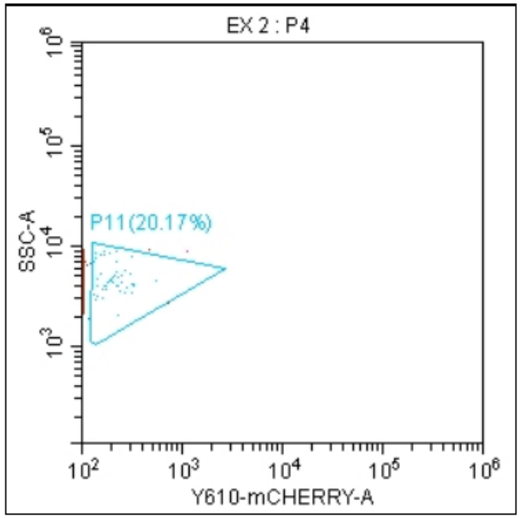

3TYP

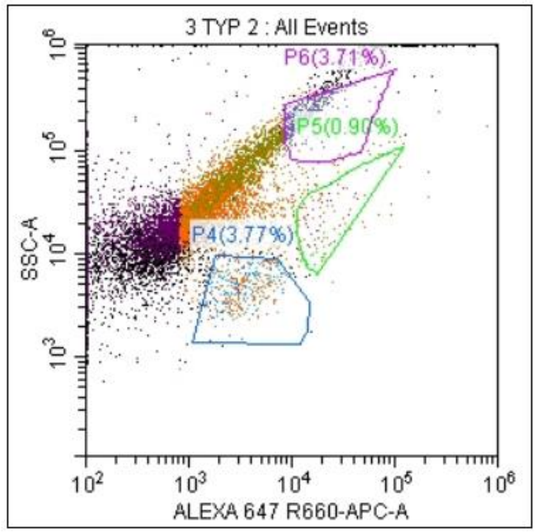

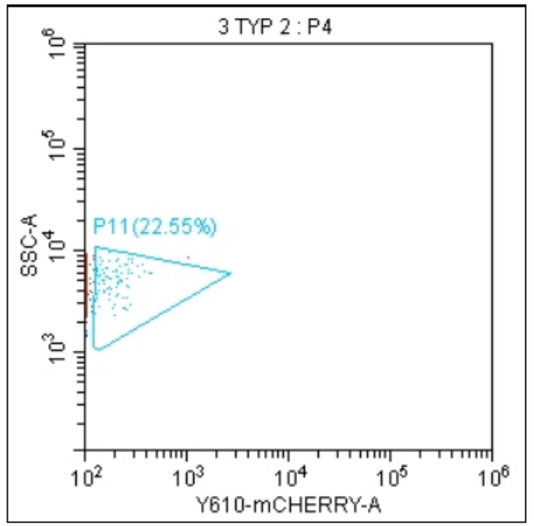

SRT1720

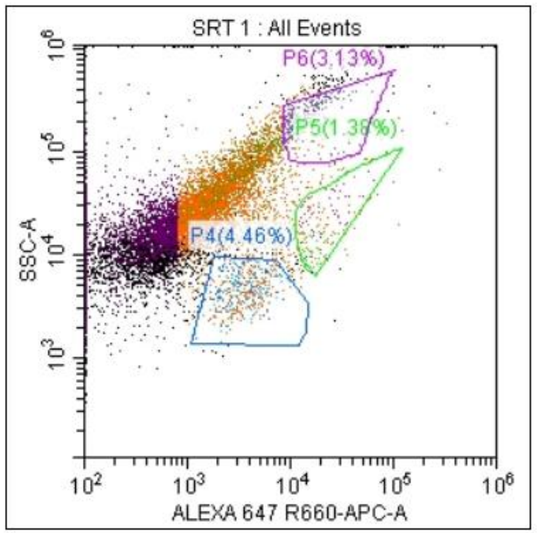

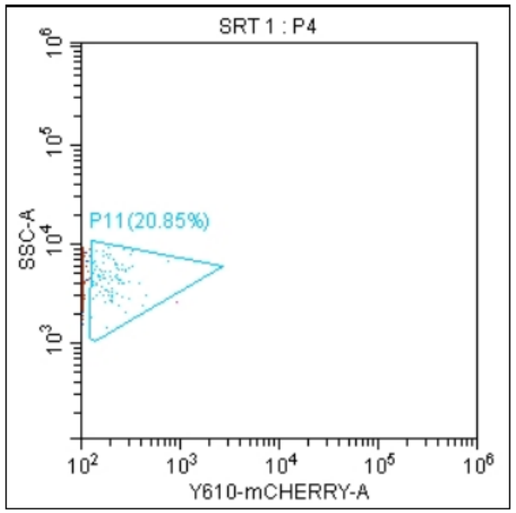

Alexa 647 CD45+ lymphocytes P4 population

Fig.S9

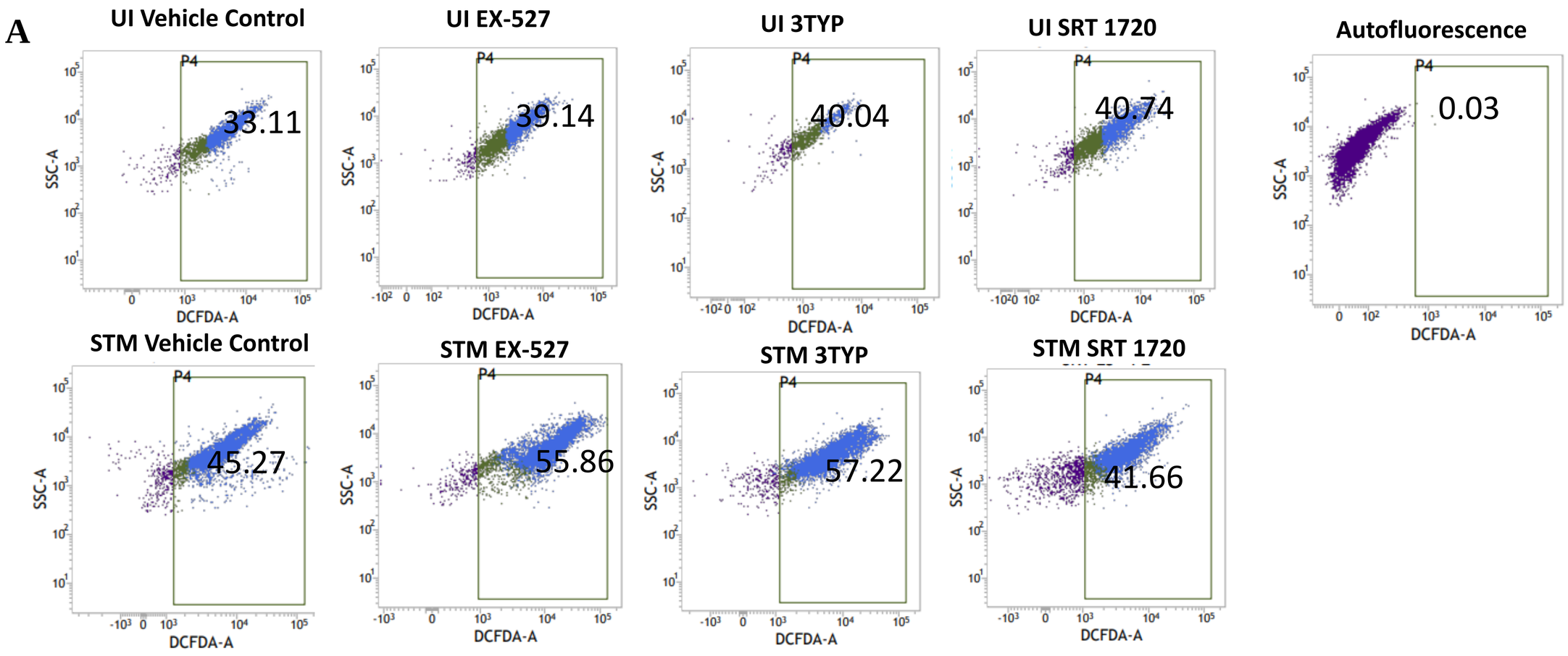
A
UI Vehicle Control
33.11
UI EX-527
39.14
UI 3TYP
40.04
UI SRT 1720
40.74
Autofluorescence
0.03
STM Vehicle Control
45.27
STM EX-527
55.86
STM 3TYP
57.22
STM SRT 1720
41.66
P4
SSC-A
DCFDA-A

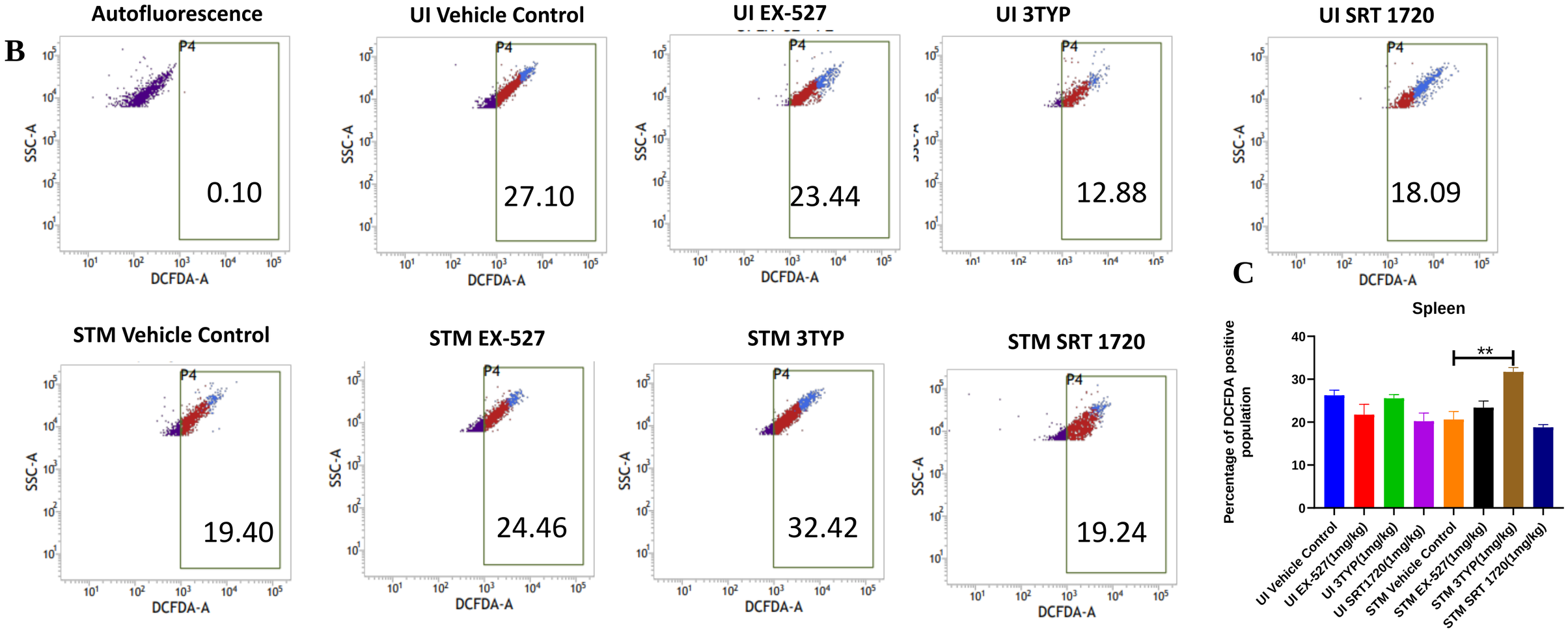
B
Autofluorescence
UI Vehicle Control
UI EX-527
UI 3TYP
UI SRT 1720
STM Vehicle Control
STM EX-527
STM 3TYP
STM SRT 1720
P4
0.10
27.10
23.44
12.88
18.09
19.40
24.46
32.42
19.24
SSC-A
DCFDA-A
C
Spleen
Percentage of DCFDA positive population
**
UI Vehicle Control
UI EX-527(1mg/kg)
UI 3TYP(1mg/kg)
UI SRT1720(1mg/kg)
STM Vehicle Control
STM EX-527(1mg/kg)
STM 3TYP(1mg/kg)
STM SRT 1720(1mg/kg)

Fig.S10

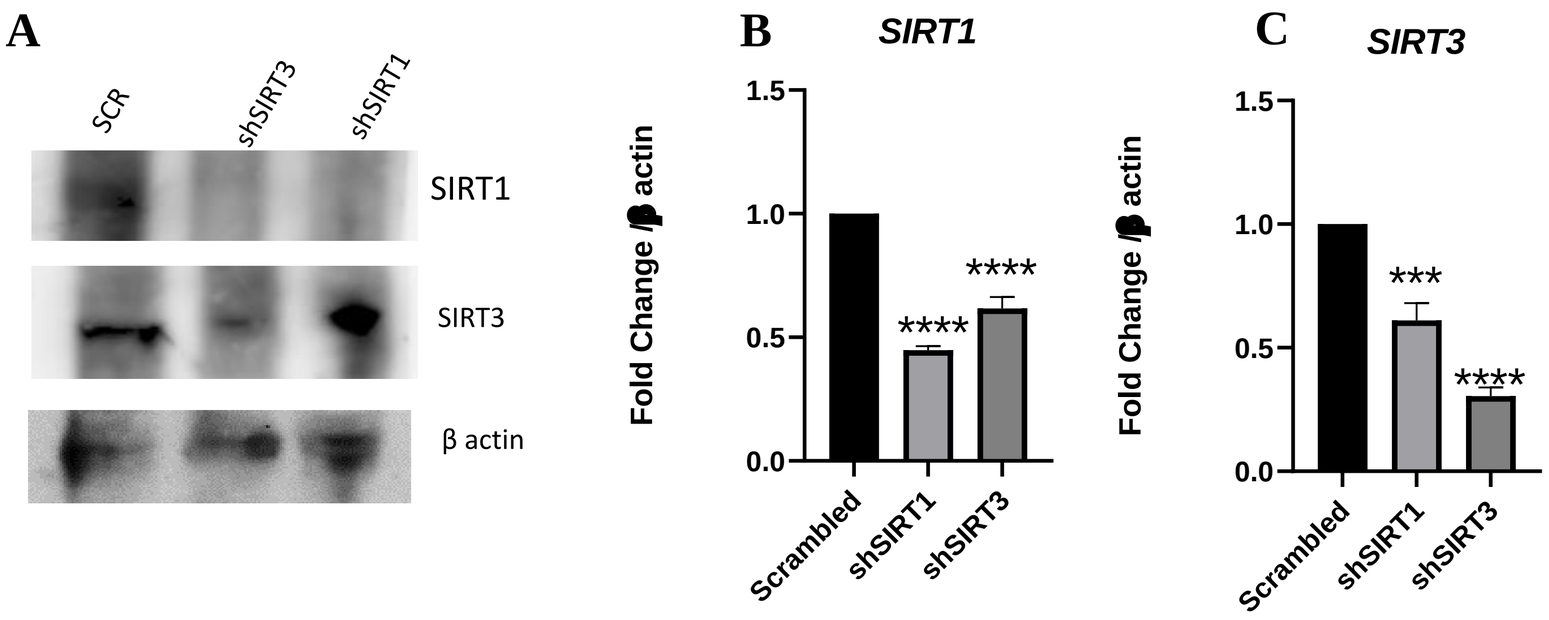
A
SCR
shSIRT3
shSIRT1
SIRT1
SIRT3
β actin
B
SIRT1
Fold Change /β actin
1.5
1.0
0.5
0.0
****
****
Scrambled
shSIRT1
shSIRT3
C
SIRT3
Fold Change /β actin
1.5
1.0
0.5
0.0
***
****
Scrambled
shSIRT1
shSIRT3

Fig.S11

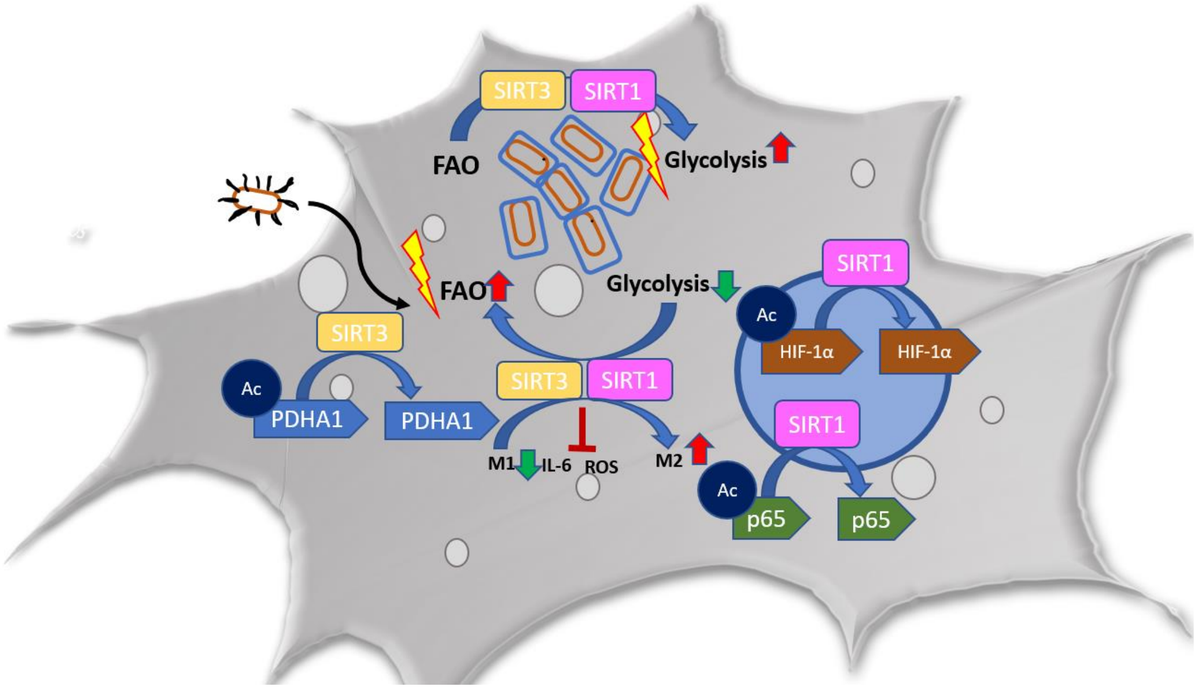
SIRT3
SIRT1
FAO
Glycolysis
FAO
Glycolysis
SIRT3
Ac
PDHA1
PDHA1
SIRT3
SIRT1
M1
IL-6
ROS
M2
SIRT1
Ac
HIF-1α
HIF-1α
SIRT1
Ac
p65
p65

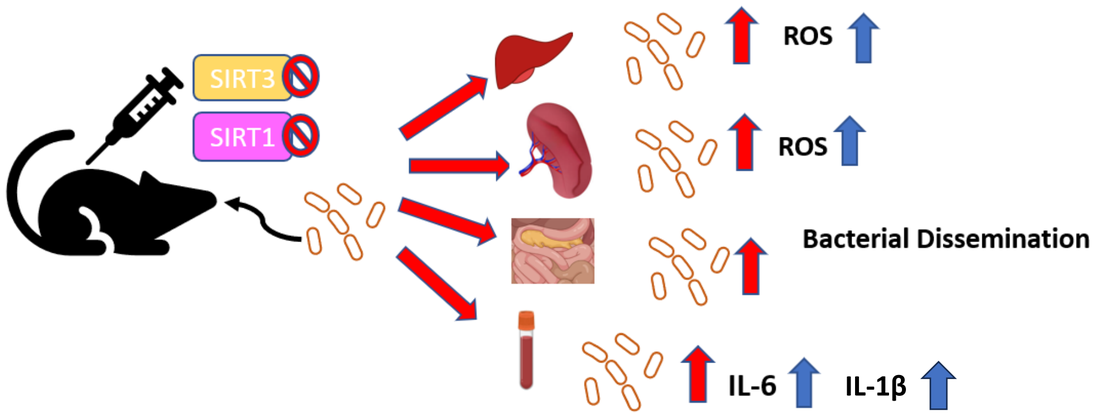
SIRT3
SIRT1
ROS
ROS
Bacterial Dissemination
IL-6
IL-1β